

AD \_\_\_\_\_

Award Number: DAMD17-02-1-0563

TITLE: Antibody Targeting of Caveolae in Breast Tumors

PRINCIPAL INVESTIGATOR: Jan E. Schnitzer, M.D.

CONTRACTING ORGANIZATION: Sidney Kimmel Cancer Center  
San Diego, California 92121

REPORT DATE: August 2004

TYPE OF REPORT: Final

PREPARED FOR: U.S. Army Medical Research and Materiel Command  
Fort Detrick, Maryland 21702-5012

DISTRIBUTION STATEMENT: Approved for Public Release;  
Distribution Unlimited

The views, opinions and/or findings contained in this report are those of the author(s) and should not be construed as an official Department of the Army position, policy or decision unless so designated by other documentation.



# REPORT DOCUMENTATION PAGE

Form Approved  
OMB No. 074-0188

Public reporting burden for this collection of information is estimated to average 1 hour per response, including the time for reviewing instructions, searching existing data sources, gathering and maintaining the data needed, and completing and reviewing this collection of information. Send comments regarding this burden estimate or any other aspect of this collection of information, including suggestions for reducing this burden to Washington Headquarters Services, Directorate for Information Operations and Reports, 1215 Jefferson Davis Highway, Suite 1204, Arlington, VA 22202-4302, and to the Office of Management and Budget, Paperwork Reduction Project (0704-0188), Washington, DC 20503

<b>1. AGENCY USE ONLY</b> (Leave blank)		<b>2. REPORT DATE</b> August 2004	<b>3. REPORT TYPE AND DATES COVERED</b> Final (1 Aug 02 - 31 Jul 04)	
<b>4. TITLE AND SUBTITLE</b> Antibody Targeting of Caveolae in Breast Tumors			<b>5. FUNDING NUMBERS</b> DAMD17-02-1-0563	
<b>6. AUTHOR(S)</b> Jan E. Schnitzer, M.D.				
<b>7. PERFORMING ORGANIZATION NAME(S) AND ADDRESS(ES)</b> Sidney Kimmel Cancer Center San Diego, California 92121  E-Mail: jschnitzer@skcc.org			<b>8. PERFORMING ORGANIZATION REPORT NUMBER</b>	
<b>9. SPONSORING / MONITORING AGENCY NAME(S) AND ADDRESS(ES)</b> U.S. Army Medical Research and Materiel Command Fort Detrick, Maryland 21702-5012			<b>10. SPONSORING / MONITORING AGENCY REPORT NUMBER</b>	
<b>11. SUPPLEMENTARY NOTES</b> Original contains color plates. All DTIC reproductions will be in black and white.				
<b>12a. DISTRIBUTION / AVAILABILITY STATEMENT</b> Approved for Public Release; Distribution Unlimited				<b>12b. DISTRIBUTION CODE</b>
<b>13. ABSTRACT (Maximum 200 Words)</b> In this project, we propose to compare, at the molecular level, protein expression in caveolae in tumor vs. normal endothelium in order to identify caveolar proteins unique to the tumor endothelium that can be used as molecular targets for therapeutic probes. We will use a novel technique developed in this lab for isolating caveolae from normal and tumor tissues at very high purity for both the proteomic analysis as well as for direct injection into mice for monoclonal antibody production. Antibodies found to be tumor caveolae-specific by Western analysis and immunostaining of tissue specimens will be assessed for tumor targeting in vivo by injecting them IV into a rat breast tumor model system. Our goal is to find a breast tumor-specific caveolae-targeted monoclonal antibody that will efficiently target the tumor and also transport drug conjugates into and even across the tumor endothelium for directed delivery to the underlying tumor cells. This approach may permit tumor ablation through localized destruction of the tumor vascular endothelium as well as increase the efficacy of chemotherapeutic agents in the treatment of solid breast tumors by improving accessibility with effective transport across the endothelial cell barrier.				
<b>14. SUBJECT TERMS</b> Tumor Targets, Antibody Therapy, Immunology, Targeted Systemic Therapy				<b>15. NUMBER OF PAGES</b> 47
				<b>16. PRICE CODE</b>
<b>17. SECURITY CLASSIFICATION OF REPORT</b> Unclassified	<b>18. SECURITY CLASSIFICATION OF THIS PAGE</b> Unclassified	<b>19. SECURITY CLASSIFICATION OF ABSTRACT</b> Unclassified	<b>20. LIMITATION OF ABSTRACT</b> Unlimited	

NSN 7540-01-280-5500

Standard Form 298 (Rev. 2-89)  
Prescribed by ANSI Std. Z39-18  
298-102



## Table of Contents

Cover.....	1
SF 298.....	2
Table of Contents.....	3
Introduction.....	4
Body.....	4
Key Research Accomplishments.....	6
Reportable Outcomes.....	7
Conclusions.....	9
Personnel.....	10
References.....	N/A

### Appendices:

Durr E, Yu J, Krasinska KM, Carver LA, Yates JR, Testa JE, Oh P, Schnitzer JE.  
Direct proteomic mapping of the lung microvascular endothelial cell surface in vivo and in cell culture.

Nat Biotechnol. 2004 22(8):985-92.

Oh P, Li Y, Yu J, Durr E, Krasinska KM, Carver LA, Testa JE, Schnitzer JE.  
Subtractive proteomic mapping of the endothelial surface in lung and solid tumours for tissue-specific therapy.

Nature. 2004 429:629-35.



## Introduction

Caveolae of vascular endothelium provide inherently accessible targets as well as a pathway for transporting antibodies across the endothelial cell barrier. Monoclonal antibodies that can target tissue-specific proteins located in caveolae permit rapid tissue-specific delivery in vivo and, perhaps more importantly, are transported into and even across the endothelium. When accessible vascular sites, such as caveolae, are targeted, tissue-specific uptake of targeting antibodies is observed in just 30 minutes with single tissue accumulation of 80% of the injected drug and up to 180-fold more than controls. Such transport pathways may be useful in improving the delivery of antibodies conjugated to agents such as chemotherapeutic drugs, toxins or even gene vectors. The goal of the proposed research was to test the hypothesis that re-directing antibody probes to accessible caveolar targets of tumor blood vessels (rather than to the breast tumor cells themselves) increases not only directed delivery to solid tumors but also increased penetration and accumulation of antibody probes into the tumor itself for greater therapeutic efficacy with fewer side effects. The focus of this project is to discover caveolar proteins that are induced specifically in the vascular endothelium of breast tumors but that are not expressed in normal tissues. We intend to generate a caveolae-targeted monoclonal antibodies that may duplicate the efficient transcytosis across the lung endothelium observed in our past work but, in this case, exhibiting breast tumor specificity. The targeting caveolae in tumor endothelium may prove useful in vivo to increase the efficacy of chemotherapeutic agents in the treatment of solid breast tumors.

## Progress Summary

**Technical Objective 1:** Proteomic analysis to identify and characterize tumor caveolae-associated proteins that may be useful for tumor vascular targeting.

**Task 1: Completed.** Isolation of caveolae from breast tumor and normal tissues.

We have successfully optimized the experimental parameters for isolating luminal endothelial cell caveolae from various normal tissues as well as breast tumor tissue from both rats and humans. Using these newly-established protocols, we can generate sufficient material to undertake the proposed proteomic analysis.

**Task 2: Completed.** Comparative protein analysis of caveolae isolates.

We have successfully performed a comparative proteomic analysis of endothelial cell caveolae from breast tumors vs. normal tissues using mass spectrometry (MS) of proteins extracted from the caveolae isolates. These experiments have resulted in the identification of numerous proteins within these isolates that appear to be induced in the breast tumor caveolae. A total of 7 MS analyses of normal and breast tumor caveolar proteins have been completed. Part of these results have recently been published (Nature 429, 629, 2004). They are also the subject of a second paper in preparation.

**Task 3: Completed.** Identification of candidate tumor-specific proteins by mass spectrometry, de novo sequencing, and classic chemical microsequencing.

We have identified 5 candidate tumor-induced proteins, designated TE1-5, found in breast tumors but not in normal tissues. Greater than 3 peptide sequences were determined for each protein by our MS analysis. Polyclonal antibodies raised to peptides of these proteins were used for validation to confirm their tumor- and caveolar-association. We find significant enrichment of TE1-5 in luminal endothelial cell plasma membrane subfractions (P) isolated from tumor-bearing tissues relative to the whole tissue lysates. Western analysis from various normal organs reveals little to no expression of TE3 and TE4 in normal tissues, some expression of TE1 and TE2 on normal liver endothelium, and some expression of TE5 in normal kidney and liver although at levels much less than breast tumor endothelium. When we immunoblotted for TE1-5 on caveolar membrane isolates (V), we found that TE1, TE3, TE4, and TE5 do indeed appear to reside in caveolae. By Western analysis, TE1 and TE3 are significantly enriched in tumor caveolae while TE2 is found enriched in tumor P but not V and remains in luminal endothelial cell plasma membrane fraction stripped of caveolae (P-V). TE5 is present in V but not enriched there. In addition, we have independently identified each of these proteins (TE1-5)



using 2-D gel maps & MS analysis of membranes isolated from various solid tumors from rat, rabbit, rhesus monkey and humans.

Because TE3 appears to be highly tumor-specific, we focused our efforts on further validation of its tumor-specificity by using tissue immunostaining of panel of normal and neoplastic tissues. TE3 is expressed selectively on the breast tumor vascular endothelium and not in nearby normal tissue. That is, TE3 is detected on the blood vessels within the growing tumor whereas there is no labeling of normal vasculature. Other tissues (heart, brain, kidney, skeletal muscle, fat, liver) were negative, consistent with the Western analysis described above. We expanded our validation of TE3 to include human tissues. Western analysis of human tumor and normal tissues revealed that TE3 is expressed in caveolae not only in breast tumors but also in tumors from kidney, liver, lung, brain, and prostate but not in various normal tissues. Thus, the tumor-induction of TE3 can be demonstrated with antibodies both in rat and human solid tumors of different types. Human tissue immunostaining using TE3 antibodies confirmed its tumor-specific expression. TE3 is expressed in the blood vessels of human breast, prostate, and liver tumor tissue whereas no labeling was detected in adjacent normal tissue vasculature (negative staining in normal brain, lung, and liver tissue). Thus, TE3 is induced quite selectively in caveolae of blood vessels of various human solid tumors, including breast, liver, and prostate.

In the last year, we have focused our efforts on identifying and cloning the protein corresponding to TE3. We have now identified TE3 as a 34 kDa form of Annexin A1 (**AnnA1**) from multiple samples by MS analysis: i) as a band found in tumor but not normal caveolae by 1-D gel analysis; ii) as a unique spot on a 2-D gel from caveolae isolated from tumor but not normal tissue; and iii) in TE3 antibody immunoprecipitates from silica-coated luminal endothelial cell plasma membranes (P) isolated from tumors. In addition to tandem MS, we have also detected AnnA1 from the TE3 fingerprint in MALDI analysis of tumor P. In all, we have identified have identified 30 peptides providing ~58% sequence coverage for AnnA1.

**Technical Objective 2:** Generate and characterize monoclonal antibodies specific for caveolae-specific molecules of rat breast tumor models.

**Task 4: Completed.** Production of monoclonal antibodies in mice using isolated caveolar membrane fractions as an immunogen or specific tumor-induced proteins identified by protein analysis (Task 3).

To better characterize TE3/AnnA1 expression and to test possible targeting of solid tumors in vivo, we needed high affinity, specific probes. Last year, we reported that we had cloned the TE3 cDNAs and begun to make monoclonal antibodies to rat, mouse and human TE3/AnnA1. Using these cDNAs, we produced recombinant protein from each of the three species for antibody generation and screening of mouse hybridomas. We have now successfully generated a panel of monoclonal antibodies (**mAbs**) recognizing rat, mouse, and human TE3/AnnA1, some of which we expect to use in an upcoming clinical trial.

**Task 5: Completed.** Establish monospecificity of candidate antibodies by Western analysis of multiple rat and human tumor and normal tissues, including blood.

We have established the monospecificity of our new TE3/AnnA1 mAbs by Western analysis of luminal endothelial cell surface membranes and caveolae isolated from various rat and human tumors.

**Task 6: Completed.** Establish tumor specificity of select candidate mAbs by analyzing multiple rat and human tumor and normal tissues by both Western analysis of isolated caveolae and by tissue immunostaining.

We have established the tumor-specificity of our new TE3/AnnA1 mAbs by both Western analysis of endothelial caveolar isolates from normal and neoplastic tissues and by tissue immunostaining of rat and human normal and tumor tissue sections. We have also determined that these new mAbs also specifically label the blood vessels of multiple rat, mouse, and human tumor types (including breast) but not in normal tissues similar to our results with the polyclonal antibodies described above in Task 3. Work using these new antibodies has recently been published (Nature 429, 629, 2004).

**Technical Objective 3:** Test the ability of developed antibodies to target specifically rat breast tumors in vivo by assessing tissue biodistribution in vivo after intravenous injection.



**Task 7: Completed.** Radiolabel candidate antibodies with I<sup>125</sup> and assess tumor targeting via IV injection and gamma counting of excised tissues.

To test whether TE3/AnnA1 is sufficiently exposed and breast tumor vessel-specific to permit immunotargeting in vivo, we performed bio-distribution analysis on our metastatic breast tumor model, whereby 13762 breast tumor cells are injected into the rat tail vein and allowed to seed the lungs with metastatic breast tumors, and the subcutaneous tumor model, whereby MDAMB435 cells are injected subcutaneously into the anterior back region, to create easily observed and palpable tumors that can be excised for analysis.

We injected <sup>125</sup>I-labeled TE3/AnnA1 antibodies intravenously to assess biodistribution in vivo and define tissue and tumor accumulation. Significant accumulation of TE3/AnnA1 antibody was observed in the whole lungs with breast tumors (metastatic model) reaching a maximum by two hours (17% ID/g). In breast tumors dissected away from normal lung tissue, TE3/AnnA1 mAb accumulation reached a maximum of 33% ID/g of tumor at 2 hours. When injected IV into normal rats without breast tumors, AnnA1 antibodies showed no targeting of normal organs, at levels <1% ID/g of tissue (data not shown). These data indicate that AnnA1 in tumor endothelial cell caveolae is exposed on the outside of the cell and is readily accessible by IV injection for breast tumor-selective delivery in vivo.

In addition, we have expanded the biodistribution studies proposed in the application (and described above) to include the use of higher resolution, state-of-the-art imaging technologies. We have used an A-SPECT high resolution small animal gamma scintigraphy imager (Gamma Medica, Northridge, CA) to rapidly visualize tumor targeting in vivo of radiolabeled TE3/AnnA1 antibodies injected intravenously. This technology, which was not available to us at the time of the original application, is far superior to the old methodology originally proposed because it provides a continuous viewing of tissue uptake, eliminates the need for single animal per data point reducing the number of test animals needed and permitting longitudinal studies, and greatly increases the quality and quantity of data collected. Radio-iodinated TE3/AnnA1 mAbs injected into the tail vein of rats with metastatic breast tumors in the lung accumulated in the tumors with a maximal saturation in the tumors of ~35% of the injected dose/gram of tumor tissue.  $\gamma$ -scintigraphic planar images captured 1-4 hours postinjection showed distinct foci of radioactivity in the lungs and little signal elsewhere in the body. Non-targeting <sup>125</sup>I-labeled IgGs did not target. When the lungs were imaged ex vivo, we observed <sup>125</sup>I-TE3/AnnA1 antibody accumulation in the tumor as a hot spot corresponding to visible tumors. Targeting was prevented by 30-fold excess unlabeled TE3/AnnA1 IgG but not control IgG. We also injected <sup>125</sup>I-AnnA1 antibodies into the tail vein of mice bearing the MDAMB435 subcutaneous breast tumor model and imaged the mice 3 hours later. Gamma scintigraphic imaging showed specific accumulation of <sup>125</sup>I-AnnA1 antibodies in the tumor but not anywhere else. Thus, AnnA1 antibodies can target multiple tumor types in rat and mouse models and is an excellent candidate for further pre-clinical testing. These data have recently been published in Nature.

#### Key research accomplishments

- Isolation of caveolae from breast tumor and normal tissues.
- Comparative protein analysis of caveolae isolates by MS analysis is underway and producing useful data.
- Identification of candidate tumor-specific proteins, TE1-5, by mass spectrometry, de novo sequencing, and classic chemical microsequencing.
- Validation of tumor- and caveolar-specificity of TE1-5 with polyclonal antibodies to peptides from TE1-5 by Western analysis and tissue immunostaining of rat and human-derived normal and neoplastic tissues.
- Identified the most promising candidate tumor-specific protein, TE3, as Annexin A1 (**AnnA1**) and cloned the cDNA for recombinant protein- and monoclonal antibody production.
- Production of new monoclonal antibodies recognizing mouse, human, and rat TE3/AnnA1.
- Established monospecificity of new TE3/AnnA1 monoclonal antibodies by Western analysis of multiple



rat and human tumor and normal tissues, including blood.

- Established tumor specificity of multiple new TE3/AnnA1 monoclonal antibodies recognizing mouse, rat, and human TE3/AnnA1 by analyzing multiple rat and human tumor and normal tissues by both Western analysis of isolated caveolae and by tissue immunostaining.
- Established that TE3/AnnA1 is both expressed and externally exposed selectively in endothelium growing in solid tumors.
- Established tumor specificity and targeting of TE3/AnnA1 monoclonal antibodies by in vitro biodistribution and state-of-the-art imaging techniques in metastatic and subcutaneous breast tumor models in rat.

## Reportable outcomes

### Publications

- Oh, P., Li, Y., Yu, J., Durr, E., Krasinska, K. M., Carver, L. A., Testa, J. E. and Schnitzer, J. E. (2004) Subtractive proteomic mapping of the endothelial surface in lung and solid tumours for tissue-specific therapy. *Nature* 429, 629-35.
- Durr, E., Yu, J., Krasinska, K. M., Carver, L. A., Yates, J. R. I., Testa, J. E., Oh, P. and Schnitzer, J. E. (2004) Direct proteomic mapping of the lung microvascular endothelial cell surface in vivo and in cell culture. *Nature Biotechnol* 22, 985-92.
- Carver, L. A. and Schnitzer, J. E. Focusing target discovery and validation through proteogenomics and molecular imaging. in The Oncogenomics Handbook: Understanding and Treating Cancer in the 21st Century. (eds. Shimkets, R. A. and LaRochelle, W. J.) In press. (The Humana Press, Inc., Totowa, NJ, 2004).
- Carver, L. A., Schnitzer, J. E., Anderson, R. G. and Mohla, S. (2003) Role of caveolae and lipid rafts in cancer: workshop summary and future needs. *Cancer Res* 63, 6571-4.
- Carver, L. A. and Schnitzer, J.E., Tissue-specific pharmacodelivery and overcoming key cell barriers in vivo: Vascular targeting of caveolae. In: Biomedical Aspects of Drug Targeting, Eds. Muzykantov, V.R., and Torchilin, B., Kluwer Academic Publishers, Boston, pp.107-128, 2002
- Carver, L. and Schnitzer, J.E. Caveolae: Mining little caves for new cancer targets; *Nature Rev Cancer* 3:571-581 (2003).

### Presentations

- 2002 First International Conference on Vascular Targeting, "The Proteome of Endothelium and its Caveolae: Organ – and Tumor – Specific Targeting and Transcytosis in vivo" (Cambridge, MA)
- 2002 Annual Meeting of the Society of Molecular Imaging, "Angiomics: Identifying & targeting accessible tissue-specific proteins on endothelium in vivo" (Boston, MA)
- 2002 National Cancer Institute Drug Discovery & Therapeutics Seminar Series, "Accessible functional proteomics: Mapping caveolae & endothelial cell surface proteins for organ- and tumor-specific targeting in vivo." (Frederick, MD)
- 2002 International Conference on Translational Cancer Research and Therapy, "Accessible Functional Proteomics: Mapping the Molecular Heterogeneity of Endothelia and Caveolae for Transcytosis & Tissue-Targeted Therapy in Vivo", (Tianjin, China)
- 2002 Schering Lecture; "Vascular proteome and targeting of specific organs and solid tumors in vivo", (Berlin, Germany)
- 2003 University of Michigan Grand Rounds Seminar: "Proteomic Mapping of Endothelium for Organ- and Tumor-Specific Delivery and Imaging in Vivo" (Ann Arbor, MI)
- 2003 2<sup>nd</sup> International Workshop on New Therapeutic Targets in Vascular Biology; "Vascular Proteomics" (Geneva, Switzerland).
- 2003 Cold Springs Harbor Laboratory International Gene Therapy Conference, Vector Targeting Strategies for Gene Therapy; "Mapping targets on endothelia and caveolae in vivo for organ- and tumor-directed delivery and transcytosis" (Cold Spring Harbor, New York)



- 2003 Xenogen Corporation Lecture: "Vascular Proteomics and Targeting for Imaging Single Organs and Solid Tumors" (Alameda, California)
- 2003 University of Miami, Department of Cell Biology and Anatomy: "Endothelium and its caveolae: From trafficking mechanisms to proteomic mapping for tumor targeting in vivo" (Miami, Florida)
- 2003 Human Genome 2003 International Conference , "Cancer angiomics: Mapping accessible vascular targets for molecular imaging and therapy" (Cancun, Mexico)
- 2003 National Cancer Institute Seminar, "Proteomic Mapping of Endothelium and Its Caveolae for Targeting Single Organs and Solid Tumors In Vivo" (Bethesda, MD)
- 2003 Stanford University, Division of Pulmonary Medicine: "Caveolae Trafficking and Vascular Proteomic Mapping for Organ- and Tumor-Specific Targeting in Vivo" (Stanford, CA)
- 2003 National Cancer Institute, The Fourth Principal Investigator's (PI) Meeting of the Innovative Molecular Analysis Technologies (IMAT) Program, Exploring Human Cancer: "Vascular Proteomics: Mapping targets on endothelia and caveolae in vivo for organ- and tumor-directed delivery and transcytosis" (San Diego, CA)
- 2003 National Heart, Lung and Blood Institute's Symposium, From Genome to Disease: A Symposium of High Throughput Biology, Microarray Technology, "The vascular proteome: Mapping endothelium and its caveolae for tissue-specific pharmacodelivery and imaging in vivo" (Bethesda, MD)
- 2003 Second Annual Meeting of The Society for Molecular Imaging. "The Vascular Proteome: Tissue-specific Imaging of the Vasculature from the Whole Body to Electron Microscopy" (San Francisco, CA)
- 2003 American Heart Association, 57th Annual Fall Conference and Scientific Sessions of the Council for High Blood Pressure Research in association with the Council on Kidney in Cardiovascular Disease, Special Keynote Lecture, "Caveolae Integrate Signaling and Trafficking as Sensore of Hemodynamic Flow and Vasoactivators" (Washington, DC)
- 2003 California Breast Cancer Research Program 2003 Symposium, From Research to Action: A Decade of Progress in San Diego, "Targeting Breast Cancer Blood Vessels" (San Diego, CA)
- 2003 University of Illinois at Chicago, Department of Pharmacology, College of Medicine, "Molecular Architecture and Function of Caveolae in Endothelium" (Chicago, IL)
- 2003 Northwestern University Division of Nephrology/Hypertension, "Function of Caveolae in Vascular Endothelium: Proteomic Mapping and Imaging for Tissue Specific Delivery" (Chicago, IL)
- 2003 Molecular Imaging Program at Stanford (MIPS) Seminar Series, "Unmasking IV-Accessible Vascular Targets Specific to Solid Tumors and Single Organs by Tissue Subfractionation, Subtractive Proteomics, and Molecular Imaging" (Stanford, CA)
- 2003 12th International Conference on Gene Therapy of Cancer, "Mapping Accessible Tumor Vascular Targets through Subtractive Proteomics and Molecular Imaging in Vivo" (San Diego, CA)
- 2003 Immunogen Corporation Lecture, "Unmasking Endothelial Cell Surface Proteins for Targeting Solid Tumors in Vivo" (Boston, MA)
- 2003 American Society of Cell Biology, 43rd Annual Meeting, "Distinct Mechanisms of Endocytosis for Antibodies Targeting Mature Caveolae vs. Sequestering GPI-AP in Lipid Rafts to Form New Caveolae" (San Francisco, CA)
- 2004 American Association of Cancer Research Advances in Cancer Research, "Unmasking IV-Accessible Tumor Vascular Targets by Tissue Subfractionation, Subtractive Proteomics and Molecular Imaging" (Waikoloa, Hawaii)
- 2004 First International Conference on Genomics, Signaling and Tumor Targeting, "Unmasking specific IV-accessible immunotargets in lung and solid tumors via prefractionated subtractive proteomics and molecular imaging in vivo." (San Diego, CA)
- 2004 Keystone Symposia, G-Protein-Coupled Receptors: Evolving Concepts and Drug Discovery, "Differential Integration of Signaling and Trafficking in Caveolae and Lipid Rafts by G Proteins and CPCRs" (Taos, New Mexico).
- 2004 Mayo Clinic, Seminar, "Proteomic Mapping of Endothelium and its Caveolae for Rapid Organ- and Tumor-specific Imaging, Transcytosis, and Therapy in Vivo" (Rochester, MN)



- 2004 Second International Conference on Vascular Targeting, Ligand Based Vascular Targeting, "Caveolar Proteins" (Miami, FL)
- 2004 Third Annual Congress on the Future of Breast Cancer, "Caveolae: Mining Little Caves for New Cancer Treatment" (Southampton, Bermuda)
- 2004 Gordon Research Conference, Endothelial Cell Phenotypes in Health and Disease, "Direct Proteomic Mapping and Functional Imaging of the Endothelial Cell Surface and its Caveolae in Vivo" (Andover, NH)
- 2004 Third Annual Meeting of the Society for Molecular Imaging, Enhancing Delivery and Traversing Barriers (co-chair), "Mapping and Targeting Caveolae to Overcome Endothelial Cell Barriers for Tissue- and Tumor-Specific Delivery in Vivo" (St. Louis, MO)
- 2004 16<sup>th</sup> EORTC – NCI – AACR Symposium on Molecular Targets and Cancer Therapeutics, "Subtractive Proteomic Mapping of the Endothelial Surface" (Geneva Switzerland)
- 2004 AACR Advances in Proteomics in Cancer Research, "Unmasking Specific IV-accessible Targets in Endothelial Caveolae of Solid Tumors via Prefractionated Subtractive Proteomics and Molecular Imaging" (Key Biscayne, FL)
- 2004 American Heart Association Annual Meeting 2004, "Cholesterol-regulated Signaling in Lipid Rafts/Caveolae" (New Orleans, LA)
- 2004 Vascular Targeting Agents Therapeutic and Diagnostic Development Conference, (Keynote Speaker) "Proteomic Mapping and Immunotargeting of Endothelium and its Caveolae for Organ- and Tumor-Specific Imaging and Therapy Tissue " (Cambridge, MA)
- 2004 Cambridge Health Institute Eighth Annual Functional Genomics Meeting, "Rapid Discovery and Validation of Accessible Tissue-Specific Targets" (Boston, MA)
- 2004 Cambridge Health Institute In Vivo Molecular Imaging Meeting, "Tumor Target Discovery and Validation through Integration of Subtractive Proteomics and Molecular Imaging InVivo" (La Jolla, CA)

## Conclusions

This has been a year of very significant progress. The work described above to validate the caveolar- and tumor-localization of TE1-5 has revealed a strong tumor- and caveolae-specificity of TE3 (identified as Annexin A1) in both rat and human normal and neoplastic tissues. We have demonstrated specific tumor accumulation of AnnA1 antibodies in rats shows that proteins expressed in caveolae can indeed be accessible by IV injection for tumor-specific delivery in vivo. These results make TE3/AnnA1 our most promising candidate for targeting breast tumor caveolae to treat human breast cancer. This proteomic analysis is providing promising candidates for breast tumor-induced proteins on endothelial cell surface caveolae that may be useful for specifically targeting drugs or genes to breast tumors while sparing bystander tissues and decreasing side effects. Thus, these studies appear promising and may provide important site-specific targets for the "magic bullets" envisioned many decades ago as a means to provide improved, more efficacious, localized anti-cancer therapy delivered to the tumor cells. These studies have recently been published in the journal *Nature*. The proteomic map of the normal lung endothelial cell surface, which was a critical control for the subtraction analysis to identify tumor-induced candidate targets, has been published recently in the journal *Nature Biotechnology*.

## References

None

## Appendices

Copies of the papers



Personnel paid from Award # DAMD17-02-1-0563:

<u>Name</u>	<u>Role on Project</u>	<u>Start Date</u>	<u>End Date</u>
J Schnitzer	PI	Dec-02	7/31/2004
P. Oh	Res Specialist	Sep-02	7/31/2004
T. Buss	Res Tech IV	Sep-02	7/31/2004
G. Angelborg	Res Tech II	Feb-03	7/31/2004
E. Durr	Postdoctoral Assoc	Oct-02	7/31/2004
Y. Li	Sr Res Sci	Oct-02	7/31/2004
J. Testa	Sr Res Sci	Oct-02	7/31/2004
P. Valadon	Sr Res Sci	Oct-02	7/31/2004
M. Gonzalez	Res Tech I	Mar-04	7/31/2004
M. Yi	Postdoctoral Assoc	Jan-04	7/31/2004



# Direct proteomic mapping of the lung microvascular endothelial cell surface *in vivo* and in cell culture

Eberhard Durr<sup>1</sup>, Jingyi Yu<sup>1</sup>, Karolina M Krasinska<sup>1</sup>, Lucy A Carver<sup>1</sup>, John R Yates III<sup>2</sup>, Jacqueline E Testa<sup>1</sup>, Phil Oh<sup>1</sup> & Jan E Schnitzer<sup>1</sup>

Endothelial cells can function differently *in vitro* and *in vivo*; however, the degree of microenvironmental modulation *in vivo* remains unknown at the molecular level largely because of analytical limitations. We use multidimensional protein identification technology (MudPIT) to identify 450 proteins (with three or more spectra) in luminal endothelial cell plasma membranes isolated from rat lungs and from cultured rat lung microvascular endothelial cells. Forty-one percent of proteins expressed *in vivo* are not detected *in vitro*. Statistical analysis measuring reproducibility reveals that seven to ten MudPIT measurements are necessary to achieve  $\geq 95\%$  confidence of analytical completeness with current ion trap equipment. Large-scale mapping of the proteome of vascular endothelial cell surface *in vivo*, as demonstrated here, is advisable because distinct protein expression is apparently regulated by the tissue microenvironment that cannot yet be duplicated in standard cell culture.

A monolayer of highly attenuated endothelial cells (ECs) lines all blood vessels to form a physiologically vital interface between the circulating blood and the underlying cells inside the tissue. This blood-tissue interface plays an important role in controlling the passage of blood molecules and cells into the tissue and in many physiological functions, including vasoregulation, coagulation and inflammation, as well as tissue nutrition, growth, survival, repair and overall organ homeostasis and function<sup>1</sup>. Disruption of the vascular endothelium and its normal barrier function can lead rapidly to tissue edema, hypoxia, pathology and even organ death<sup>2</sup>.

Although the microenvironment of the tissue surrounding the blood vessels clearly influences EC phenotype<sup>3–8</sup>, little molecular information is available regarding vascular endothelium as it exists in native tissue. This is in large part because of technical limitations in molecular profiling of a cell type that represents such a small percentage of the cells in the tissue. Past approaches have analyzed endothelial cells isolated from tissue by enzymatic digestion and sorting of the released single cells using EC markers<sup>9–12</sup>. Although the study of isolated and even cultured ECs *in vitro* has yielded much functional and molecular information, both enzymatic and mechanical tissue disassembly and growth in culture contribute to phenotypic changes that result in morphological alterations as well as loss of native function and protein expression<sup>3</sup>. Although expected to be substantial, the molecular differences between ECs *in vivo* and *in vitro* are unknown. The reported ability of cells and phage-displayed peptides to home to specific tissues of the body after intravenous injection also provides indirect evidence supporting the molecular heterogeneity of the endothelial cell surface among organs<sup>13,14</sup> but has not yet facilitated global mapping of EC surface proteins *in vivo*.

Here, we report our initial efforts to provide a large-scale mapping of the cell-surface proteome of microvascular endothelium as it exists in rat lung tissue *in vivo* and in cultured rat lung ECs.

## RESULTS

### Sample preparation and quality control

The silica-coating methodology<sup>15–19</sup> was used to isolate luminal EC plasma membranes from rat lungs and from cultured rat lung microvascular ECs (RLMVEC; isolated and grown in culture as in our past work<sup>20</sup>) for comparative proteomic analysis by two-dimensional liquid chromatography tandem mass spectrometry (2D LC-MS/MS). Rigorous quality control testing established  $\geq 95\%$  purity for silica-coated luminal EC plasma membranes (P) in EC plasma membranes based on a  $>20$ -fold enrichment relative to total homogenate/lysate (H) in more than two EC surface marker proteins and  $>20$ -fold depletion in well-established markers of subcellular organelles (Fig. 1a and Methods). For rat lung P, we also required  $>20$ -fold depletion in membrane protein markers from other cell types present in lung or blood (Fig. 1b and Methods).

### Analytical completeness of large scale MS/MS analysis

To analyze rat lung EC surface proteins comprehensively, we did  $>30$  measurements using MudPIT<sup>21</sup> on P isolated from rat lungs and RLMVEC. These data were entered into a relational database that allowed us to combine results of individual measurements for analysis separately or in totality.

To estimate the number of MudPIT measurements required for completing as comprehensive an analysis as possible with our instrumentation and protein database, we statistically analyzed repeated MudPIT

<sup>1</sup>Sidney Kimmel Cancer Center, 10835 Altman Row, San Diego, California 92121, USA. <sup>2</sup>The Scripps Research Institute, La Jolla, California 92037, USA. Correspondence should be addressed to J.E.S. (jschnitzer@skcc.org).

Published online 18 July 2004; doi:10.1038/nbt993



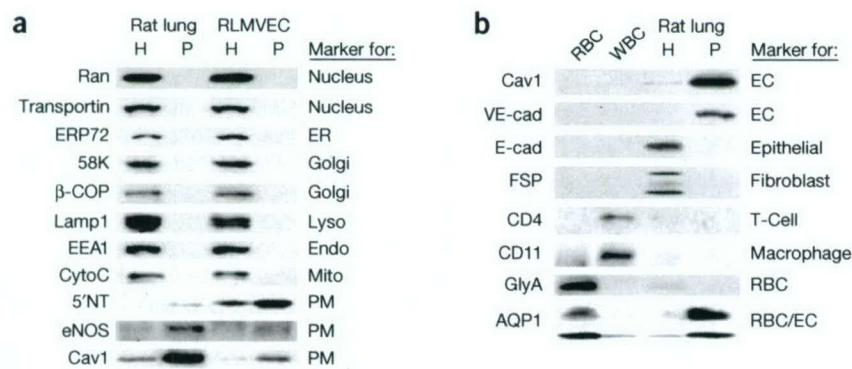


**Figure 1** Quality analysis of rat lung P and RLMVEC P by western blot analysis. Proteins (5  $\mu$ g) were resolved by SDS-PAGE, transferred to nitrocellulose and immunoblotted with antibodies to the indicated proteins. **(a)** Western blot analysis of proteins from rat lung P versus RLMVEC P using antibodies to the indicated organellar membrane proteins. **(b)** Western blot analysis of proteins isolated from rat lung P using antibodies for the indicated cell types. Note that AQP1 has been found at the surfaces of both ECs and erythrocytes<sup>19</sup>. H, total homogenate/lysate; P, silica-coated endothelial cell plasma membranes; VE-cad, vascular endothelial cadherin; E-cad, epithelial cadherin; FSP, fibroblast surface protein; GlyA, glycophorin A; AQP1, aquaporin 1; ERP72, protein disulfide isomerase A4; 58K, Golgi marker p58;  $\beta$ -COP, coatamer beta subunit; EEA1, early endosomal antigen 1; CytoC, cytochrome c; 5'NT, 5' nucleotidase; eNOS, endothelial nitric oxide synthase; Cav1, caveolin 1; WBC, leukocyte; RBC, erythrocyte; EC, endothelial cell; ER, endoplasmic reticulum; lyso, lysosome; endo, endosome; mito, mitochondria; PM, plasma membrane.

measurements to determine at which point additional experiments produce few newly identified proteins. Using an identification criterion of two or more MS/MS spectra of true tryptic peptides, we found that ~66% of the identified proteins in any measurement of rat lung P were confirmed by any second measurement and 34% of the proteins remained unconfirmed (Fig. 2). Adding a third measurement decreased newly identified proteins to 20%. After ten measurements, this number leveled off at 4.2% (that is, proteins not found in the other nine measurements). We use the term "confidence of analytical completeness" to describe this definition for reproducibility. There were no differences in this statistical curve when the comparatively analyzed measurements were from the same rat lung P sample or from P samples produced independently. An average 260 ( $\pm$ 47) unique proteins were identified in each MudPIT experiment with two or more MS/MS spectra. The same 95%

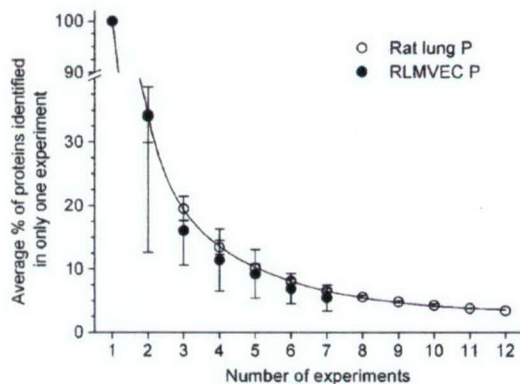


**Figure 2** Reproducibility of protein identification in rat lung P. The confidence of analytical completeness is calculated as a function of the number of analytical runs. Each point represents the percentage of proteins identified only in an individual run compared to all preceding experiments.  $\circ$ , rat lung P;  $\bullet$ , RLMVEC P.

confidence of analytical completeness was achieved for the RLMVEC P analysis after seven measurements (Fig. 2).

### Endothelial cell surface proteome in lung

In rat lung P, we identified 450 nonredundant proteins with three or more distinguishable MS/MS spectra of true tryptic peptides (see Supplementary Table 1 online). Although proteins covered by three MS/MS spectra accounted for the largest subpopulation, 70% of all proteins listed in Supplementary Table 1 were covered by more than three MS/MS spectra (Fig. 3a). The distribution of MS/MS spectrum coverage followed roughly a single exponential decay in the range of 3 to 12 MS/MS spectra. Exceptions included highly abundant, highly covered proteins, such as fodrin, spectrin or plectin.

To assess possible analytical bias in the protein identification, we calculated the molecular weights and isoelectric points (pIs) of each protein based on its primary amino acid sequence. All 450 proteins identified in rat lung P showed a typical molecular weight distribution (15–600 kDa) with a maximum of 29% between 25 and 50 kDa and >80% below

200 kDa (Fig. 3b). Their pIs ranged from 4.0 to 12.0 with bimodal distribution maxima at 5.75 and 9.0 (Fig. 3c). About 25% of these proteins fall outside the typical limits of protein resolution by 2D-gel electrophoresis ( $\leq$ 100 kDa; pI 4.5–8.5) (Fig. 3d).

We classified the proteins identified in rat lung P according to currently available data. All proteins fit in two broad categories within the current rat protein database (Fig. 4a): characterized proteins (74%) and proteins yet-to-be-characterized (26%), which includes entries described as genes of unknown function and hypothetical proteins. Of the characterized proteins (Fig. 4b), 81% can be associated with the plasma membrane. The remainder are reported to localize primarily to ribosomes (3.6%), endoplasmic reticulum (ER) (4.5%), mitochondria (5.1%) and/or the nucleus (6.3%) and may include proteins that may exist at more than one site in the cell.

We also classified the identified proteins according to their interaction with the plasma membrane as well as their orientation and structure in the membrane. Of the proteins residing at the plasma membrane, 31% were integral or lipid-anchored membrane proteins, 25% were cytoskeletal and/or junctional proteins, 35% were inner peripheral membrane proteins and 8.6% were externally bound (Fig. 4c).

Cytoskeletal proteins had the best MS/MS spectrum coverage in our sample (23.6 spectra/protein) followed by inner peripheral membrane-associated proteins (8.9 spectra/protein). Transmembrane spanning and lipid-anchored proteins had less coverage (both with 6.9 spectra/protein) (Fig. 5a). The majority of the transmembrane spanning proteins identified in rat lung P contained a single transmembrane domain (Fig. 5b). Integral membrane proteins that are more hydrophobic, especially those with multiple transmembrane domains, have fewer tryptic cleavage sites (hydrophilic residues R and K) and are frequently glycosylated, which may prevent access of the protease and reduce the number of possible identifiable tryptic peptides. For example, based on a calculation of theoretical tryptic digests, G-protein-coupled receptors have only 1.25 tryptic peptides/10 kDa with properties likely to produce good MS/MS spectra (based on an evaluation of  $\alpha$ 2-adrenergic receptor,



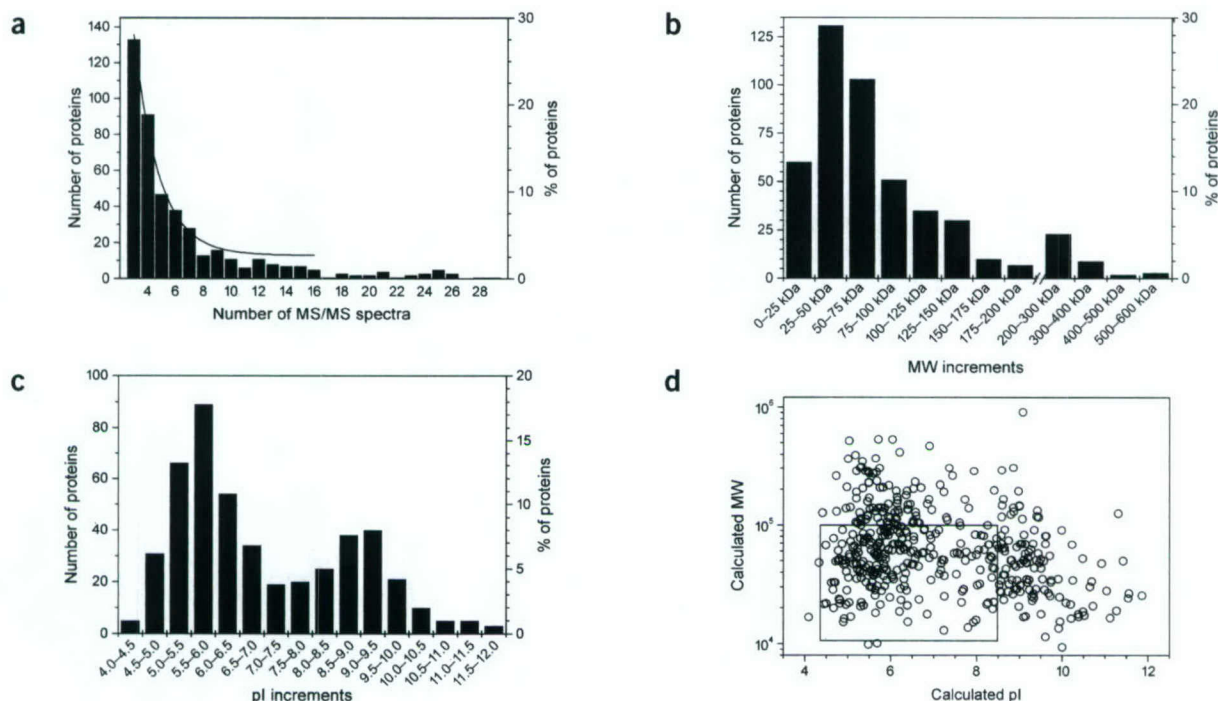


**Figure 3** Spectrum coverage per protein and physicochemical properties. **(a)** Distribution of MS/MS spectrum coverage of proteins identified in rat lung P. The fitting parameters of this curve have no physical meaning. **(b)** Molecular weight distribution of identified proteins. **(c)** pI distribution of identified proteins. **(d)** The calculated pI of identified proteins were plotted against their calculated molecular weight on a logarithmic scale. Box indicates typical limitations for resolving proteins within 2D gels. In **a–c**, the number of proteins falling into each classification is plotted (left y-axis) as well as the percentage of the total number proteins identified falling into each classification (right y-axis).

$\beta$ 1B adrenergic receptor, muscarinic receptor M1, B1 bradykinin receptor and angiotensin II receptor 1A). Soluble proteins such as bovine serum albumin average about six tryptic peptides/10 kDa of protein mass. We identified 19 G-protein-coupled receptors in lung P, but only with one or two spectra. Therefore, the relative abundance of membrane proteins in the sample may be higher than indicated by our data.

Lastly, we categorized the identified proteins according to their reported function (Fig. 4d): 29% and 25% of the identified proteins were signaling and structural proteins, respectively; 7.8% were involved in caveolae- or clathrin-mediated cell surface membrane trafficking; 5.2% were involved in cell-cell adhesion, including junctional proteins;

4.5% were exterior enzymes, an important group known to be especially enriched on the lung endothelium, and which metabolize blood-borne hormones and vasoactive compounds; 4.1% were transporter molecules mediating the movement of small molecules (ions and water) across the membrane bilayer; and 25% of the proteins were not easily categorized and labeled 'other.'

#### Comparison of EC surface proteins *in vivo* and *in vitro*

To assess protein expression of ECs growing in native conditions *in vivo* versus in cell culture *in vitro*, we compared proteins in RLMVEC P versus rat lung P (Fig. 5c and Supplementary Table 1 online). We allowed a

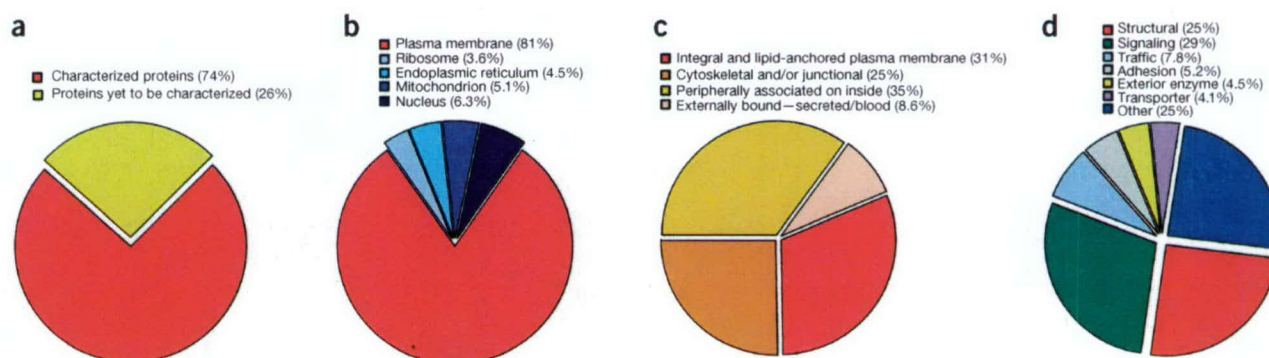


**Figure 4** Classification of proteins identified in rat lung P. **(a–d)** Pie charts of the identified proteins classified according to their degree of characterization in the rat database **(a)**; the expected primary subcellular localization of the characterized proteins **(b)**; subclasses of plasma membrane proteins **(c)**; and functional characterization of the plasma membrane proteins **(d)**.



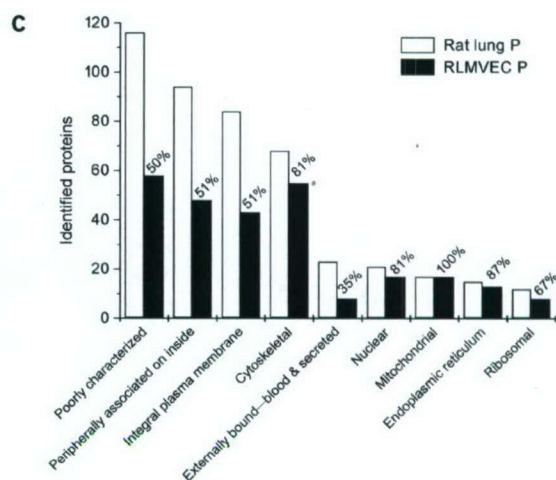
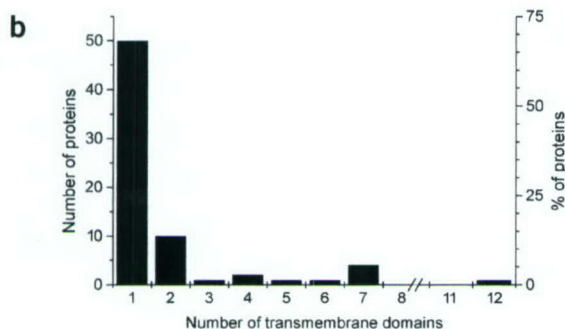
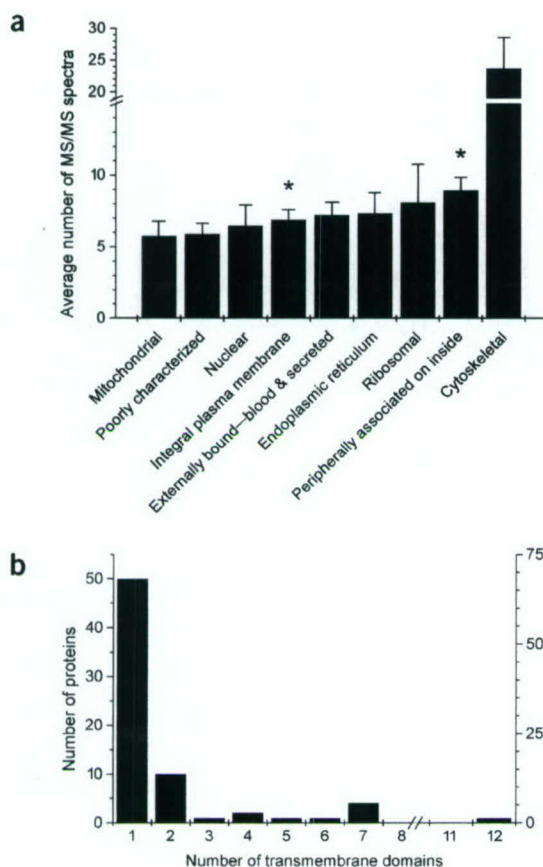


**Figure 5** Analysis of identified proteins. (a) Spectrum coverage per subcellular location. The average MS/MS spectrum coverage per protein is shown for each subcellular location. Error bars indicate standard deviation; \* denotes proteins that are frequently underrepresented in proteomics analysis usually showing lower spectrum coverage because of low accessibility and biophysical properties. (b) Distribution of the number of known or predicted transmembrane-spanning alpha helices in all integral membrane proteins identified in rat lung P. The number of predicted transmembrane domains per protein is plotted against the number of proteins falling into each classification (left y-axis) and as a percentage of the total number of integral membrane proteins identified (right y-axis). (c) Localization of proteins identified in rat lung P and RLMVEC P. Histogram of the number of proteins identified in RLMVEC P and rat lung P plotted according to their subcellular location. Percentage indicates proportion of proteins identified in RLMVEC P versus lung P in each category.

minimum coverage of one high-quality MS/MS spectrum to identify a protein in RLMVEC P as long as the protein had been identified previously with higher stringency (three or more spectra) in rat lung P. We found 263 out of the 450 proteins identified in rat lung P also in RLMVEC P with the remaining 187 proteins (42%) detected only in rat lung P, suggesting possible modulation by the *in vivo* tissue microenvironment not reproduced in cell culture. If we used the same three peptide criteria as for rat lung P, only 32% (145 of 450 proteins) overlapped with RLMVEC P. Even greater differences were apparent in select categories of proteins. Approximately 50% of the integral and peripheral membrane proteins as well as yet-to-be-characterized proteins were solely identified in rat lung P. Only 35% of blood and secreted proteins from rat lung P were detected in RLMVEC P. We identified in RLMVEC P only ~30% of the trafficking proteins detected in rat lung P, consistent with cultured ECs expressing greater than tenfold less caveolae relative to native ECs *in vivo*. Proteins primarily localized to the cytoskeleton, mitochondria, ER and nucleus were identified in similar proportions in RLMVEC P and rat lung P.

#### High prevalence of known EC surface proteins

We identified 73 known vascular EC surface proteins in rat lung P and RLMVEC P (see Supplementary Table 2 online). Because these proteins are known markers of the EC surface, we lowered the stringency for identification to one or more true tryptic peptide MS/MS spectra of high quality as determined by manual inspection. Of the 65 EC marker proteins identified in rat lung P, 22 (34%) were identified with one spectrum, 12 (18%) with two spectra and 31 (48%) with three or more spectra. Moreover, 41 of the 65 proteins (63%) were identified solely in rat

lung P. In RLMVEC P, we found 32 EC marker proteins (12 (38%) with one spectrum, 3 (9%) with two spectra and 17 (53%) with three or more spectra), of which 8 were not identified in lung P. This list could be increased greatly by adding cytoskeletal proteins shown to exist in ECs.

#### Validation of protein expression

To validate proteins identified by MS/MS, we performed western blot analysis for a subset of 22 proteins (chosen relatively randomly based on antibody availability; Fig. 6a). We identified 16 of these proteins by MS/MS in rat lung P but not in RLMVEC P. This finding was confirmed by western blot analysis in 14 out of the 16 cases (87.5%) with only Trk-A and Lyn B also detected in RLMVEC P. Nine proteins not detected in RLMVEC P were known EC markers (aquaporin, angiotensin converting enzyme (ACE), carbonic anhydrase (CA), endothelin-converting enzyme (ECE), podocalyxin, receptor for advanced glycation end product (RAGE), zona occludens (ZO)-2, TIE-2, VE-cadherin) and four of the remaining seven proteins had either a predicted transmembrane domain (Trk-A, P2Z receptor, seven transmembrane receptor) or a lipid anchor (LynB), suggesting plasma membrane localization. Western blot analysis confirmed all five proteins (aminopeptidase N (APN), caveolin-1, HSP47, FLJ10849 and ICAM-1) identified by MS in both rat lung P and in RLMVEC P. We detected 5'NT by MS analysis solely in RLMVEC P with ten MS/MS spectra, but we detected it enriched in P over H in both lung P and RLMVEC P by western blot analysis, albeit with far more expression in RLMVEC P. The amount of 5'NT in rat lung P may have been below the detection sensitivity of the MS analysis.

This western blot analysis confirmed the expression of several proteins that apparently have not been identified before. Monospecific,



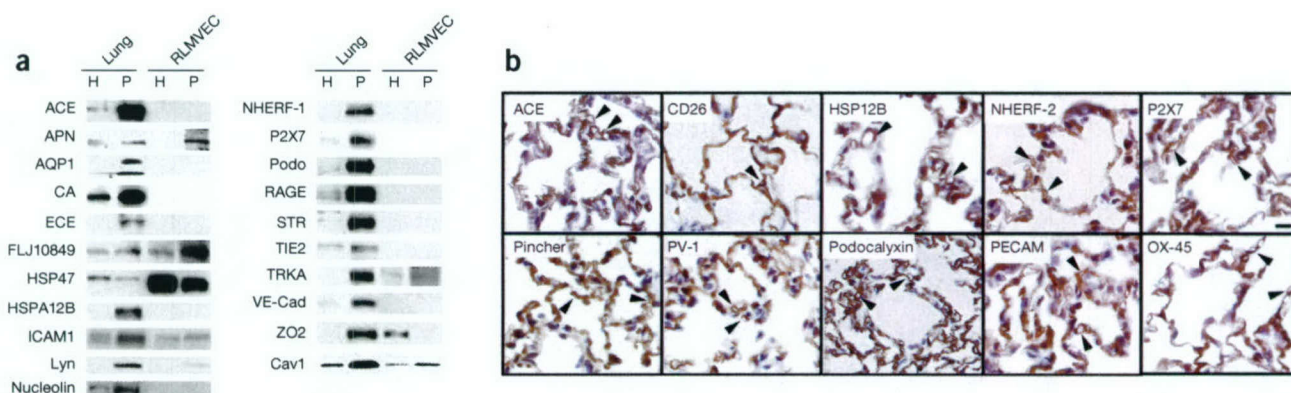


**Figure 6** Protein validation. (a) Western blot analysis was performed on 5 μg of total tissue or cell homogenates (H) and EC plasma membranes (P) of rat lung endothelium and RLMVEC using the indicated antibodies. (b) Tissue immunostaining of select proteins identified in endothelial membranes. Cryosections of rat lung tissue stained with antibodies recognizing the indicated proteins. Arrowheads denote typical examples of open blood microvessels. Bar, 10 μm. ACE, angiotensin converting enzyme; APN, aminopeptidase N; AQP1, aquaporin 1; CA, carbonic anhydrase; ECE, endothelin-converting enzyme; HSP47, 47-kDa heat shock protein; ICAM-1, intercellular adhesion molecule 1; NHERF-2, Na<sup>+</sup>/H<sup>+</sup> exchange regulatory cofactor NHE-RF2; P2X7, P2X purinergic receptor 7; Podo, podocalyxin; RAGE, receptor for advanced glycation end products; STR, seven transmembrane receptor; VE-cad, vascular endothelial-cadherin; ZO-2, zona occludens 2; cav1, caveolin-1.

affinity-purified polyclonal antibodies that we generated to synthetic peptides confirmed not only our MS findings but also the existence of two proteins listed as hypothetical in the database. The antibodies detected a 59-kDa protein (FLJ10849) in both rat lung P and RLMVEC P and an 82-kDa protein (HSPA12B) only in rat lung P, consistent with the predicted molecular weight of these proteins. Other verified new findings included the enrichment in P of TIE-2, APN, ICAM-1 and nucleolin, whose expression at the EC surface was reported to be induced during angiogenesis and/or inflammation (TEM4 and TEM6<sup>10</sup> were also identified but no antibodies are available for validation). Two proteins, P2Z7 and Trk-A, have not previously been localized to ECs but rather to neuronal cells and tissues.

We also used immunohistochemical staining of rat lung tissue sections to validate EC expression of 23 proteins (chosen randomly by availability of antibodies suitable for immunohistochemistry). ACE, CD26, HSPA12B, NHERF-2, P2X7, Pincher, PV-1, podocalyxin, PECAM (CD31) and OX-45 were expressed on lung blood vessels (Fig. 6b). Caveolin-1, ECE, aquaporin 1, Nedd5, CA, TIE2, RAGE, Glut4, ZO-1, ICAM-1, thrombomodulin, CD39 and aminopeptidase P were similarly detected on lung endothelium (data not shown). Tissues stained with secondary antibody alone were negative. Thus, these analyses together validated 27 proteins newly identified on the lung endothelial cell surface through our MS analysis of rat lung P (e.g., Trk-A, P2X7, seven transmembrane receptor, NHERF-2, HSPA12B, pincher, Nedd 5, Glut4). See Supplementary Notes online for an expanded description of findings and validation.

## DISCUSSION

Our estimation of the confidence of completeness provides a useful gauge of the reproducibility and relative comprehensiveness of individual MudPIT measurements as well as the number of measurements required to achieve a statistically defined level of completeness. The probability that the acquisition of tandem mass spectra will be exactly reproduced is inversely proportional to the complexity and dynamic range of the peptide mixture. Likewise, reproducibility of the data depends on the complexity of the sample as well as the quality and composition of peptides from independent sample preparations originating from different animals. Thus, it seems prudent to do a statistical analysis

from several measurements to assess this variation and to estimate the degree to which the sample can be comprehensively described with a given amount of independent measurements. Our analysis here required 7–10 MudPit measurements to achieve >95% confidence of analytical completeness possible with the current equipment, database and analytical approach. Note that the confidence of analytical completeness may depend on many factors—including the complexity of the individual sample being analyzed, sample preparation, the quality of the chromatography, the sensitivity of the instrument and the completion of the rat protein database—and must be reevaluated for each project.

Based on the current rat database, 74% of the proteins identified in the isolated EC surface have been characterized to some extent, including functionally, structurally and/or with localization data. But 26% are new and not yet characterized in the rat database. Based on the current literature, >80% of the characterized proteins have a solid reason or experimental evidence supporting their association with the plasma membrane. Yet, despite rigorous quality testing of each membrane preparation by western blot analysis, we have identified some proteins that at first glance may not appear to belong at the plasma membrane, including blood proteins and proteins of intracellular organelles.

Consistent with flushing the vasculature free of blood, our quality testing detects little to no presence of well-known marker proteins for erythrocytes and leukocytes in P. Nevertheless, we identified 21 known blood proteins. Given that there are >500 blood plasma proteins and even more blood cell proteins, this number appears too low to be explained by general contamination. In fact, the presence of a small subset of blood proteins may be expected in rat lung P and RLMVEC (grown in serum). For example, albumin and transferrin can interact specifically with the EC surface via specific binding proteins<sup>22–24</sup>. Hemoglobin alpha and beta chains may come from small amounts of cell-free hemoglobin in the blood rather than simply erythrocyte contamination, especially in light of the lack of erythrocyte markers in P (Fig. 1).

Likewise, we detected proteins currently considered to be located primarily in ER, mitochondria, Golgi, ribosomes or nuclei, which cumulatively were ~15% of the total proteins identified (20% of the characterized proteins). But, given our stringent quality criteria of



≥20-fold enrichment of EC markers and ≥20-fold depletion of specific markers of these subcellular organelles, we may expect ≤5% contaminants. Thus, general contamination of membranes from these organelles seems remote, even more so if one considers the few sometimes low-abundance proteins identified (~15 average per organelle) relative to the many hundreds of proteins in each organelle. Of course, it is possible that polycationic proteins, such as histones and ribosomal subunit proteins, released by tissue homogenization can adsorb electrostatically to the polyanionic polyacrylic acid crosslinker of the silica-coated membranes. But it seems more likely that most of these proteins simply reside in more than one subcellular location. It is not unusual for proteins initially categorized as organelle-specific to later be discovered elsewhere in the cell. So far, four proteins identified here are examples of this. Nucleolin is a well-characterized nuclear protein but is expressed also at the cell surface<sup>25</sup>. Elongation factor-1 alpha is known primarily as a component of the protein synthesis machinery but has a less well-known function in cytoskeletal reorganization<sup>26</sup>. Protein disulfide isomerase, commonly classified as an ER protein, has recently been detected at the plasma membrane of platelets and liver<sup>27</sup>. Hsp47 was initially assigned to the ER, but later discovered to be transported to the plasma membrane<sup>28</sup>. Thus, this analysis may provide, for some proteins, the first evidence of a secondary localization at the plasma membrane. Protein-protein interactions may further explain the presence of select proteins (see Supplementary Note online). Considering all of these issues, our list of identified proteins seems rather consistent with our quality control data showing ≥95% purity of the isolated membranes.

Comparative proteomic analysis of EC surface membranes isolated from rat lung versus cultured RLMVEC revealed striking differences. Only ~51% of the integral membrane proteins and plasma membrane-associated proteins identified were expressed in common between rat lung P and RLMVEC P. Interestingly, 65 of 73 (89%) total known EC marker proteins detected in this study were found in rat lung P versus only 32 (43.8%) in RLMVEC P (see Supplementary Table 2 online). We detected 41 known markers, such as ACE and ECE, in rat lung P but not in RLMVEC P. Overall, more than 180 (41%) proteins were detected in rat lung P *in vivo* but not at all in RLMVEC P *in vitro* (see Supplementary Note online for additional discussion).

It is quite apparent through studying vasculogenesis, angiogenesis and the modulation of EC phenotype in culture and *in vivo* that EC morphology, protein expression and function are affected greatly by physical and molecular cues from the basement membrane, perivascular cells, circulating blood and even other cells deeper within the tissue<sup>3,10,17,29</sup>. EC isolation as well as standard, albeit limited, cell culture conditions seem not to maintain the expression of proteins found *in vivo*, which may have functional consequences. Here, we provide a glimpse of how wide the microenvironment-induced molecular differences between ECs *in vivo* and *in vitro* can be. Of course, some of these differences may relate to the derivation of the RLMVEC from one segment of the pulmonary microvasculature (arterioles, capillaries and venules) whereas rat lung P is primarily EC plasma membranes from all microvessel segments, which constitute >90% of the total vascular surface area. Obviously, more sophisticated culturing conditions are needed to maintain proteins expressed in native tissue. Towards this end, our results begin to identify a set of promising tissue-modulated EC markers that can now be used to monitor future attempts to reproduce native EC phenotype *in vitro* and may contribute to a deeper understanding of how the tissue environment controls EC phenotype.

We have described a large-scale proteomic analysis of *in vivo* vascular endothelium—more specifically, the luminal EC surface in lung tissue. Our identification of 450 proteins using rigorous criteria (more than three peptides) is an improvement over many proteomic analyses that

found similar numbers of proteins in whole cells, bacteria, yeast and tissue preparations but usually with less demanding selection criteria (one to two peptides)<sup>30</sup>. Moreover, two MS analyses of whole cultured ECs recently identified less than 60 proteins, including only a few proteins found here: hemoglobin, albumin, heat shock proteins, actin, nucleophosmin, vimentin and tubulins<sup>11,12</sup>. These studies did not identify any cell surface enzymes or transmembrane proteins.

A more detailed understanding of the proteome of specialized cell types may help elucidate how cells fulfill their biological function in a systems biological context. Differences in protein expression patterns between differentiated cells as well as changes occurring during disease are of great interest in experimental medicine for diagnosis and treatment. Cell surface mapping of normal lung endothelium *in vivo* and *in vitro* is a necessary prelude to understanding the extent to which the tissue microenvironment can modulate EC function and protein expression not only in normal tissues but also perhaps in diseases. This specialized proteome may have value clinically because proteins expressed at this blood-tissue interface are accessible to the circulating blood and may serve as targets for tissue-specific drug and gene delivery *in vivo*<sup>29,31,32</sup>. The technology described here may help exploit such possibilities in the future.

## METHODS

**Materials.** Standard laboratory chemicals were high-performance liquid chromatography (HPLC) grade or higher if available and purchased from VWR unless otherwise noted. Tris (2-carboxyethyl)-phosphine hydrochloride (TCEP) was obtained from Pierce. Iodoacetamide was obtained from Aldrich. Porozyme bulk-immobilized trypsin was purchased from Applied Biosystems. Endoproteinase Lys-C was purchased from Roche Diagnostics. 3× cell lysis buffer (CLB) contains 6 M Urea, 0.5 M Trisbase, 9 mM EDTA, 3.6% β-mercaptoethanol and 9% SDS.

We obtained antibodies against the following: ACE, APN, caveolin-1, E-cadherin, Tie 2, PECAM and VE-cadherin from Santa Cruz Biotechnology; aquaporin-1, cytochrome C, ERp72, EEA1, eNOS, Lamp1, Lyn, P2X7, Ran, Transportin, CD26 and ZO-2 from BD Biosciences/Pharmingen; β-COP, fibroblast surface protein, glycophorin A and p58K from Sigma; CD4 and CD11 from Serotech; HSP47 from Stressgen Biotechnologies; RAGE from Affinity Bioreagents; ECE from Zymed Lab; Trk-A from ABCam nucleolin from Leinco Technologies. Antibodies against the following were kind gifts: carbonic anhydrase IV from W.S. Sly, St. Louis University; NHERF-2 from E.J. Weinman, University of Maryland Hospital<sup>33</sup>; 5' nucleotidase from Paul Luzzio (Cambridge, England); seven transmembrane protein (Ig-hepta) from Shigehisa Hirose, Tokyo Institute of Technology (Yokohama, Japan)<sup>34</sup>; OX-45 from Neil Barclay, University of Oxford (Oxford, UK)<sup>35</sup>; Pincher from Simon Haleguola, State University of New York (Stony Brook, NY); podocalyxin, PV-1 and ICAM-1 were produced in house.

**Animals.** Sprague-Dawley male rats (150–250 g; Charles River Laboratories) were used unless otherwise indicated. Animal experiments were done in accordance with federal guidelines following review and approval by the Institutional Animal Care and Use Committee.

**Cell culture.** Rat lung microvascular ECs (RLMVEC) were isolated and grown as described originally<sup>36</sup>.

**SDS page and western blot analysis.** SDS PAGE and western blot analysis were done as described previously<sup>18</sup>.

**Tissue immunostaining.** Frozen rat lung tissue was cut (5 μm) on a Microm HM505E cryomicrotome. Sections were fixed with neutral buffered formalin for 5 min at 25 °C then incubated for 1 h at 25 °C in blocking solution (5% FBS, 0.1% Tween 20 in PBS). After a 2-h incubation at room temperature in primary antibodies (diluted in blocking solution), the sections were washed, treated with the biotin-conjugated secondary antibody (KPL Laboratories) for 1 h at 25 °C, washed again and treated with a streptavidin-conjugated horseradish peroxidase



(KPL Laboratories) for 1 h at 25 °C. Immune complexes were detected using a Liquid DAB staining kit from BioGenex. Sections were counterstained with hematoxylin, dehydrated, mounted in Permount (Fisher Scientific) and imaged digitally by light microscopy using a Nikon Eclipse E800 equipped with a Nikon digital camera DXM1200.

**Production of polyclonal antibodies.** Antigenicity predictions for HSPA12B and septin homolog FLJ10849 were done with Lasergene (DNASTar) using the prediction methods of Margalit and Berzofsky, Rothbard and Taylor and Jameson Wolf. Polyclonal antibodies in rabbit were produced for HSPA12B against the peptide Ac-CGYTARDYYHDLPEEAR-CONH<sub>2</sub> and for FLJ10849 against the peptide Ac-CQLLQSAQQAQQAQTKK-CONH<sub>2</sub> by Biosource.

**Isolation of luminal EC plasma membranes from rat lungs and RLMVEC.** The luminal EC plasma membranes were isolated directly from rat lung tissue or cell culture using a silica-coating procedure as described<sup>15,16</sup>. Briefly, a solution of cationic colloidal silica particles was used to selectively coat the EC surface either by perfusing the lung vasculature via the pulmonary artery *in situ* or by overlaying RLMVEC confluent monolayers. After electrostatic cross-linking and quenching with polyacrylic acid to form a stable membrane pellicle, the tissue or cells were homogenized and the sheets of P are sedimented by two rounds of ultracentrifugation through high-density media away from all the other much less dense tissue component in the lung homogenate or the total RLMVEC lysate (H). This subfractionation yielded a membrane pellet highly enriched in EC surface markers and markedly depleted of markers of other cell types and subcellular organelles<sup>15-19</sup>.

To ensure that we use consistently high-quality material, each lot of H and isolated P was subjected to rigorous quality control testing before analysis. Using standard immunoblotting, we required the purity level of plasma membranes in P relative to H to be at least 20-fold enriched in at least two EC surface marker proteins, such as caveolin, 5'-nucleotidase (5'NT), VE-cadherin-1, angiotensin converting enzyme (ACE) or endothelial nitric oxide synthase (eNOS). In addition, P had to be depleted by >20-fold relative to H in well-established organellar membrane markers, including nuclear (ran, transportin), endosomal (early endosome antigen 1 (EEA1)), Golgi (p58,  $\beta$ -COP), lysosomal (lamp1), mitochondrial (cytochrome c) and endoplasmic reticulum (ERp72). For rat lung P, we also required a >20-fold depletion in protein markers of membranes from other cell types present in lung or blood, including epithelial cells (E-cadherin), fibroblasts (FSP), white blood cells (CD11, CD4) and red blood cells (glycophorin A).

**Preparation of enzymatic digest of protein mixtures for mass spectrometric analysis.** The proteins in P were solubilized using CLB before vortexing and boiling for 5 min. The protein concentration was determined by the micro BCA assay from Pierce. Silica particles were sedimented by centrifugation to collect the solubilized proteins in the supernatant, which was then precipitated with chloroform/methanol and resolubilized in 8 M urea adjusted to pH 8.5 with 100 mM ammonium bicarbonate. Protein disulfide bonds were reduced with 2.5 mM Tris (2-carboxyethyl)-phosphine hydrochloride (TCEP) for 15 min at 60 °C; carboxyamidomethylated with 3.75 mM iodoacetamide for 15 min at 25 °C in the dark; digested by a first-site-specific enzymatic digestion with endoproteinase lys-C for 4 h at 37 °C, 1:100 (wt/wt); digested for a second time. After the protein mixture was diluted to 1.6 M urea with 100 mM ammonium bicarbonate, pH 8.5, it was digested a second time with porozyme-immobilized trypsin (10  $\mu$ l/100  $\mu$ g protein) overnight at 37 °C (with agitation). The immobilized trypsin was then removed by centrifugation and the peptides in the supernatant concentrated by solid phase extraction with SPEC-PLUS PTC18 cartridges (Anslys Diagnostics) following the manufacturer's instructions. After lyophilizing the peptide mixture to near dryness the samples were stored in sample buffer (5% acetonitrile, 0.3% formic acid) at a concentration of 5  $\mu$ g/ $\mu$ l (calculated from the initial amount of protein) at -20 °C before mass spectrometric analysis.

**MudPIT.** In each experiment approximately 150  $\mu$ g of complex peptide mixture was separated by 2D LC. The first dimension was based on strong cation exchange and the second dimension on C<sub>18</sub> reversed-phase hydrophobic interaction chromatography. Both chromatographic materials were packed seamlessly into a fritless microcolumn. A 5- $\mu$ m tip was pulled on a fused-silica microcapil-

lary (100  $\mu$ m inner dimension (i.d.)  $\times$  365  $\mu$ m outer dimension (o.d.)) using a Model P-2000 laser puller (Sutter Instrument). The microcolumn was then packed with three phases of chromatographic material as follows: 8.5 cm of 5  $\mu$ m C<sub>18</sub> reversed-phase material (Polaris C18-A, Metachem), then 4 cm of 5  $\mu$ m, 300-Å strong cation exchanger (PolyLC) and lastly 3.5 cm of C<sub>18</sub> material using a helium pressure cell operated at 600–900 p.s.i. (Mass Evolution). After equilibrating the microcapillary column with sample buffer, 30  $\mu$ l of the complex peptide mixture (150  $\mu$ g) was loaded off-line onto the microcapillary column which was then mounted onto a microcross (Upchurch Scientific) and placed in-line with an Agilent 1100 quaternary HPLC. Peptides were directly eluted into the mass spectrometer using 2D LC with 18 step-elutions from the strong cation exchanger followed by a gradient elution of the reversed-phase material<sup>30</sup>. The buffer solutions used were: buffer A, 5% (vol/vol) acetonitrile and 0.1% (vol/vol) formic acid; buffer B, 80% (vol/vol) acetonitrile and 0.1% (vol/vol) formic acid; buffer C, 500 mM ammonium acetate, 5% (vol/vol) acetonitrile and 0.1% (vol/vol) formic acid. Step 1 consisted of a 110-min gradient from 0 to 100% buffer B and was followed by steps 2–18. Each step consisted of a 135-min gradient including pregradient salt steps with increasing concentrations of ammonium acetate. The profile of steps 2–18 was: 5 min 100% buffer A; 3 min x% buffer C (x% corresponding to: 25, 37.5, 50, 58.5, 67, 75, 83.5, 91.5, 100, 125, 150, 175, 200, 225, 250 and 500 mM ammonium acetate); 5 min 100% buffer A; a 5-min gradient to 15% buffer B; a 60-min gradient to 45% buffer B; a 32-min gradient to 100% buffer B; 5 min 100% buffer B; a 10-min gradient to 100% buffer A; and 10 min isocratic re-equilibration at 100% buffer A. The 100  $\mu$ l/min flow rate at the HPLC was reduced 400-fold by a fused silica capillary (50  $\mu$ m i.d., 365  $\mu$ m o.d.) splitter placed on the microcross.

Mass spectrometric measurements were done on a LCQ Deca XP ion trap mass spectrometer (ThermoFinnigan) equipped with a modified microelectrospray ionization source from Mass Evolution. A spray voltage of 2.0 kV was applied precolumn at the liquid junction of the microcross as described<sup>37</sup>. Operation of the quaternary Agilent 1100 HPLC pump and the mass spectrometer was fully automated during the entire procedure using the Excalibur 1.2 data system (ThermoFinnigan). Continuous cycles of one full scan ( $m/z$  400 to 1400) followed by three data-dependent MS/MS measurements at 35% normalized collision energy were done. MS/MS measurements were allowed for the three most intense precursor ions with an enabled exclusion list of 25  $m/z$  values ( $\pm 1.5$  Da) or a maximum time limit of 5 min. The zoom scan function to determine the charge state was disabled to increase the duty cycle of the instrument.

**Database search and analysis of tandem mass spectra.** MS/MS spectra were extracted from raw files requiring a minimum of 21 signals with an intensity of at least  $7.5 \times 10^4$  arbitrary units. Extracted MS/MS spectra were automatically assigned to the best matching peptide sequence using the SEQUEST algorithm<sup>38</sup> and the Sequest Browser software package (ThermoFinnigan). SEQUEST searches were done on independent dual processor (2.0–2.6 GHz) personal computers against a rat protein database containing 40,800 protein sequences downloaded as FASTA-formatted sequences from Entrez (NCBI; <http://www.ncbi.nlm.nih.gov/entrez>). Sequence redundancies were removed using Perl script. To increase the search speed the protein database was preprocessed to create a binary database containing all possible tryptic peptides of the searched database. Any static and dynamic modifications that would account for post-translational and chemical modifications were neglected. The peptide mass search tolerance was set to 3 Da. Spectral matches were retained with a minimal cross-correlation score (XCorr) of 1.5, 2.2 and 3.3 for charge states +1, +2 and +3 respectively. DeltaCN (top match's XCorr minus the second-best match's XCorr divided by top match's XCorr) had to be  $\geq 0.07$ . Retained spectral matches were filtered and reassigned to proteins using DTASelect<sup>39</sup>. DTASelect outputs of independent measurements were entered into Accessible Vascular Targets database (AVATAR). AVATAR was designed to store a large amount of mass spectrometric data and to provide tools to analyze the data to extract valuable information. We used relational models for database design based on Entity-Relationship and implemented the database in the MySQL relational database management system to support database query and management. This relational database plus Perl-based user-friendly interface have greatly improved data organization, data consistency and integrity, and facilitated data comparison and information retrieval. To increase coverage of known EC markers in some of the analysis, we also used a larger database containing over 200,000 protein sequences (human, mouse and rat).



**Removal of protein redundancy.** AVATAR allowed a detailed analysis of parameters such as reproducibility and combined sequence coverage. The final protein list created from all peptide sequences obtained by MS/MS was compiled using AVATAR to retrieve the minimum number of proteins identified by three or more peptide spectra. If multiple entries of the same protein from different species (that is, mouse and human) other than rat were present only the species with the better spectrum coverage was manually retained. If it was not unambiguously possible to distinguish multiple isoforms or splice variants of a protein being assigned to the same set of peptides from each other, we manually reduced this list to one primary entry.

**Analysis of the reproducibility of MudPIT measurements.** Twelve independent 18-step MudPIT experiments of rat lung P sample were statistically analyzed to evaluate the benefit of repetitive MudPIT measurements. After each additional experiment we determined the fraction of proteins that were represented in at least two experiments and the percentages of proteins that were present in only one single experiment. Because this analysis can depend on the sequence by which the experiments are analyzed, we limited potential bias from any particular order of experiments by analyzing 12 different experiment sequences where the order of the experiments was systematically permuted by shifting the first experiment to the last position.

**In silico protein analysis.** The molecular weights and pIs of each protein based on its primary amino acid sequence were calculated using the ExPasy web server ([http://us.expasy.org/tools/pi\\_tool.html](http://us.expasy.org/tools/pi_tool.html)). The actual molecular weights and pIs may differ slightly from the calculated values because post-translational modifications are not considered by the program at this time. SwissProt (<http://us.expasy.org/sprot/sprot-top.html>) and the National Center Biotechnology Information (NCBI; <http://www.ncbi.nlm.nih.gov/entrez/query.fcgi>) protein and literature databases were used to classify proteins according to their currently known predominant subcellular location. Known or predicted transmembrane-spanning alpha helices were determined through the literature or by using the web-based prediction program TMHMM v2.0 (provided by the Center for Biological Sequence Analysis of the Technical University in Denmark, <http://www.cbs.dtu.dk/services/TMHMM-2.0>). Only 100% probabilities were taken into consideration. Searches for protein families and hidden Markov models were done using pfam (<http://www.sanger.ac.uk/software/pfam/index.html>).

Note: Supplementary information is available on the Nature Biotechnology website.

#### ACKNOWLEDGMENTS

We thank Michelle Bourne, Lisa Randall and Traci Smith for technical assistance; David Tabb for help setting up DTASelect; and Yan Li for helpful discussion. This research was supported by grants to J.E.S. from the National Institutes of Health (Heart, Lung and Blood nos. R01 HL52766, R01 HL58216), National Cancer Institute (no. R01 CA83989, R24 CA095893, R33 CA97528), Sidney Kimmel, Schut Foundation, California Tobacco-related Disease Research Program (no. 11RT-0167) and California Breast Cancer Research Program (no. 8WB-00114).

#### COMPETING INTERESTS STATEMENT

The authors declare that they have no competing financial interests.

Received 19 December 2003; accepted 13 May 2004

Published online at <http://www.nature.com/naturebiotechnology/>

1. Schnitzer, J.E. Update on the cellular and molecular basis of capillary permeability. *Trends Cardiovasc. Med.* **3**, 124–130 (1993).
2. Michiels, C. Endothelial cell functions. *J. Cell. Physiol.* **196**, 430–443 (2003).
3. Madri, J.A. & Williams, S.K. Capillary endothelial cell culture: Phenotype modulation by matrix components. *J. Cell Biol.* **97**, 153–165 (1983).
4. Goerdt, S. et al. Characterization and differential expression of an endothelial cell-specific surface antigen in continuous and sinusoidal endothelial, in skin vascular lesions and *in vitro*. *Exp. Cell Biol.* **57**, 185–192 (1989).
5. Gumkowski, F., Kaminska, G., Kaminski, M., Morrissey, L.W. & Auerbach, R. Heterogeneity of mouse vascular endothelium. *Blood Vessels* **24**, 11–23 (1987).
6. Aird, W.C. et al. Vascular bed-specific expression of an endothelial cell gene is programmed by the tissue microenvironment. *J. Cell Biol.* **138**, 1117–1124 (1997).
7. Janzer, R.C. & Raff, M.C. Astrocytes induce blood-brain barrier properties in endothelial cells. *Nature* **325**, 253–257 (1987).
8. Stewart, P.A. & Wiley, M.J. Developing nervous tissue induces formation of blood-brain barrier characteristics in invading endothelial cells: a study using quail-chick transplantation chimeras. *Dev. Biol.* **84**, 183–192 (1981).

9. Auerbach, R., Alby, L., Morrissey, L.W., Tu, M. & Joseph, J. Expression of organ-specific antigens on capillary endothelial cells. *Microvasc. Res.* **29**, 401–411 (1985).
10. St. Croix, B. et al. Genes expressed in human tumor endothelium. *Science* **289**, 1197–1202 (2000).
11. Obermeyer, N., Janson, N., Bergmann, J., Buck, F. & Ito, W.D. Proteome analysis of migrating versus nonmigrating rat heart endothelial cells reveals distinct expression patterns. *Endothelium* **10**, 167–178 (2003).
12. Bruneel, A. et al. Proteomic study of human umbilical vein endothelial cells in culture. *Proteomics* **3**, 714–723 (2003).
13. Pasqualini, R. & Ruoslahti, E. Organ targeting *in vivo* using phage display peptide libraries. *Nature* **380**, 364–366 (1996).
14. Rajotte, D. et al. Molecular heterogeneity of the vascular endothelium revealed by *in vivo* phage display. *J. Clin. Invest.* **102**, 430–437 (1998).
15. Schnitzer, J.E., McIntosh, D.P., Dvorak, A.M., Liu, J. & Oh, P. Separation of caveolae from associated microdomains of GPI-anchored proteins. *Science* **269**, 1435–1439 (1995).
16. Oh, P. & Schnitzer, J.E. Isolation and subfractionation of plasma membranes to purify caveolae separately from glycosyl-phosphatidylinositol-anchored protein microdomains in *Cell Biology: A Laboratory Handbook*, vol. 2 (ed. Celis, J.) 34–45 (Academic Press, Orlando, 1998).
17. Rizzo, V., Morton, C., DePaola, N., Schnitzer, J.E. & Davies, P.F. Recruitment of endothelial caveolae into mechanotransduction pathways by flow conditioning *in vitro*. *Am. J. Physiol. Heart Circ. Physiol.* **285**, H1720–H1729 (2003).
18. Schnitzer, J.E., Liu, J. & Oh, P. Endothelial caveolae have the molecular transport machinery for vesicle budding, docking, and fusion including VAMP, NSF, SNAP, annexins, and GTPases. *J. Biol. Chem.* **270**, 14399–14404 (1995).
19. Schnitzer, J.E. & Oh, P. Aquaporin-1 in plasma membrane and caveolae provides mercury-sensitive water channels across lung endothelium. *Am. J. Physiol.* **270**, H416–H422 (1996).
20. Schnitzer, J.E. & Oh, P. Antibodies to SPARC inhibit albumin binding to SPARC, gp60, and microvascular endothelium. *Am. J. Physiol.* **263**, H1872–H1879 (1992).
21. Wolters, D.A., Washburn, M.P. & Yates, J.R., III. An automated multidimensional protein identification technology for shotgun proteomics. *Anal. Chem.* **73**, 5683–5690 (2001).
22. Jeffries, W.A. et al. Transferrin receptor on endothelium of brain capillaries. *Nature* **312**, 162–163 (1984).
23. Schnitzer, J.E. & Oh, P. Albondin-mediated capillary permeability to albumin. Differential role of receptors in endothelial transcytosis and endocytosis of native and modified albumins. *J. Biol. Chem.* **269**, 6072–6082 (1994).
24. Schnitzer, J.E. gp60 is an albumin-binding glycoprotein expressed by continuous endothelium involved in albumin transcytosis. *Am. J. Physiol.* **262**, H246–H254 (1992).
25. Christian, S. et al. Nucleolin expressed at the cell surface is a marker of endothelial cells in angiogenic blood vessels. *J. Cell Biol.* **163**, 871–878 (2003).
26. Negrutskii, B.S. & El'skaya, A.V. Eukaryotic translation elongation factor 1 alpha: structure, expression, functions, and possible role in aminoacyl-tRNA channeling. *Prog. Nucleic Acid Res. Mol. Biol.* **60**, 47–78 (1998).
27. Honscha, W., Ottallah, M., Kistner, A., Platte, H. & Petzinger, E. A membrane-bound form of protein disulfide isomerase (PDI) and the hepatic uptake of organic anions. *Biochim. Biophys. Acta* **1153**, 175–183 (1993).
28. Hebert, C. et al. Cell surface colligin/Hsp47 associates with tetraspanin protein CD9 in epidermoid carcinoma cell lines. *J. Cell. Biochem.* **73**, 248–258 (1999).
29. Schnitzer, J. The endothelial cell surface and caveolae in health and disease. in *Vascular Endothelium: Physiology, Pathology and Therapeutic Opportunities* (eds. Born, G.V.R. & Schwartz, C.J.) 77–95 (1997).
30. Washburn, M.P., Wolters, D. & Yates, J.R., III. Large-scale analysis of the yeast proteome by multidimensional protein identification technology. *Nat. Biotechnol.* **19**, 242–247 (2001).
31. McIntosh, D.P., Tan, X.Y., Oh, P. & Schnitzer, J.E. Targeting endothelium and its dynamic caveolae for tissue-specific transcytosis *in vivo*: a pathway to overcome cell barriers to drug and gene delivery. *Proc. Natl. Acad. Sci. USA* **99**, 1996–2001 (2002).
32. Carver, L.A. & Schnitzer, J.E. Caveolae: mining little caves for new cancer targets. *Nat. Rev. Cancer* **3**, 571–581 (2003).
33. Weinman, E.J., Steplock, D. & Shenolikar, S. Acute regulation of NHE3 by protein kinase A requires a multiprotein signal complex. *Kidney Int.* **60**, 450–454 (2001).
34. Abe, J., Suzuki, H., Notoya, M., Yamamoto, T. & Hirose, S. Ig-hepta, a novel member of the G protein-coupled hepta-helical receptor (GPCR) family that has immunoglobulin-like repeats in a long N-terminal extracellular domain and defines a new subfamily of GPCRs. *J. Biol. Chem.* **274**, 19957–19964 (1999).
35. van der Merwe, P.A. et al. The NH2-terminal domain of rat CD2 binds rat CD48 with a low affinity and binding does not require glycosylation of CD2. *Eur. J. Immunol.* **23**, 1373–1377 (1993).
36. Magee, J.C., Stone, A.E., Oldham, K.T. & Guice, K.S. Isolation, culture, and characterization of rat lung microvascular endothelial cells. *Am. J. Physiol.* **267**, L433–L441 (1994).
37. Link, A.J. et al. Direct analysis of protein complexes using mass spectrometry. *Nat. Biotechnol.* **17**, 676–682 (1999).
38. Eng, J. & McCormac, A. & Yates, J.R. An approach to correlate tandem mass spectral data of peptides with amino acid sequences in a protein database. *J. Am. Soc. Mass Spectrom.* **5**, 976–989 (1994).
39. Tabb, D.L., McDonald, W.H. & Yates, J.R., III. DTASelect and Contrast: tools for assembling and comparing protein identifications from shotgun proteomics. *J. Proteome Res.* **1**, 21–26 (2002).



## Supplementary Notes

**Diversity of identified proteins.** Proteins associated with the plasma membrane that are not integral membrane proteins or lipid-anchored may exist in our preparation through protein complex formation and interaction partners. For example, sodium hydrogen exchanger regulatory factor 2 (NHERF-2) is not membrane-bound but rather associates with podocalyxin, a pan-endothelial integral membrane protein marker<sup>1</sup>, via its PDZ domain<sup>2</sup>. NHERF-2 in turn interacts with ezrin and EBP50-PDZ interactor<sup>3</sup>, both of which were also identified in rat lung P. Another example is dedicator of cytokinesis protein 1 (Dock180), which is recruited to the plasma membrane via its interaction with phosphatidylinositol 3,4,5-triphosphate<sup>4</sup> where it has been implicated in regulation of cytoskeletal rearrangements required for cell motility<sup>5</sup>. Moreover, its activation has been found to be enhanced by binding to engulfment and cell motility proteins (ELMO) 1 and 2, also found in P. Such similar interactions may explain the presence of many cytosolic and even other proteins in our preparation because of yet to be discovered recruitments.

**Distinct EC surface proteome in vivo vs. in vitro.** The tight junction protein ZO-2 is readily detected by MS in rat lung P but not in RLMVEC. Western analysis (Fig. 6a) and immunofluorescence (our unpublished observations) confirms the expression of ZO-2 in RLMVEC cells. It is in the total cell lysate (H) and not P. The lack of ZO-2 and other junctional complex proteins (VE-cadherins and ZO-1) in RLMVEC P but not rat lung P suggest that the junctional complex remains in P from tissue but not cultured EC monolayers. The intercellular junctions of ECs in vivo are more developed and tighter than those in culture so that during homogenization of the lung tissue, membrane breakage may occur to include along with the rest of the silica-coated plasma membranes only the junctions that are tightly interdigitated.

**Novel findings.** In addition to identifying multiple known plasma membrane and EC marker proteins, we also detected a number of proteins that were unexpected, such as TIE-2, APN, TEM4, TEM6, ICAM-1, and nucleolin. TIE2 and ICAM-1 expression in lung endothelium was also validated by tissue immunostaining (Fig. 6b) whereas APN and nucleolin were detected by Western analysis enriched in lung P. These molecules are all thought to be endothelial markers induced during angiogenesis and/or inflammation despite being clearly present in rat lung P from multiple samples. Given the mechanical forces involved with respiration, lung endothelium may undergo recurrent damage requiring more self-renewal and be less quiescent than in other tissues. Conversely, the inherent highly oxygenated state of the tissue would render unlikely typical triggers of angiogenesis, such as hypoxia. In the end, strategies of targeting tumors through these proteins should assess possible lung targeting in vivo.



We also identified two neuronal receptors, P2Z receptor (P2X7)<sup>6</sup> and Trk-A<sup>7</sup>. Although Trk-A (isoform I) can be expressed in a wide range of non-neuronal tissues such as connective tissue (fibroblasts), kidney, lung, breast and esophagus<sup>8,9</sup>, to the best of our knowledge this is the first time that either of these neuronal cell surface receptors are detected at the EC surface (**Fig. 6**). Given the enrichment in P and the lack of previous detection in lung tissue<sup>6</sup>, their EC surface expression appears real and may reflect the high sensitivity of this analytical approach. Other proteins, such as aquaporin and synaptobrevin, previously thought to be specific for other cell types (epithelial and neuronal, respectively) have also been discovered in endothelium using similar tissue subfractionation techniques<sup>10,11</sup>. The P2X7 antibody is effective for both Western analysis and tissue immunostaining so that we have confirmed P2X7 expression on lung endothelium on frozen tissue sections.

In addition to known proteins, we also detected a number of yet-to-be-characterized proteins (25%). This group includes proteins discovered through EST and cDNA cloning initiatives as well as proteins that are "similar to a known gene from the human or mouse database" predicted by automated annotation of the rat genome. These predicted proteins require further structural and functional characterization before they can be classified outside this category. We chose to generate specific antibodies to two proteins (FLJ10849 and HSPA12B) in this category for validation of the MS findings. FLJ10849 is a hypothetical protein supported by expressed sequence tag (EST) evidence that was identified with good sequence coverage (28.6%; 18 spectra; Supplementary Fig. 1 and Supplementary Table 4 online). A BLAST<sup>12</sup> search of the sequence revealed its closest relative to be human septin 6 with 81% identity and a pfam search showed that it contained a CDC\_GTP motif that is common to proteins involved in cell division as well as in endocytosis or GTP-driven vesicle formation<sup>13</sup>. HSPA12B, identified in rat lung P (26 spectra, 28.4% coverage of the predicted primary sequence), is an apparent member of the Hsp70 super family (see Supplementary Fig. 2 and Supplementary Table 5 online). HSPA12B is supported by EST findings and Northern analysis reveals expression in atherosclerotic lesions<sup>14</sup>. HSPA12B expression was also confirmed in the lung endothelium by tissue immunostaining (**Fig. 6b**) but, unfortunately, the FLJ10849 antibody was suboptimal and gave significant background staining. They are both enriched in P relative to H so that it is very likely based on our experience that they both are indeed expressed at the lung EC surface. To the best of our knowledge this is the first time that the translation of these 2 proteins has been confirmed on a primary sequence level.

**Protein validation.** Given that a protein not identified by MS out of a complex mixture is not necessarily absent in the sample, we have used Western analysis to test for many proteins not detected in RLMVEC P. 87.5% of the tested proteins that are not detected in RLMVEC by MS are also not detected by Western analysis and 91% of all tested proteins that are detected in either rat lung or RLMVEC P are



confirmed by Western analysis (see Supplementary Table 3 online). All detected protein bands agree with the predicted molecular weights and, given the relative specificity of each antibody this analysis provides good evidence that the peptides identified by MS truly corresponded to the identified proteins. Yet, it remains problematic that the public protein databases are as yet incomplete so that we cannot rule out the possibility for the existence of other, yet-to-be-identified proteins that share peptide sequences. Western analysis also has the advantage of providing quantitative information on the relative levels of each protein. Proteins depleted in P relative to total cell/tissue lysate (H) have a greater probability of being contaminants revealed by the high sensitivity of the mass spectrometer whereas proteins enriched in P over H are expected rarely to be contaminants.

Immunohistochemical staining of lung tissue can provide additional validation beyond subfractionation to show clearly lung EC expression of identified proteins. Unfortunately, many antibodies do not work both in Western analysis and immunohistology. Proteins are denatured to varying degrees after SDS-PAGE and transfer to filters whereas proteins in frozen tissue may be more native in structure and may be interacting with other proteins to block possible antibody reactivity. Tissue immunostaining can be extremely laborious and time consuming requiring careful preparation and optimization. In our experience of testing >500 antibodies in the last decade,  $\geq 50\%$  of all the antibodies that we get either from other labs or from commercial sources are not monospecific by Western analysis and thus cannot be used for immunohistochemistry: at least 50% of these monospecific antibodies do not work for tissue immunostaining.

### Supplementary References

1. Horvat, R., Hovorka, A., Dekan, G., Poczewski, H. & Kerjaschki, D. Endothelial cell membranes contain podocalyxin--the major sialoprotein of visceral glomerular epithelial cells. *J Cell Biol* **102**, 484-491 (1986).
2. Li, Y., Li, J., Straight, S.W. & Kershaw, D.B. PDZ domain-mediated interaction of rabbit podocalyxin and Na(+)/H(+) exchange regulatory factor-2. *Am J Physiol Renal Physiol* **282**, F1129-1139 (2002).
3. Reczek, D. & Bretscher, A. Identification of EPI64, a TBC/rabGAP domain-containing microvillar protein that binds to the first PDZ domain of EBP50 and E3KARP. *J Cell Biol* **153**, 191-206 (2001).
4. Brugnera, E. et al. Unconventional Rac-GEF activity is mediated through the Dock180-ELMO complex. *Nat Cell Biol* **4**, 574-582 (2002).
5. Cote, J.F. & Vuori, K. Identification of an evolutionarily conserved superfamily of DOCK180-related proteins with guanine nucleotide exchange activity. *J Cell Sci* **115**, 4901-4913 (2002).



6. Deuchars, S.A. et al. Neuronal P2X7 receptors are targeted to presynaptic terminals in the central and peripheral nervous systems. *J Neurosci* **21**, 7143-7152 (2001).
7. Esposito, D. et al. The cytoplasmic and transmembrane domains of the p75 and Trk A receptors regulate high affinity binding to nerve growth factor. *J Biol Chem* **276**, 32687-32695 (2001).
8. Barker, P.A. et al. Tissue-specific alternative splicing generates two isoforms of the trkA receptor. *J Biol Chem* **268**, 15150-15157 (1993).
9. Koizumi, H., Morita, M., Mikami, S., Shibayama, E. & Uchikoshi, T. Immunohistochemical analysis of TrkA neurotrophin receptor expression in human non-neuronal carcinomas. *Pathol Int* **48**, 93-101 (1998).
10. Schnitzer, J.E., Liu, J. & Oh, P. Endothelial caveolae have the molecular transport machinery for vesicle budding, docking, and fusion including VAMP, NSF, SNAP, annexins, and GTPases. *J. Biol. Chem.* **270**, 14399-14404 (1995).
11. Schnitzer, J.E. & Oh, P. Aquaporin-1 in plasma membrane and caveolae provides mercury-sensitive water channels across lung endothelium. *Am J Physiol* **270**, H416-422 (1996).
12. Altschul, S.F., Gish, W., Miller, W., Myers, E.W. & Lipman, D.J. Basic local alignment search tool. *J Mol Biol* **215**, 403-410 (1990).
13. Kartmann, B. & Roth, D. Novel roles for mammalian septins: from vesicle trafficking to oncogenesis. *J Cell Sci* **114**, 839-844 (2001).
14. Han, Z., Truong, Q.A., Park, S. & Breslow, J.L. Two Hsp70 family members expressed in atherosclerotic lesions. *Proc Natl Acad Sci U S A* **100**, 1256-1261 (2003).

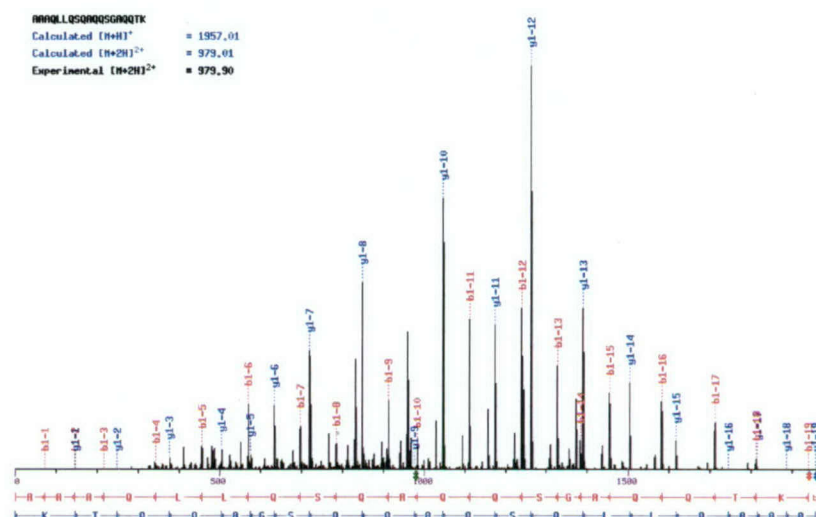


Supplementary Table 3: Summary of Western analysis

Protein name	Rat Lung		Cell Culture		MS		MS result confirmed
	H	P	H	P	Lung P	RLMVEC P	
<i>Angiotensin-converting enzyme</i>	-	+	O	O	yes	no	yes
<i>Aquaporin 1</i>	-	+	O	O	yes	no	yes
<i>Carbonic anhydrase IV</i>	-	+	O	O	yes	no	yes
<i>Endothelin converting enzyme</i>	O	+	O	O	yes	no	yes
<i>High affinity nerve growth factor receptor</i>	O	+	-	-	yes	no	no
<i>Lyn B tyrosine kinase</i>	O	+	O	-	yes	no	no
<i>Nucleolin</i>	-	+	O	O	yes	no	yes
<i>P2Z receptor</i>	-	+	O	O	yes	no	yes
<i>Podocalyxin</i>	-	+	O	O	yes	no	yes
<i>Receptor for advanced glycosylation end products</i>	-	+	O	O	yes	no	yes
<i>Seven transmembrane receptor</i>	-	+	O	O	yes	no	yes
<i>Sodium-hydrogen exchanger 3 regulatory factor 2</i>	O	+	O	O	yes	no	yes
<i>Tight junction protein 2 - ZO2</i>	O	+	+	O	yes	no	yes
<i>Tyrosine-protein kinase receptor TIE-2</i>	+	+	O	O	yes	no	yes
<i>HSPA12B (HSP70 motif containing protein)</i>	O	+	O	O	yes	no	yes
<i>Vascular endothelial cadherin</i>	O	+	O	O	yes	no	yes
<i>Aminopeptidase N</i>	+	+	O	+	yes	yes	yes
<i>Caveolin-1</i>	-	+	+	+	yes	yes	yes
<i>Heat shock protein 47</i>	+	+	+	+	yes	yes	yes
<i>Hypothetical protein FLJ10849 (septin homolog)</i>	+	+	-	+	yes	yes	yes
<i>Intercellular adhesion molecule-1</i>	-	+	+	+	yes	yes	yes
<i>Ox-45</i>	-	+	O	O	yes	yes	no
<i>5'-nucleotidase</i>	O	+	+	+	no	yes	yes

The table summarizes the results from Western analysis in comparison to MS analysis. Proteins are listed in alphabetical order in three categories. The three categories are *i)* not found by MS in RLMVEC P; *ii)* found by MS in RLMVEC P and rat lung P; *iii)* not found by MS in rat lung P. Open circles indicate no signal, minus signs indicate lower signal intensity and plus signs indicate higher signal intensity.



Supplementary Figure 1: **MS/MS spectrum of peptide of FLJ10849**

Tandem mass spectrum of the doubly charged tryptic peptide "AAAQLLSQAQQSGAQQTK" corresponding to amino acid positions 400 - 418 in septin homolog FLJ10849 (NCBI: gi|34876531|). The overlapping amino acid sequence "QLLSQAQQSGAQQTKKD" corresponding to positions 403 - 420 was used as antigen for the production of polyclonal antibodies in rat. Mass spectral fragment ions cover 63.9% of the peptide sequence. The calculated precursor  $m/z$  (979.01) differs by 0.89 mass units from the observed  $m/z$  of the precursor ion (979.90).

Supplementary Table 4: **Peptide and spectrum coverage of FLJ10849**

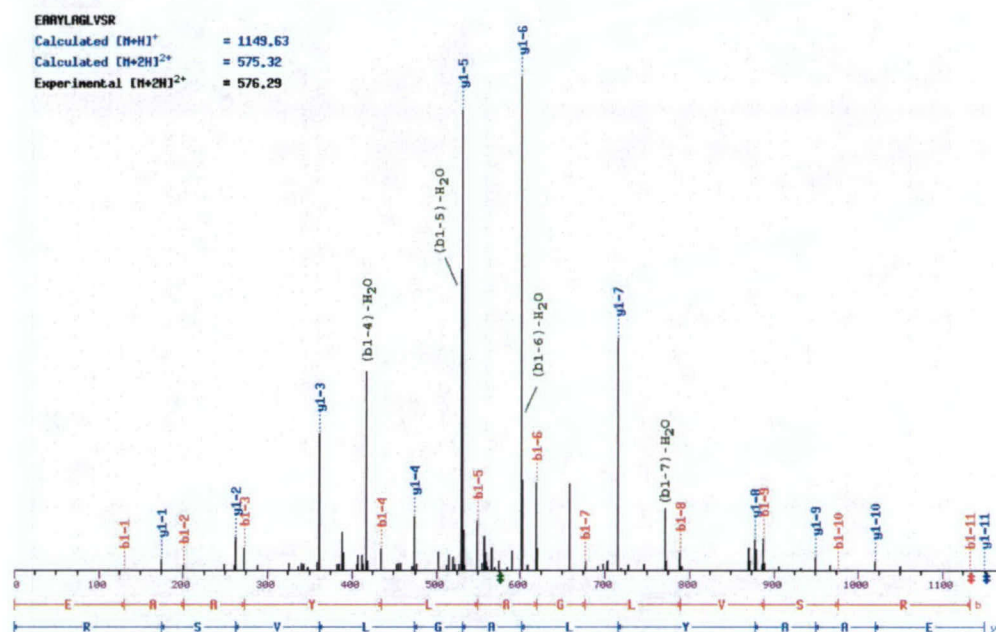
Septin 6 homolog FLJ10849		Charge state		
position	sequence	1	2	3
(15 - 34)	NLSLSGHVGFDSLDPQLVNK		x/o	
(55 - 65)	STLMDTLFNTK	x/o	x/o	
(66 - 80)	FESDPATHNEPGVRL		x/o	
(84 - 93)	SYELQESNVR	x	x	
(96 - 110)	LTIVDTVGFGDQINK		o	
(111 - 130)	DDSYKPIVEYIDAQFEAYLQEELK			o
(138 - 146)	SLFNYHDTR	x/o	x/o	
(163 - 170)	SLDLVTMK	x/o		
(176 - 184)	VNIIPPIAK	x/o	x/o	
(275 - 286)	EMLIRVNMEDLR		x	
(293 - 298)	HYELYR	x/o	x	
(309 - 326)	DTDPDSKPFSLQETYEAK		x	
(327 - 336)	RNEFLGELQK	o	x/o	
(399 - 418)	KAAAQLLSQAQQSGAQQTK			x
(400 - 418)	AAAQLLSQAQQSGAQQTK		x/o	o

Tryptic peptides of Septin homolog FLJ10849 (NCBI: gi|34876531|) identified by MS/MS in rat lung P are listed with their primary sequence positions and the precursor charge state. The sequence coverage per amino acid is 28.6%. (x) indicates peptides identified in rat lung P and (o) indicates peptides identified in RLMVEC P.



## Supplementary Figure 2:

## (A) MS/MS spectrum peptide of HSPA12B



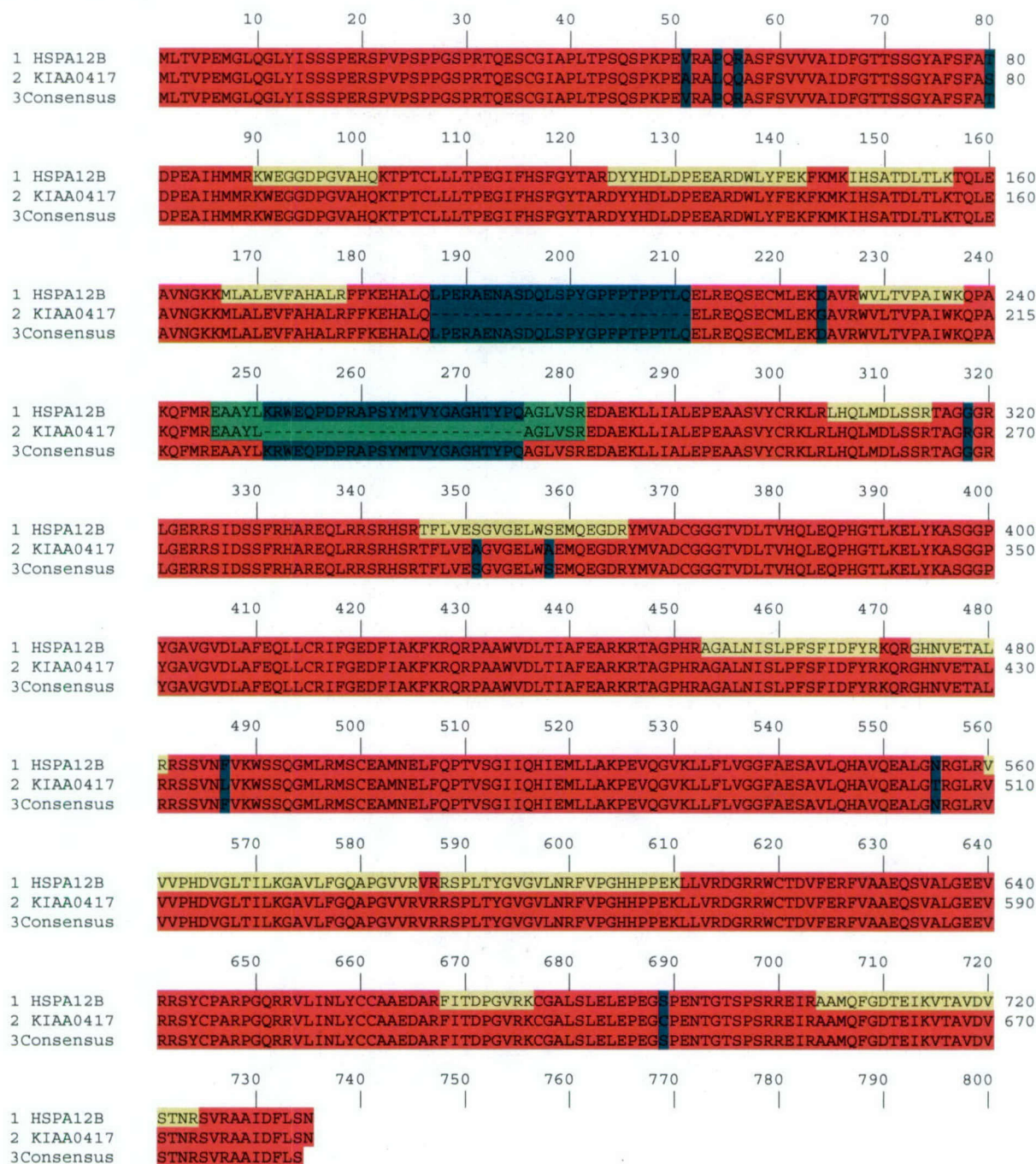
Tandem mass spectrum of the doubly charged tryptic peptide "EAAYLAGLYSR" corresponding to amino acid positions 246 - [...] - 281 in HSPA12B *Rattus norvegicus* (NCBI: gi|34858716|) or amino acid positions 221 - 231 of HSPA12B *Mus musculus* (NCBI: gi|21312236|) found in RLMVEC P sample. Mass spectral fragment ions cover 90.0% of the peptide sequence. The calculated precursor m/z (575.32) differs by 0.04 mass units from the observed m/z of the precursor ion (575.29).



## Supplementary Figure 2:

## (B) Sequence coverage of HSPA12B

Comparison of HSPA12B rat sequence with mouse sequence (KIAA0417)



Amino acid sequences of HSPA12B of *Rattus norvegicus* (NCBI: gi|34858716|) and *Mus musculus* (NCBI: gi|21312236|) are aligned and the tryptic peptides identified by tandem mass spectra are highlighted in yellow. The sequence coverage per amino acid is 28.4%. Peptide EAYLAGLVSR (position 246 - [...] - 281 in rat and highlighted in green) is specific for the mouse sequence of HSPA12B (positions 221 - 231). Its occurrence in rat lung P strongly suggests a sequence conflict. See also supplemental Table 5.



Supplementary Table 5: **Peptide and spectrum coverage of HSPA12B**

HSPA12B		Charge state		
position	sequence	1	2	3
(90 - 101)	KWEGGDPGVAHQ		x	
(91 - 101)	WEGGDPGVAHQ		x	
(124 - 135)	DYYHDLDPPEAR		x	
(136 - 142)	DWLYFEK	x		
(147 - 157)	IHSATDLTLK	x		
(167 - 178)	MLALEVFAHALR		x	
(228 - 238)	WVLTVP AIWK		x	
(246 - [...] - 281)	EAAYL-----AGLVSR		x	
(305 - 314)	LHQLMDLSSR	x	x	
(346 - 366)	TFLVESGVGELWSEMQEGDR			
(453 - 469)	AGALNISLPFSFIDFYR		x	
(473 - 481)	GHNVELALR	x	x	
(559 - 572)	VVVP HDVGLTILK	x	x	
(573 - 586)	GAVLFGQAPGVVR	x	x	
(588 - 600)	RSPLTYGVGV LNR		x	
(589 - 600)	SPLTYGVGV LNR	x	x	
(601 - 610)	FVPGHHPPEK		x	
(668 - 676)	FITDPGVRK		x	
(704 - 714)	AAMQFGDTEIK	x		
(715 - 724)	VTAVDVSTNR	x	x	

Tryptic peptides of HSPA12B (NCBI: gi|34858716|) identified by MS/MS in rat lung P are listed with their primary sequence position and the precursor charge state. The sequence coverage per amino acid is 28.4%. Peptide EAAYLAGLVSR (position 246 -[...] -281) is specific for the mouse sequence of HSPA12B (NCBI: gi|21312236| position 221 - 231). See also supplemental Figure 2.



Supplementary Table 1

## Integral and lipid-anchored plasma membrane proteins

Protein name	NCBI locus	SwissProt or Trembl locus	Number of MS/MS spectra				Function	Predicted TMs
			Lung P	RLMVEC	PI	MW		
ADP/ATP translocase 2	728810	Q09073	3	7	9.74	32901	transport	2
ADP-ribosyl cyclase 1 (CD38H)	2493428	Q64244	4	3	8.83	34436	other	1
ALCAM (CD166)	2589007	O35112	3	-	5.77	65022	adhesion	1
Aminopeptidase N	113750	P15684	3	4	5.30	109317	ee	1
Angiotensin-converting enzyme (CD134)	11493661	P12821	44	-	5.95	149715	ee	1
Antigen peptide transporter 2	407477	P36372	3	2	6.27	77713	transport	5
Aquaporin 1	312924	P29975	3	-	7.70	28830	transport	6
Atrial natriuretic peptide receptor A	204270	P18910	5	-	6.59	118951	signaling	1
Carbonic anhydrase IV	544726	P48284	11	-	6.31	35076	ee	GPI
Caveolin-1	17017233	Q8VIK9	13	5	5.30	20553	traffick	1
Caveolin-2	17017237	Q8VIK7	4	1	5.65	18175	traffick	2
CD9 antigen	729088	P40241	3	2	7.25	25084	adhesion	4
CDC42	31542368	Q8CFN2	3	2	5.76	21311	signaling	prenylate
Cell surface glycoprotein MUC18	10566949	x	5	-	5.74	71373	other	1
Cerebral protein-11	34880202	O75069	5	-	5.87	81692	other	2 ion
Chloride intracellular channel 5	12232044	Q9EPT8	12	-	5.64	28299	transport	channel
Complement component C1q receptor (endothelial-CD93 antigen)	9886763	Q9ET61	4	-	4.87	68782	other	1
C-Yes	12539401	Q99PW1	4	5	6.22	60588	signaling	myristate
Cytolysin	203894	P35763	6	-	8.18	61513	other	channel
Dipeptidyl peptidase IV (CD26)	118905	P14740	31	-	5.87	88003	ee	1
Ecto-apyrase (CD39)	1754710	P97687	4	-	7.48	57408	ee	2
Ecto-ATPase	203990	P16573	3	-	5.62	57264	ee	1
Endothelial cell-selective adhesion molecule	27720013	x	8	-	8.53	31382	adhesion	1
Endothelin converting enzyme	529085	P42893	7	-	6.37	86126	ee	1
Flotillin-2	4097589	Q9Z2S9	3	4	5.13	47038	traffick	-
FYN	1101768	Q62844	3	-	6.23	60702	signaling	myristate
G protein beta 1 subunit	31669	P04901	10	-	5.60	37377	signaling	-
G protein beta 2 subunit	1730215	P54313	6	-	5.61	37500	signaling	-
G protein G alpha 11	8925964	Q9JID2	10	2	5.91	42026	signaling	palmitate
G protein G alpha 13	27690213	x	4	3	8.38	43811	signaling	palmitate
G protein Gi alpha 2	71896	P04897	7	3	5.28	40368	signaling	palmitate
G protein Gi alpha 3	6980964	P08753	6	1	5.51	40391	signaling	palmitate
G protein Go alpha 2	27808491	P30033	6	3	5.62	40073	signaling	palmitate
G protein Gq alpha	7329187	P82471	8	3	5.58	41425	signaling	palmitate
G protein Gs alpha	14161099	Q63803	6	2	5.50	45709	signaling	palmitate
Giantin	516826	Q63714	4	-	5.01	364297	other	1
Glut4	4193489	Q9Z1X1	4	6	5.47	121159	transport	1
High affinity nerve growth factor receptor (TRK-A)	549122	P35739	4	-	5.98	87868	signaling	1
Integrin alpha-1 (CD49a)	124941	P18614	8	18	5.65	130809	adhesion	1
Integrin alpha-5 (CD49c)	34868649	Q80YP5	4	6	5.70	115016	adhesion	1
Integrin alpha-6 (CD49e)	13992591	Q924W2	4	1	6.53	108807	adhesion	1
Integrin beta-1 (CD29)	520566	P49134	11	10	5.77	88495	adhesion	1
Intercellular adhesion molecule-1 (CD54)	124100	Q00238	6	10	6.53	60142	adhesion	1
Intercellular adhesion molecule-2	34873952	-	3	-	8.02	31091	adhesion	1
K-Ras 2B	1172844	P46203	3	1	8.24	21425	signaling	0
Lipoprotein lipase	462538	Q06000	3	-	8.36	53082	ee	0
Low-density lipoprotein receptor-related protein 2	13562118	P98158	3	1	5.03	519276	other	1
Lutheran antigen	10566957	Q9ESS6	7	-	5.52	67512	other	1
Lyn tyrosine kinase	2105002	Q07014	13	-	6.76	58529	signaling	prenylation
Membrane-bound aminopeptidase P	13560983	Q99MA2	25	-	5.49	76080	ee	GPI
MHC class I protein, isoform a	3493247	x	3	-	6.35	39348	other	1
MHC class I protein, isoform b (RT1.A1(f) protein)	1483574	Q31257	15	1	5.64	39246	other	1
MHC class I protein, isoform c	7453015	x	5	-	7.17	41718	other	1
MHC class I protein, isoform d	1263198	x	6	-	5.55	41473	other	1
Microsomal dipeptidase	459933	P31430	7	2	5.67	45506	ee	GPI
Myoferlin	23597920	Q9NZM1	9	21	6.19	126162	other	1
Na <sup>+</sup> K <sup>+</sup> transporting ATPase alpha-1	114376	P06685	20	18	5.30	113054	transport	7
Na <sup>+</sup> K <sup>+</sup> transporting ATPase beta-3	3121778	Q63377	4	2	8.08	31830	transport	1
Neural visinin-like protein 3	8393864	P35333	4	-	5.32	22207	transport	myristate
Nogo-A protein	6822247	Q9JK11	4	5	4.41	126388	signaling	2



<i>OX-2 membrane glycoprotein</i>	129300	P04218	4	-	9.02	31088	other	1
<i>OX-45 antigen (CD48)</i>	56805	P10252	9	-	7.67	27680	adhesion	GPI
<i>P2Z receptor (P2X7)</i>	2499425	Q64663	3	-	8.30	68392	signaling	2
<i>Plasma membrane calcium-transporting ATPase 1</i>	92025	P11505	5	1	5.71	138719	transport	7
<i>Plasma membrane calcium-transporting ATPase 4</i>	1054879	Q64542	5	-	6.17	133094	transport	7
<i>Platelet-endothelial cell adhesion molecule-1 (CD31)</i>	1684839	P97635	4	-	8.63	38164	adhesion	1
<i>Podocalyxin</i>	4996222	Q9WVQ2	5	-	4.81	51545	adhesion	1
<i>Progesterone receptor component 1</i>	6647578	P70580	4	1	4.45	21467	signaling	1
<i>PV-1</i>	5281517	Q9WV78	21	-	8.80	50033	other	1
<i>Rab-11B</i>	9837357	O35509	6	3	5.98	24509	signaling	prenylation
<i>Rab-5b</i>	27689505	x	5	2	8.64	23426	signaling	prenylation
<i>Ral-A</i>	131836	P05810	4	1	6.66	23553	signaling	prenylation
<i>Ral-B</i>	310212	P36860	6	1	6.24	23317	signaling	prenylation
<i>Rap-1a</i>	27660326	P10113	4	1	6.39	20987	signaling	prenylation
<i>Rap1b</i>	595280	Q62636	4	2	5.37	20929	signaling	prenylation
<i>Ras-like protein TC25</i>	27662306	x	3	1	9.10	16797	signaling	prenylation
<i>Receptor for advanced glycosylation end products</i>	498034	Q63495	12	-	5.83	42664	signaling	1
<i>Seven transmembrane receptor</i>	5525078	Q9WV70	4	-	6.46	149446	signaling	7
<i>Tapasin</i>	13399280	Q99JC6	4	1	7.74	50045	other	1
<i>Thrombomodulin</i>	2502062	P07204	6	-	4.78	60329	signaling	1
<i>TIE-2</i>	34869831	Q9QW24	5	-	5.94	95115	signaling	1
<i>Transmembrane 4 superfamily member 3</i>	6179618	O55158	5	-	5.64	25545	signaling	4
<i>VAMP-associated protein A</i>	4240462	Q9Z270	3	4	8.58	27223	traffick	1
<i>Vascular endothelial-cadherin</i>	34851204	P55284	7	-	5.12	83275	adhesion	1

## Cytoskeletal and/or junctional proteins

Protein name	NCBI locus	SwissProt or Trembl locus	Number of MS/MS spectra		PI	MW	Function	predicted TMs
			Lung P	RLMVEC				
<i>Actin - alpha</i>	511131	P04270	29	30	5.23	42019	structural	
<i>Actin - beta</i>	13592133	P02570	30	21	5.29	41737	structural	
<i>Actin - gamma</i>	27714843	x	9	14	5.21	35162	structural	
<i>Actinin 1- alpha</i>	4210985	Q9Z1P2	15	35	5.23	102960	structural	
<i>Actinin alpha-4</i>	6636119	Q9QXQ0	9	19	5.24	104786	structural	
<i>Adducin, alpha</i>	1200129	Q63028	9	1	5.81	80355	structural	
<i>Adducin, gamma</i>	1041240	Q62847	4	3	5.46	78804	structural	
<i>Afadin (I)</i>	2555011	O35889	8	1	5.82	207678	structural	
<i>Ankyrin G</i>	3885972	x	3	1	7.94	284459	other	
<i>Catenin alpha</i>	34878659	x	34	1	5.92	105787	structural	
<i>Catenin beta</i>	16758082	Q9WU82	16	1	5.53	85455	structural	
<i>Catenin delta-1</i>	34856482	x	18	1	5.96	101396	structural	
<i>Desmin</i>	1352241	P48675	5	6	5.21	53326	structural	
<i>Desmoplakin I</i>	34875216	x	3	-	5.92	105787	structural	
<i>Desmoslin</i>	27676906	Q810D0	3	-	5.06	140733	structural	
<i>Dynein, heavy chain</i>	31377489	P38650	5	30	6.04	532025	structural	
<i>Epiplakin 1</i>	34867002	x	6	3	5.65	368204	structural	
<i>ERM-binding phosphoprotein</i>	8132349	Q9JJ19	12	1	5.70	38830	structural	
<i>Ezrin</i>	17902245	x	60	21	5.59	138687	structural	
<i>F-actin capping protein alpha-1</i>	34859736	x	5	3	5.43	32910	structural	
<i>F-actin capping protein alpha-2</i>	34883261	x	5	3	5.57	32967	structural	
<i>F-actin capping protein beta</i>	34872216	x	7	3	5.69	30629	structural	
<i>Filamin 1</i>	34881882	x	61	81	5.67	279442	structural	
<i>Fodrin alpha chain</i>	3462887	P16086	227	109	5.20	284638	structural	
<i>Gelsolin</i>	34853856	x	9	4	6.22	84946	structural	
<i>Junction plakoglobin</i>	1497985	P14923	16	-	5.95	81498	structural	
<i>Kinesin heavy chain 5B</i>	27687147	x	5	5	6.25	97300	other	
<i>Kinesin heavy chain 5C</i>	34854278	x	6	3	5.99	114413	other	
<i>Microtubule-associated protein 1B</i>	1083716	x	5	2	4.73	259025	structural	
<i>Microtubule-associated protein 4</i>	34866431	x	8	7	5.29	303149	structural	
<i>Moesin</i>	2218139	x	94	41	5.75	206407	structural	
<i>Myosin heavy chain, smooth muscle</i>	92503	x	7	5	5.19	47803	structural	
<i>Myosin heavy chain-A, nonmuscle</i>	967249	x	142	139	5.49	226338	structural	
<i>Myosin heavy chain-B, nonmuscle</i>	7381235	x	51	112	5.49	228965	structural	
<i>Myosin I beta</i>	13431669	Q05096	10	4	9.42	131918	structural	
<i>Myosin I gamma</i>	23821864	Q63357	4	3	9.45	116137	structural	



Myosin light chain 1	56670	x	6	-	5.03	22156	structural
Myosin light chain 1, atrial	57513	x	8	1	4.96	21282	structural
Myosin regulatory light chain 2-A, smooth muscle isoform	57087	x	15	15	4.67	19895	structural
Myosin VI	34865321	x	5	-	8.59	116960	structural
Myosin, unconventional Myr2 I heavy chain	12831209	x	15	29	9.41	118090	structural
Myotonic dystrophy kinase-related Cdc42-binding kinase beta	7446380	O54875	11	1	6.38	194020	signaling
N-WASP	2274845	O08816	4	1	8.33	54325	structural
Periplakin	34868748	x	7	1	5.35	204147	structural
Plectin	1709655	P30427	160	24	5.71	533540	structural
Radixin	34863387	x	60	26	5.69	66125	structural
Spectrin, beta	34879632	x	137	52	5.48	278423	structural
Spectrin-like protein GTRAP41	11066461	Q9QWN8	11	1	5.59	271064	structural
Tau -big	207158	x	5	-	5.54	71774	other
Tensin	27684945	x	16	2	6.29	64171	structural
Tight junction protein 1 - ZO1	34857171	x	26	-	5.96	215532	structural
Tight junction protein 2 - ZO2	1839162	Q9UDY2	15	-	6.96	133972	structural
Transgelin 2	27678408	x	3	2	8.41	22393	other
Tripartite motif protein TRIM2	34857890	x	3	-	6.78	90452	other
Tripartite motif protein TRIM3	21362968	O70277	5	-	8.17	80796	other
Tropomodulin 1	1628561	P70567	4	-	4.97	40480	structural
Tropomodulin 2	13928838	P70566	3	-	5.34	39492	structural
Tropomodulin 3	34864364	x	6	4	4.91	46416	structural
Tropomyosin 2	112442	P04692	11	6	4.71	32695	structural
Tropomyosin 3	17105362	Q63600	13	4	4.68	32819	structural
Tropomyosin 4	136081	P09495	7	4	4.66	28510	structural
Tubulin, alpha-1	55777	x	14	11	4.94	50136	structural
Tubulin, Beta 3	21245098	x	6	3	4.88	50303	structural
Tubulin, beta-2	37494	P05217	22	7	4.79	49831	structural
Tubulin, beta-5	27465535	P05218	25	11	4.78	49640	structural
Utrrophin	2960013	x	16	2	5.18	391075	structural
Vimentin	57480	P31000	26	42	5.06	53602	structural
WASP interacting protein	12275264	x	5	-	11.42	49751	structural

### Peripherally associated on inside

Protein name	NCBI locus	SwissProt or Trembl locus	Number of MS/MS spectra			MW	Function	predicted TMs
			Lung P	RLMVEC	PI			
Abl-interactor 1	13242310	x	3	1	6.57	51705	signaling	
Adaptin, alpha A	113337	x	5	1	6.51	104045	traffick	
Adaptin, alpha-C	90292	P18484	14	1	6.53	103913	traffick	
Adaptin, beta	18034787	P21851	11	1	5.19	105691	traffick	
Adaptin, beta-3A	34857415	x	3	1	5.47	119142	traffick	
Annexin A11	1351943	P48037	6	-	5.39	75623	signaling	
Annexin A2	294518	Q07936	39	33	7.53	38547	signaling	
Annexin A3	113955	P14669	4	-	6.04	36322	signaling	
Annexin A4	1703320	P55260	14	-	5.32	35744	signaling	
Annexin A6	763181	P48037	24	8	5.39	75623	signaling	
Arginosuccinase	31377525	x	3	-	5.88	51391	ee	
Arrestin beta-1	203102	P29066	9	-	5.84	47066	traffick	
Arrestin C	543855	P36576	3	-	5.48	9878	traffick	
Beta-adrenergic receptor kinase 1	114153	P26817	7	-	6.54	79785	signaling	
Calgranulin A	13638435	P50115	4	-	5.69	10107	other	
Calgranulin B	478287	P50116	10	-	7.24	13014	other	
Calmodulin	230824	P02593	4	3	4.09	16706	other	
Cdc42 guanine nucleotide exchange factor zizimin 1	34876077	x	4	-	7.44	260094	signaling	
Centaurin-alpha2	7636039	Q9JK15	4	-	9.35	43524	other	
Clathrin coat assembly protein AP50	113332	P20172	7	1	9.57	49655	traffick	
Cytosolic sorting protein PACS-1a	3347953	O88588	6	-	7.61	104700	traffick	
Dynamin II	729380	P39052	6	4	6.30	44036	traffick	
E3KARP, NHE3 kinase A regulatory protein	13925523	x	24	-	5.36	84531	signaling	
EBP50-PDZ interactor	34879000	x	4	1	7.61	56788	other	
Exo70	2827160	O54922	3	-	6.27	75046	traffick	
Exocyst complex component Sec3	27694722	x	3	1	6.93	64552	traffick	
Exocyst complex component Sec5	19705549	O54921	4	3	6.67	104031	traffick	
G-protein-coupled receptor kinase 5	2499663	Q62833	4	-	8.48	67783	signaling	



Granzyme K	1708036	P49864	4	-	9.59	28465	signaling
Growth-arrest-specific protein 7	25742641	x	4	2	7.24	50394	other
GTPase activating protein 1	34857388	x	26	3	6.13	193859	signaling
Heat shock cognate 71 kDa protein (HSC73)	56379	P08109	13	2	5.37	70871	other
Hic-5/ARA55 protein	12659068	Q99PD6	3	-	8.36	36181	other
Integrin-linked kinase	13111653	O55222	24	6	8.30	51373	signaling
Janus protein tyrosine kinase 1	2288925	O35803	3	-	8.26	99649	signaling
Latent TGF-beta binding protein-2 like protein	2463409	O35806	3	12	5.20	189867	structural
Lim protein 1 (FHL-1)	4894849	Q9WUH4	3	1	8.76	31904	other
Methionine aminopeptidase 2	204004	P38062	7	-	5.72	53052	ee
Munc18-3	12583689	Q99PV2	3	-	8.28	68021	transport
Neurofibromin 2	32363191	Q63648	3	1	6.20	68712	structural
Numb protein isoform	34867377	x	7	-	9.32	69246	other
Parvin-alpha	13526899	Q9HB97	5	2	5.69	42292	structural
Parvin-beta	34867494	x	3	-	5.90	41701	structural
Peptide N-myristoyltransferase 1	22507314	x	7	1	9.14	56937	other
Periaxin	18642399	Q63425	28	1	8.60	146400	other
Peroxiredoxin 4	4336879	Q9Z0V5	3	1	5.86	30540	other
Phosphatidylinositol 4-kinase, 230kDa	1944499	O08662	3	-	6.57	231320	signaling
Phosphatidylinositol-4-phosphate 5-kinase type II alpha	16758974	Q9R0I8	5	-	6.50	46225	signaling
Phosphatidylinositol-4-phosphate 5-kinase type II beta	16758316	O88377	5	-	7.18	47264	signaling
Phosphatidylinositol-4-phosphate 5-kinase type II gamma	17978457	O88370	4	1	6.39	47336	signaling
Phosphatidylinositol-binding clathrin assembly protein	16758324	O55012	4	2	8.58	69286	traffick
Phospholipase C-beta-1	91896	P10687	10	1	5.86	138344	signaling
Phospholipase C-beta-3	13177635	P51432	21	1	5.77	139492	signaling
Phospholipase C-beta-4	435757	Q9QW07	13	1	6.41	134497	signaling
Phospholipase C-beta-4B	4063009	x	10	1	6.11	116040	signaling
Phospholipase C-gamma-2	130230	P24135	4	-	6.40	147735	signaling
Pincher	20135683	Q8R3Z7	19	2	6.33	61468	traffick
Prohibitin	13937353	x	3	11	5.57	29820	other
Proline rich synapse associated protein 2	5262748	Q9JLU4	13	2	8.98	193258	traffick
Protein kinase A anchoring protein 2	34868424	x	9	-	4.88	90962	signaling
Protein kinase C delta bindig protein	4092842	x	8	5	5.79	27910	signaling
Protein tyrosine phosphatase, non-receptor type 6	16758788	P81718	8	-	7.63	69578	signaling
Protein-tyrosine phosphatase, non-receptor type 6	16758788	x	9	-	7.63	69578	signaling
Ral simian leukemia viral oncogene homolog A	29741807	x	3	-	9.34	24325	signaling
Ras suppressor protein 1	34877253	x	18	5	5.34	347557	signaling
Ras-binding protein SUR-8	27685625	x	4	-	9.19	32823	signaling
Rho- and Arf-GTPase activating protein 1	27682975	x	6	-	5.68	235892	signaling
Rho GTPase activating protein 5	34865207	x	4	1	6.15	172287	signaling
RhoGEF glutamate transport modulator GTRAP48	13027442	x	3	-	5.50	168534	signaling
Rho-interacting protein 3	10803059	Q9ERE6	7	13	5.95	117113	signaling
Scaffolding protein SLIPR	7650497	x	5	-	5.80	129405	other
Septin 2	13928415	x	14	16	6.15	41593	structural
Septin 4	34872968	x	7	-	5.81	53083	structural
Septin 7 (CDC10)	9789715	Q9WVC0	20	15	8.82	50508	structural
Septin-like protein	28849875	Q9QZR6	3	2	8.65	63792	structural
Serine proteinase inhibitor 3	111807	P09006	3	-	5.32	46652	other
Serine/threonine kinase 10	9507151	x	5	-	9.44	57390	signaling
Serine/threonine kinase MARK2	2052191	O08679	3	-	9.63	80872	signaling
Serine/threonine protein kinase TAO1	7514084	O88664	3	-	7.30	115952	signaling
Serine/threonine protein phosphatase PP1 M110 subunit	802105	x	4	-	5.30	109720	signaling
Serine/threonine protein phosphatase PP1B	585712	P37140	4	4	5.84	37187	signaling
Serum deprivation response	34875838	x	12	2	5.21	46386	signaling
Smad1	3192871	P97588	3	-	6.90	52713	signaling
SNAP-23	2970673	O70377	5	3	4.82	23235	traffick
Sodium-hydrogen exchanger 3 regulatory factor 1	11024674	x	7	-	5.70	38830	signaling
Sodium-hydrogen exchanger 3 regulatory factor 2	15419607	x	23	-	7.25	37369	signaling
Syndapin 2	6651167	Q9QY17	12	-	5.04	55978	traffick
Thioredoxin-dependent peroxide reductase 2	2499470	Q63716	7	4	8.27	22109	other
Thrombospondin 1	33340123	AAQ14549	4	9	4.74	129671	adhesion
TOAD-64	1351260	P47942	3	9	5.95	62278	other
TPR-containing Rab8b-interacting protein	27465633	Q925N3	3	-	5.12	64885	other
Ubiquitin	20302085	x	4	5	6.94	34361	other



## Outside bound - secreted / blood

Protein name	NCBI locus	SwissProt or Trembl locus	Number of MS/MS spectra		PI	MW	Function	predicted TMs
			Lung P	RLMVEC				
Apolipoprotein A-I	91984	P04639	3	-	5.52	30088	other	
Beta-2-microglobulin	999862	P07151	4	-	7.80	13720	other	
Fetuin	112459	P24090	5	-	6.05	37982	other	
Fibrinogen B, beta chain.	455105	P14480	6	-	7.89	54303	other	
Fibronectin	120178	P04937	3	117	5.50	272511	other	
Glutathione peroxidase	121668	P04041	7	2	7.65	22258	other	
Hemoglobin, alpha chain	1304381	P01946	12	-	7.93	15197	other	
Hemoglobin, beta chain	204570	P02091	5	-	7.99	15848	other	
Hepatoma-derived growth factor related protein 3	21955178	Q9D2M7	6	-	8.4	22447	other	
Histidine-rich glycoprotein 1	13358876	x	13	-	7.76	59049	other	
Histidine-rich glycoprotein 2	13358878	x	14	-	7.55	58056	other	
Inter-alpha-inhibitor H4P heavy chain	7441758	O35802	4	-	6.08	103607	other	1
Laminin alpha-5	34860912	x	3	6	6.21	415468	other	
Laminin beta-1	27717157	x	3	2	4.82	21738	other	
Laminin gamma-1	27712576	P11047	3	3	5.20	167423	other	
Mast cell protease 8	8928167	P97594	6	-	9.02	27486	other	
Mast cell protease 9 (Granzyme J)	1763232	P97595	6	-	9.33	26314	other	
Prolargin	10834558	Q9EQP5	15	1	9.51	43179	other	
Serum albumin	55628	P02770	16	1	6.09	68719	other	
Spondin	544353	P35446	7	-	5.85	90773	other	
Transferrin	1854476	P12346	7	1	6.94	76364	other	
Vitronectin	1255044	Q62905	6	-	5.68	54679	other	
Von Willebrand factor	4467984	P04275	12	-	5.32	309299	other	

## Poorly characterized proteins (unknown localization, structure, and function)

Protein name	NCBI locus	SwissProt or Trembl locus	Number of MS/MS spectra		PI	MW	Function	predicted TMs
			Lung P	RLMVEC				
Ac2-233	32527749	Q7TPJ1	3	-	6.16	161633		
Brain-enriched WD-repeat protein	13660779	x	6	-	6.74	57551		
cDNA Sequence BC019977	34871032	x	3	-	9.99	90565		
DAMP-1 protein	28070980	Q811A2	4	-	8.38	19674		2
EH-domain containing protein 2	34452241	Q8R491	5	2	5.95	61106		
EH-domain containing protein 3	34536836	x	6	2	6.04	60807		
Granzyme-like protein II	296176	Q06606	7	-	8.74	27463		
Hypothetical protein FLJ10849	34876531	x	18	20	6.47	58774		
Hypothetical protein FLJ13187	34866158	x	3	-	8.55	27741		
Hypothetical protein FLJ20401	34856089	x	6	-	7.62	98851		
Hypothetical protein FLJ30973	34864323	x	4	-	5.55	61017		
Hypothetical protein KIAA0332	27721099	x	3	-	7.32	110303		
Hypothetical protein KIAA0635	27694697	x	3	2	5.66	55620		
Hypothetical protein KIAA0763	27712638	x	3	1	8.86	139934		
Hypothetical protein KIAA0915	27672832	x	8	-	8.66	91406		
Hypothetical protein KIAA0982	27688091	x	4	-	5.69	57127		
Hypothetical protein KIAA1902	27699143	x	3	-	6.16	89929		
Hypothetical protein XP_238419	27716235	x	4	1	10.00	9379		
Hypothetical RNA binding protein RDA288	18041977	x	6	16	8.42	43012		
Similar to KIAA1185 protein	34872773	x	6	1	8.52	63531		
Lethal giant larvae-like protein 1 homolog	22779849	x	3	-	6.14	112495		
Neuronal tissue-enriched acidic protein	11560135	x	3	5	4.50	21790		
Protein kinase SK2	7514055	x	12	1	4.96	137888		
RIKEN cDNA 2010012F05	34859075	x	3	2	4.80	23760		
Similar to a C.elegans protein RW1	34875601	x	3	1	7.24	190311		2
Similar to actin binding protein-278	34869526	x	23	30	5.41	284704		
Similar to Brain-Specific Protein p25 Alpha	27729783	x	3	-	9.71	54772		
Similar to BUB3	34859446	x	12	-	6.32	30535		
Similar to cask-interacting Protein 2	34875360	x	4	-	6.58	127726		
Similar to CGI-74 protein	34855164	x	3	-	11.56	26564		
Similar to chromodomain-helicase-DNA-binding protein 5	34860336	x	3	5	5.74	301239		



Similar to cleavage and polyadenylation specific factor 6	34864893	x	4	1	9.14	69006	
Similar to cobl-related protein 1	34854739	x	3	-	6.39	135106	
Similar to cytochrome b5 Reductase 1	27712062	x	3	1	8.95	34233	
Similar to DEAD-box protein 05	27690065	x	14	6	9.06	69239	
Similar to DEAD-box protein 17	34866944	x	8	5	8.75	73945	
Similar to DEAH box protein 15	34878065	x	4	1	7.12	90977	
Similar to dJ1033H22.1 (KIAA0554)	34860217	x	9	-	6.40	68740	
Similar to DNA-PKcs	34870011	x	3	1	6.90	470420	
Similar to DOCK180 protein	34874363	x	4	-	7.15	218571	
Similar to DRIM (downregulated in metastasis) protein	27717947	x	3	1	8.59	289353	
Similar to ELMO1	34876187	x	6	-	5.86	44456	
Similar to ELMO2 (KIAA1834)	34860711	x	3	-	5.91	86108	
Similar to eukaryotic translation initiation factor 5A	27672956	Q8VHU8	5	6	5.07	16832	
Similar to fibrillarin	34855407	x	3	10	10.25	34222	
Similar to FK506 binding protein 3	27664664	x	5	2	9.29	25148	
Similar to FSHD region gene 1 protein	34872381	x	5	-	8.95	29031	
Similar to Hbs1l protein	34852821	x	3	-	9.17	47772	
Similar to heat shock 70 kDa protein 12A (HSPA12A)	34864793	x	3	1	8.87	129368	
Similar to heat shock 70 kDa protein 12B (HSPA12B)	34858716	x	25	-	8.58	81822	
Similar to HSPC315	34871854	x	3	-	6.37	28146	
Similar to hypothetical protein	27710240	x	6	-	8.47	77072	
Similar to hypothetical protein MGC29390	34869210	x	3	1	6.53	202867	
Similar to Integrin alpha-L	34859294	x	5	-	6.15	151135	
Similar to KIAA1083 protein	34862486	x	3	-	9.61	69002	
Similar to KIAA1230 protein	27713641	x	3	-	5.43	111708	1
Similar to KIAA1849 protein	27731437	x	6	-	11.27	18939	
Similar to LD39815p	27716313	x	3	1	6.23	29077	
Similar to leiomodlin 1	34880269	x	3	-	9.27	62197	
Similar to Map4k6-pending protein	34871056	x	4	-	8.00	56056	
Similar to mBLVR	34862288	x	4	-	8.11	81993	
Similar to mitochondrial import receptor subunit TOM34	34860666	x	3	-	9.23	34461	
Similar to mKIAA0219	34872627	Q92616	4	7	7.36	303089	
Similar to myeloperoxidase	34873270	x	3	-	9.61	80883	
Similar to Na <sup>+</sup> and H <sup>+</sup> -coupled glutamine transporter	16923996	Q8VEK3	9	16	5.92	87748	0
Similar to nebulin	34854661	x	3	1	9.08	909311	
Similar to nicotinamide nucleotide transhydrogenase	34854180	Q13423	3	9	9.17	34922	12
Similar to nuclear receptor coactivator NCoA-62	34867492	x	3	2	9.00	145690	
Similar to OSBP-related protein 6	34856448	x	3	-	6.63	105187	
Similar to osmotic stress protein	34856875	x	3	3	9.91	35022	2
Similar to p53 inducible protein	34870680	x	7	-	6.10	127654	
Similar to polymerase I-transcript release factor	27689507	x	25	5	5.43	43909	
Similar to pre-mRNA cleavage factor Im (25kD)	12655103	x	13	3	8.85	26227	
Similar to protein disulfide isomerase A5	34869214	x	3	-	6.35	89317	
Similar to protein disulfide isomerase-related protein	34869214	x	4	2	6.35	89317	
Similar to PTB-associated splicing factor	34871066	x	6	10	8.94	65137	
Similar to PTPL1-associated RhoGAP 1	34862742	x	6	-	5.83	128868	
Similar to Rab8-Interacting Protein	34861505	x	3	-	6.06	91387	
Similar to rho/rac guanine nucleotide exchange factor ,GEF	27693092	x	4	-	5.39	72437	
Similar to ribosome binding protein 1	34858829	x	8	9	9.00	143328	
Similar to RIKEN cDNA 1190003A07	34861128	x	3	1	5.46	156956	
Similar to RIKEN cDNA 1500019M23	34932774	x	3	2	8.99	20550	
Similar to RIKEN cDNA 1810013P09	34855823	x	3	-	8.66	38164	
Similar to RIKEN cDNA 3010001A07	34868074	x	4	1	6.92	82148	2
Similar to RNA helicase (DEAD-box protein 03)	34933204	x	7	13	6.18	69437	
Similar to Schwachman-Bodian-Diamond syndrome protein	27664348	x	4	1	8.91	28753	
Similar to selective hybridizing clone (SHYC)	34856144	x	9	-	6.89	164053	
Similar to SET binding factor 1	34867669	x	3	1	8.41	196456	
Similar to slingshot 1	34872826	x	4	1	6.36	178058	
Similar to small nuclear ribonucleoprotein associated protein N	27687269	Q63747	6	3	11.31	124746	
Similar to small nuclear ribonucleoprotein Sm D2	27676406	x	3	3	9.92	13527	
Similar to small nuclear ribonucleoprotein Sm D2	27676406	x	3	3	9.92	13527	
Similar to small nuclear ribonucleoprotein U1A	34855379	x	4	-	6.40	15295	
Similar to splicing factor (CC1.3)	34860256	x	4	-	10.23	68157	
Similar to splicing factor PRP8	34872765	x	3	-	8.86	304438	
Similar to splicing factor SC35	27691222	x	3	-	11.86	25476	
Similar to splicing factor U2AF 65 kDa subunit	34854490	x	9	-	4.98	28114	
Similar to sulfide quinone reductase	34856819	x	5	5	9.02	69000	
Similar to SWI/SNF complex 170 kDa subunit	34862210	x	5	2	5.28	126799	
Similar to talin 2	34864297	x	77	37	5.47	284529	



Similar to Tenc1 protein	34868665	x	3	-	8.63	164794		
Similar to TMP 2	34862084	x	3	-	7.73	163993		1
Similar to transcription factor BTF3	27686915	x	8	3	6.85	17699		
Similar to transcription factor CA150	34879270	x	10	-	8.80	123020		2
Similar to Transcription Initiation Factor IIE, Alpha Subunit	27666810	x	3	1	4.72	49229		
Similar to transcription termination factor I interacting peptide 20	34854655	x	3	-	8.69	42723		
Similar to transcriptional activator Pur-alpha	34878862	x	4	2	6.07	34884		
Similar to tyrosyl-tRNA ligase	34871588	x	7	1	8.61	63026		
Similar to U2 small nuclear ribonucleoprotein B	34858820	x	3	-	9.72	25352		
Similar to vinculin	34868946	x	12	7	5.52	135513		
Similar to WD repeat endosomal protein	34866638	x	3	-	7.05	84698		
Similar to Werner syndrome helicase homolog	34878743	x	3	-	5.31	99948		
Similar to zinc finger protein Cezanne	34858073	x	3	2	6.85	150318		
Similar to zinc finger transcription factor ZNF207	34872895	x	4	-	9.20	52779		
TEMO (novel testicular molecule)	9954445	Q9ESY1	3	-	6.71	206589		
Thyroid hormone receptor interactor 10 (salt tolerant protein)	16758800	P97531	4	3	5.23	62788		

### Ribosomal proteins

Protein name	NCBI locus	SwissProt or Trembl locus	Number of MS/MS spectra		PI	MW	Function	predicted TMs
			Lung P	RLMVEC				
ABC50	10863747	Q9ERQ2	4	-	6.79	92749		
Acidic ribosomal phosphoprotein P0	11693176	P19945	4	-	5.91	34215		
Elongation factor 1-alpha 1	1220484	Q64718	31	20	9.10	50150		
Elongation factor 1-alpha 2	206440	P27706	5	1	9.11	50454		
Eukaryotic translation initiation factor 1, alpha subunit	1352425	P47813	3	-	4.91	46416		
Eukaryotic translation initiation factor 2, alpha subunit	325	P05199	9	2	5.02	35977		
Eukaryotic translation initiation factor 2, beta subunit	27703942	x	7	1	5.61	38243		
Eukaryotic translation initiation factor 2, gamma subunit	27663888	x	10	3	9.51	17740		
Eukaryotic translation initiation factor 5	585303	Q07205	5	1	5.36	48954		
Ribosomal proteins large subunit family	x	x	x	x	basic	x		
Ribosomal proteins small subunit family	x	x	x	x	basic	x		
Ribosomal S6 kinase alpha 1	13592065	Q63531	3	-	7.97	82883		

### Endoplasmic reticulum proteins

Protein name	NCBI locus	SwissProt or Trembl locus	Number of MS/MS spectra		PI	MW	Function	predicted TMs
			Lung P	RLMVEC				
78 KD Glucose-regulated protein	121574	P06761	10	50	5.07	72347		
Calnexin	543922	P35565	7	23	4.49	67255		1
Calreticulin	55855	P18418	10	15	4.33	47995		
Cytochrome b5, ER	231928	P00173	3	1	4.90	15224		
Cytochrome P450 2B1	223633	P00176	3	-	7.00	55934		1
Flavin-containing monooxygenase 1	204152	P36365	5	-	8.66	59781		1
Heat shock protein 47 kDa	8393057	P29457	6	15	8.88	46518		
NADH-cytochrome b5 reductase	127847	P20070	7	3	8.57	34043		
NADPH-cytochrome P450 reductase	3318958	P00388	5	5	5.30	76832		1
Peptidyl-prolyl cis-trans isomerase B	2143900	P24368	19	15	9.30	23025		
Prostaglandin F2 receptor negative regulator	2497303	Q62786	3	1	6.16	98731		1
Protein disulfide isomerase A3	56905	P11598	21	36	5.88	56623		
Protein disulfide isomerase A6	2501206	Q63081	3	15	4.95	47220		
Ribophorin I	132560	P07153	4	16	6.05	68304		1
Ribophorin II	132562	P25235	4	5	5.72	69061		3



**Mitochondrial proteins**

Protein name	NCBI locus	SwissProt or Trembl locus	Number of MS/MS spectra		PI	MW	Function	predicted TMs
			Lung P	RLMVEC				
Acetoacetyl-CoA thiolase	135757	P17764	4	3	8.92	44695		
Acetyl-CoA acyltransferase	135762	P13437	3	3	8.09	41871		
Aldehyde dehydrogenase, mitochondrial	118505	P11884	3	4	6.63	56488		
ATP synthase CF(0) - B chain, mitochondrial	114625	P19511	3	6	9.39	28869		
ATP synthase CF(0) - D chain, mitochondrial	220904	P31399	4	8	6.21	18632		
ATP synthase CF(1) - alpha chain, mitochondrial	6729934	P15999	14	22	9.22	58826		
ATP synthase CF(1) - beta chain, mitochondrial	1374715	P10719	17	23	5.18	56354		
Cytochrome b5, mitochondrial	2253161	P04166	3	1	4.92	16265		
Cytochrome c, somatic	118008	P00009	4	6	9.61	11474		
Glutamate dehydrogenase	6980956	P10860	12	13	8.05	61428		
Heat shock 40 kDa protein 4	1706475	P54102	4	3	6.65	44868		
NADP+-specific isocitrate dehydrogenase	13928690	x	4	7	6.53	46734		
PDC-E2	266685	P08461	3	3	5.70	58764		
Succinyl-CoA synthetase, alpha chain	135025	P13086	4	9	9.54	35032		
Trifunctional enzyme, alpha subunit	510108	Q64428	8	14	9.11	82513		
Trifunctional enzyme, beta subunit	543387	Q60587	5	3	9.50	51414		
Ubiquinol-cytochrome C reductase complex core protein 2	418146	P32551	3	6	9.16	48373		

**Nuclear proteins**

Protein name	NCBI locus	SwissProt or Trembl locus	Number of MS/MS spectra		PI	MW	Function	predicted TMs
			Lung P	RLMVEC				
2',3'-cyclic nucleotide 3'-phosphodiesterase	294527	Q64575	4	-	9.03	47268		
Centrosomal protein 2	27704348	Q9BV73	3	2	4.98	208800		
DNA mismatch repair protein Msh2	1709122	P54275	3	1	5.77	104028		
DNA topoisomerase I	4809197	x	5	1	9.35	90760		
FBP-interacting repressor	5524727	Q9NZA0	6	1	5.25	58171		
G10 protein homolog (edg-2)	3064070	Q70454	6	-	9.15	17069		
High mobility group protein 1	1708258	P07155	24	8	5.70	24894		
High mobility group protein 2	1708260	P52925	20	1	7.10	24028		
Histones	x	x	x	x	x	x		
La Ribonucleoprotein	729919	P38656	4	4	9.47	47777		
Lamin A	1346413	P48679	25	53	6.54	74324		
Lamin B1	1575794	P70615	9	16	5.16	66475		
Lamin C2	1556433	P48679	21	42	6.54	74324		
Nucleolin	92559	P13383	3	-	4.67	77016		
Nucleophosmin	114763	P13084	3	7	4.62	32560		
Poly [ADP-ribose] polymerase-1 (PARP-1)	3123251	P27008	10	1	9.07	112529		
Pyrimidine binding protein 1	13487910	Q00438	3	6	9.14	56937		
Spliceosomal protein SAP155	9885342	Q9ET34	3	-	5.67	54496		
Structural maintenance of chromosome 3	29336525	P97690	3	1	7.82	138448		
Thymopoietin beta (LAMINA-associated polypeptide 2)	6981660	Q62733	4	4	9.40	50278		1
Transcription factor MTSG1	30017413	Q80Z99	3	1	7.20	50728		
Transcription initiation factor RAP30	220891	Q63489	5	1	9.24	28380		



Supplementary Table 2

## Endothelial cell associated marker proteins

Protein name	NCBI locus	SwissProt or TrEMBL locus	Species	Number of MS/MS spectra		predicted TMs
				Rat	Lung	
5'-nucleotidase (CD73)	112826	P21588	R	-	10	1
Adrenergic receptor alpha 2B	2245628	x	H	1	-	7
Alpha-2 macroglobulin	112914	P28666	M	1	-	0
Aminopeptidase N (CD13)	2499898	P97449	R	3	4	1
Angiotensin II receptor (1 or 2)	13591910		R	1	1	7
Angiotensin-converting enzyme (CD134)	11493661	P12821	R	44	-	1
Annexin IV	1703320	P55260	R	14	-	0
Annexin V	4033508	P14668	R	2	2	0
APC protein	114033	P25054	H	2	-	0
Aquaporin-CHIP	267413	P29975	R	3	-	6
Bradykinin receptor B2	456684		R	-	1	7
Carbonic anhydrase IV	544726	P48284	R	11	-	0
Caveolin-1	17017233	Q8VIK9	R	13	5	1
Chemokine receptor CXCR	19879587		M	1	-	7
Dipeptidyl peptidase IV (CD26)	118905	P14740	R	31	-	1
Ecto-apyrase (CD39)	2499219	P55772	M	1	-	2
EDG-1	1352343	P48303	R	1	-	7
EDG-2	729546	P41223	H	3	-	0
EGF	181980	x	H	1	-	1
EGF	1071851	x	M	-	2	2
Endomucin	34860660	x	R	1	-	1
Endothelial actin-binding protein	17486458	P21333	H	61	81	0
Endothelial cell-selective adhesion molecule	13991773	Q925F2	M	5	-	1
Endothelial collagen	17738302	P27658	H	-	3	0
Endothelial differentiation-related factor 1	4503453	O60869	H	2	-	0
Endothelial plasminogen activator inhibitor	129578	P20961	R	0	4	0
Endothelin converting enzyme	529085	P42893	R	7	-	1
H-CAM (CD44)	19923703	O08779	R	2	4	1
Integrin alpha V	1170592	P43406	M	2	5	1
Integrin alpha-1 (CD49a)	124941	P18614	R	8	18	2
Integrin alpha-3 (CD49c)	3183040	Q62470	M	7	-	2
Integrin alpha-5 (CD49e)	1708569	P11688	M	4	6	1
Integrin beta-1 (CD29)	520566	P49134	R	11	10	1
Intercellular adhesion molecule-1 (I-CAM1; CD54)	124100	Q00238	R	6	10	2
Intercellular adhesion molecule-2 (I-CAM2; CD102)	462381	P35330	M	3	-	1
MAC-inhibitor (CD59)	2507508	P27274	R	1	-	2
MDR 1A	266517	P21447	R	1	9	11
MECA32	14161394	x	M	2	1	1
Microvascular endothelial differentiation gene 1	10732861	P97554	R	-	1	1
MRP-1 (CD9)	729088	P40241	R	3	2	4
MUC18	13095926	x	R	5	-	1
Muscarinic acetylcholine receptor M3	92492	x	R	1	1	7
Na <sup>+</sup> /K <sup>+</sup> transporting ATPase alpha 1	18204493	P06685	M	20	18	10
Nicotinic acetylcholine receptor alpha 3	19073315		M	1	-	4
Nicotinic acetylcholine receptor beta 3	113108	P12391	R	1	-	4
Nitric-oxide synthase	266646	P29476	R	1	1	0
P2Y purinoceptor 6	2495019		R	-	1	6
PAR-1B alpha	15042611	x	H	1	-	0
Platelet endothelial tetraspan antigen-3	11968106	Q9QZA6	R	1	3	4
Platelet-derived growth factor receptor	129891	P05622	M	1	1	1
Platelet-endothelial cell adhesion molecule-1 (CD31)	1684839	x	R	4	-	1
Podocalyxin	4996222	x	R	5	-	1
Purinergic receptor 5	34223726	P43657	H	1	-	7
PV-1	5281517	Q9WV78	R	21	-	1
RAGE	2497319	Q63495	R	11	-	1
Scavenger receptor (CD36)	3243055	x	R	1	-	2
Scavenger receptor class B type I	4210542	x	R	1	1	2
Scavenger receptor class F	4507203	x	H	1	-	0
Sialomucin (CD34)	495716	Q64314	M	1	-	1
Thrombomodulin	13929084	x	R	6	-	1
Tight junction protein 1 - ZO1	303710	P39447	M	26	-	0
Tight junction protein 2 - ZO2	1839162	Q9UDY2	R	15	-	0
Transferrin receptor (CD71)	136378	P02786	H	2	1	1
Tumor endothelial marker 4 (TEM4)	15987489	Q96PFE	H	2	-	0
Tumor endothelial marker 6 (TEM6, Tensin 3)	17511209	Q96PE0	H	2	1	0
Tyrosine-protein kinase receptor TIE-2	34869831	Q9QW24	R	5	-	1
Vascular adhesion protein-1	5902787	O70423	M	2	-	1
Vascular cell adhesion protein 1	267284	P29534	R	-	8	1
Vascular endothelial cell specific protein 11	13928415	x	R	14	16	0
Vascular endothelial junction-associated molecule	10720348	P57087	H	2	-	1
Vascular endothelial-cadherin 1	1150514	P55284	M	7	-	2
Vascular endothelial-cadherin 2	8164037	Q9NPG4	H	2	1	1
Von Willebrand factor	4467984	P04275	R	12	-	0



# Subtractive proteomic mapping of the endothelial surface in lung and solid tumours for tissue-specific therapy

Phil Oh, Yan Li, Jingyi Yu, Eberhard Durr, Karolina M. Krasinska, Lucy A. Carver, Jacqueline E. Testa & Jan E. Schnitzer

Sidney Kimmel Cancer Center, 10835 Altman Row, San Diego, California 92121, USA

**The molecular complexity of tissues and the inaccessibility of most cells within a tissue limit the discovery of key targets for tissue-specific delivery of therapeutic and imaging agents *in vivo*. Here, we describe a hypothesis-driven, systems biology approach to identifying a small subset of proteins induced at the tissue–blood interface that are inherently accessible to antibodies injected intravenously. We use subcellular fractionation, subtractive proteomics and bioinformatics to identify endothelial cell surface proteins exhibiting restricted tissue distribution and apparent tissue modulation. Expression profiling and  $\gamma$ -scintigraphic imaging with antibodies establishes two of these proteins, aminopeptidase-P and annexin A1, as selective *in vivo* targets for antibodies in lungs and solid tumours, respectively. Radio-immunotherapy to annexin A1 destroys tumours and increases animal survival. This analytical strategy can map tissue- and disease-specific expression of endothelial cell surface proteins to uncover novel accessible targets useful for imaging and therapy.**

New targets are needed for detecting disease through molecular imaging<sup>1–4</sup> and for treating disease through directed delivery *in vivo*<sup>5–9</sup>. Sequencing the human genome has identified a target pool of 40,000 genes which may translate into a million possible protein targets<sup>10</sup>. Genomic and proteomic analysis of normal and diseased tissues has yielded thousands of genes and gene products for diagnostic and tissue assignment as well as potential therapeutic targets<sup>5–11</sup>. But the sheer number of candidates can overwhelm the required *in vivo* validation process, leading some to question the ultimate impact of these approaches on speeding up drug discovery<sup>5–7,10</sup>. Reducing tissue data complexity to a manageable subset of candidates most relevant to targeting, imaging and treating disease is clearly desired but requires new discovery and validation strategies, that effectively focus the power of global identification technologies.

Selectively targeting a single organ or diseased tissue (such as a solid tumour) *in vivo* remains a desirable but elusive goal for molecular medicine<sup>12,13</sup>. This targeting would allow more effective imaging as well as drug and gene therapies for many acquired and genetic diseases<sup>1–4,6,7,10–13</sup>. Most tissue- and disease-associated proteins are expressed by cells inside tissue compartments not readily accessible to intravenously injected biological agents such as antibodies. This inaccessibility hinders many site-directed therapies<sup>5–7,12,13</sup> and imaging agents<sup>1–4</sup>. For example, multiple barriers to delivery prevent effective immunotherapy for solid tumours *in vivo*, despite efficacy and specificity *in vitro*<sup>12–17</sup>. Conversely, the nearly universal access of chemotherapeutics dilutes efficacy requiring increased dosages, leading to unwanted systemic side effects. Thus, new approaches are required to filter the overabundance of molecular information to allow rapid discovery and validation of accessible tissue-specific targets that can direct molecular imaging and pharmacodelivery *in vivo*.

Here, we divert analytical focus from the poorly accessible cells inside tissues to the critical tissue–blood interface, inherently accessible to agents absorbed or injected into the blood. The endothelium is a minor tissue component that exists as an attenuated cell monolayer lining all blood vessels and is in direct contact with the circulating blood. The tissue microenvironment surrounding blood vessels seems to control the endothelial cell phenotype

*in vivo*<sup>18–22</sup>. But the degree to which normal and diseased tissues can modulate endothelial cell surface protein expression is unknown. Indirect evidence of endothelial cell molecular heterogeneity comes from the reported ability of certain cells and peptide sequences to home to specific tissues after intravenous injection<sup>23–25</sup>. Several receptors to angiogenic factors have been identified<sup>26–28</sup> and genomic analysis of endothelial cells isolated from tumours has provided angiogenic markers of unknown subcellular localization<sup>29</sup>. Genetically induced endothelial cell targets provide ‘proof of principle’ that immuno-targeting endothelium can cause tumour regression<sup>30</sup>; however, few probes to native endothelial cell surface proteins show validated tissue-specific pharmacodelivery *in vivo*<sup>14,15,17,24,31,32</sup>. This paucity of molecular information may reflect the lack of tissue-induced proteins or, perhaps more likely, the difficulty in studying such a minor cell type as it exists natively in the tissue without tissue disruption and isolation. Although gene and immune targeting of tumour neovasculature seems promising<sup>33,34</sup>, the ultimate potential of endothelial targeting in creating new drug delivery systems remains unclear<sup>16,17</sup>. The actual existence of tissue-specific endothelial cell surface targets will remain uncertain until we overcome current technical barriers to comprehensively map and validate tissue-induced endothelial cell surface proteins *in vivo*.

## Molecular diversity of endothelium *in vivo*

To investigate endothelial cell surface heterogeneity *in vivo*, we performed subcellular fractionation to isolate silica-coated luminal endothelial cell plasma membranes and their caveolae directly from normal organs<sup>35,36</sup>. These plasma membranes and their caveolae displayed a greater than 20-fold enrichment for endothelial cell surface or caveolar markers (angiotensin converting enzyme (ACE), vascular endothelial (VE)-cadherin and caveolin-1), whereas markers of intracellular organelles (for example, the Golgi protein  $\beta$ -COP), other tissue cells (for example, E-cadherin for epithelium, fibroblast surface protein) and blood (for example, glycophorin A, CD4 and CD11) were greater than 20-fold depleted (Fig. 1c; data not shown and as shown previously<sup>19,35,36</sup>). This quality control analysis was applied to each isolate.

We analysed these isolated plasma membranes by two-



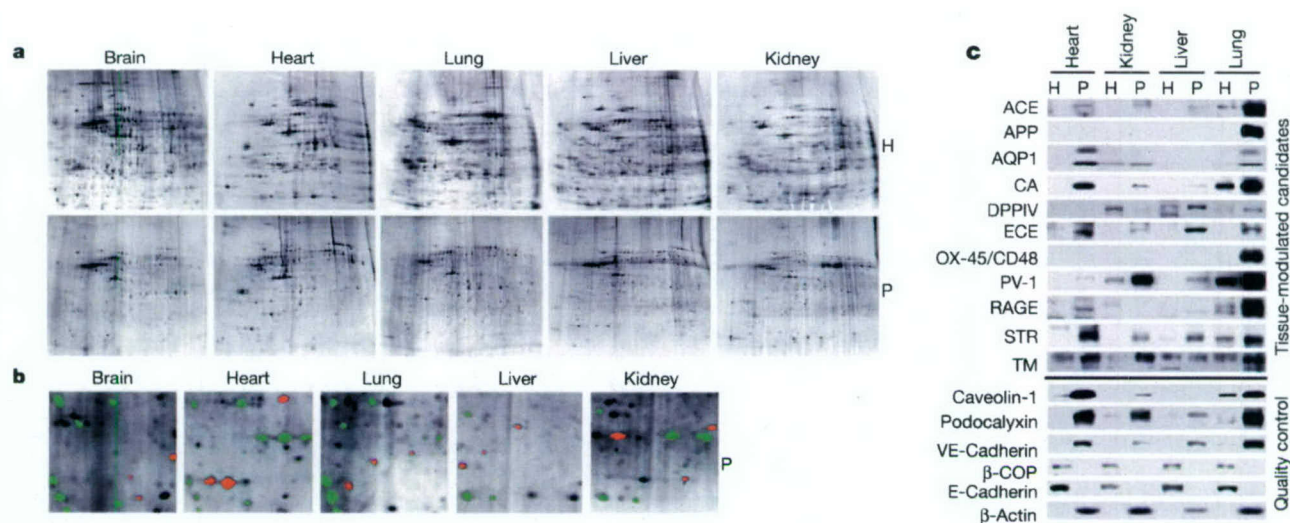


**Figure 1** Molecular heterogeneity of endothelial cell surface in multiple rat organs *in vivo*. **a**, Silver-stained 2D gels of proteins from the whole tissue homogenates (H) and the isolated luminal cell endothelial plasma membranes (P). **b**, Comparison of representative region of 2D gels of endothelial plasma membrane from the indicated rat tissues. Green, protein spots found in  $\geq 2$  tissues; Red, spots not detected elsewhere. **c**, Western blot analysis of proteins from endothelial plasma membranes (10  $\mu$ g) from multiple rat organs

using the antibodies to the indicated proteins. ACE, angiotensin converting enzyme; APP, aminopeptidase P; AQP1, aquaporin 1; CA, carbonic anhydrase; DPPIV, dipeptidyl peptidase IV; ECE, endothelin converting enzyme; RAGE, receptor for advanced glycation end products; STR, seven transmembrane receptor; TM, thrombomodulin.  $\beta$ -COP, coatomer beta subunit.

dimensional (2D) gel electrophoresis to produce high-resolution vascular endothelial protein maps of the major rat organs, that were distinct and much reduced in complexity from that of the starting tissue homogenate (Fig. 1a). Differential spot analysis detected many distinct proteins in plasma membrane versus the homogenate and also in the plasma membrane between organs (Fig. 1b). Western blot analysis further confirmed this heterogeneity (Fig. 1c; data not shown). In many cases, antigens difficult to detect in tissue homogenates were readily apparent in the isolated plasma membranes, reflecting the significant enrichment and increased sensitivity provided by subfractionation to unmask proteins located on the endothelial cell surface. Unique 'molecular fingerprints or signatures' that may include tissue- and cell-specific proteins were apparent for each endothelium.

### Subtractive analysis and profiling

To identify specific proteins expressed at the endothelial cell surface we used mass spectrometry, database searching and immunoblotting, to analyse endothelial plasma membranes and caveolae isolated from rat tissues<sup>35,36</sup>, as well as cultured rat lung microvascular endothelial cells (RLMVEC), isolated and grown in culture<sup>37</sup>. So far, we have identified nearly 2,000 non-redundant proteins (our unpublished observation) which were entered into a database (Accessible Vascular Targets, AVATAR) that was designed and annotated to provide relational analysis between measurements and samples. To identify lung-induced, and possibly, lung-specific endothelial cell surface proteins we used a systems biology approach, based on the hypothesis that the surrounding tissue microenvironment (normal or diseased) modulates protein expression in the vascular endothelium. We subtracted, *in silico*, the proteins identified in endothelial plasma membranes from rat lungs versus RLMVEC because tissue-dependent protein expression may be reduced in cell culture that cannot yet duplicate conditions *in vivo*. To increase certainty of expression *in vivo* versus *in vitro*, we applied a strict identification criterion of  $\geq 6$  tandem mass spectrometry (MS/MS) spectra to rat lung endothelial plasma membranes versus low stringency of  $\geq 1$  MS/MS spectra to RLMVEC

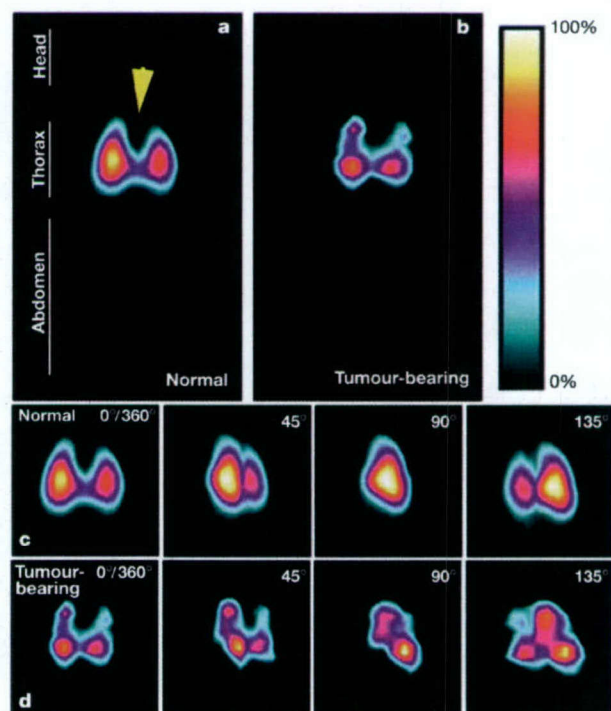


**Figure 2** *In vivo*  $\gamma$ -scintigraphic imaging of APP antibody targeting in normal and tumour-bearing rats. **a**, **b**, Planar images collected 20 min after an intravenous injection of  $^{125}$ I-APP monoclonal antibody into normal female rats (**a**) and female rats bearing metastatic breast adenocarcinoma in the lung (**b**). **c**, **d**, SPECT imaging using a parallel hole collimator of female normal rats (**c**) or rats bearing breast adenocarcinoma tumours in their lungs (**d**) 20 min after tail vein injection with  $^{125}$ I-APP antibodies (50  $\mu$ Ci of IgG at 10 Ci g<sup>-1</sup>). Representative re-projected frames at the indicated degree of rotation are shown. Arrowhead in (**a**) denotes heart cavity.



plasma membranes. From the current rat database of approximately 40,000 entries, we identified 37 differentially expressed proteins. To meet our objective of direct exposure to circulating antibodies, we applied bioinformatic interrogation of structure, glycosylation and membrane orientation to reduce the list to 11 proteins likely to have domains outside the cell.

To confirm the original mass spectrometry findings and to assess organ-specificity, we performed expression profiling with specific antibodies. Consistent with our hypothesis, western blot analysis detected all 11 proteins enriched in lung endothelial plasma membranes (Fig. 1c) but not in RLMVEC plasma membranes (data not shown). Each of these proteins exhibited a different pattern of restricted expression. Two proteins, aminopeptidase P (APP) and OX-45, were detected only in endothelial plasma membranes from lung. Staining of tissue sections with antibodies (including to APP and OX-45) confirmed this restricted expression (data not shown). This profiling by western blot analysis was very sensitive and reliable, even at low expression levels. Thus subtractive

proteomic analysis provided a subset of endothelial cell proteins not expressed *in vitro* and differentially expressed *in vivo*, apparently regulated by the unique tissue microenvironment in each organ.

### Lung-specific targeting *in vivo*

To assess the immuno-accessibility of APP and OX-45 *in vivo*, including possible lung-specific targeting, we intravenously injected  $^{125}$ I-labelled monoclonal antibodies into rats and performed whole-body imaging using planar  $\gamma$ -scintigraphy. Within 20 min, we observed clear lung images, indicating rapid and specific targeting of APP antibody to the lung (Fig. 2a, c). Region-of-interest and biodistribution analysis confirmed this lung-specific targeting with 65% of the injected dose per gram of tissue accumulating in the lungs and less than 2% injected dose per gram of tissue in other organs and blood. Consistent with the low blood levels, the heart cavity was readily apparent (Fig. 2a, arrowhead). Furthermore, this lung targeting was inhibited by addition of a 50-fold excess of unlabelled APP IgG but not with control IgG (data not

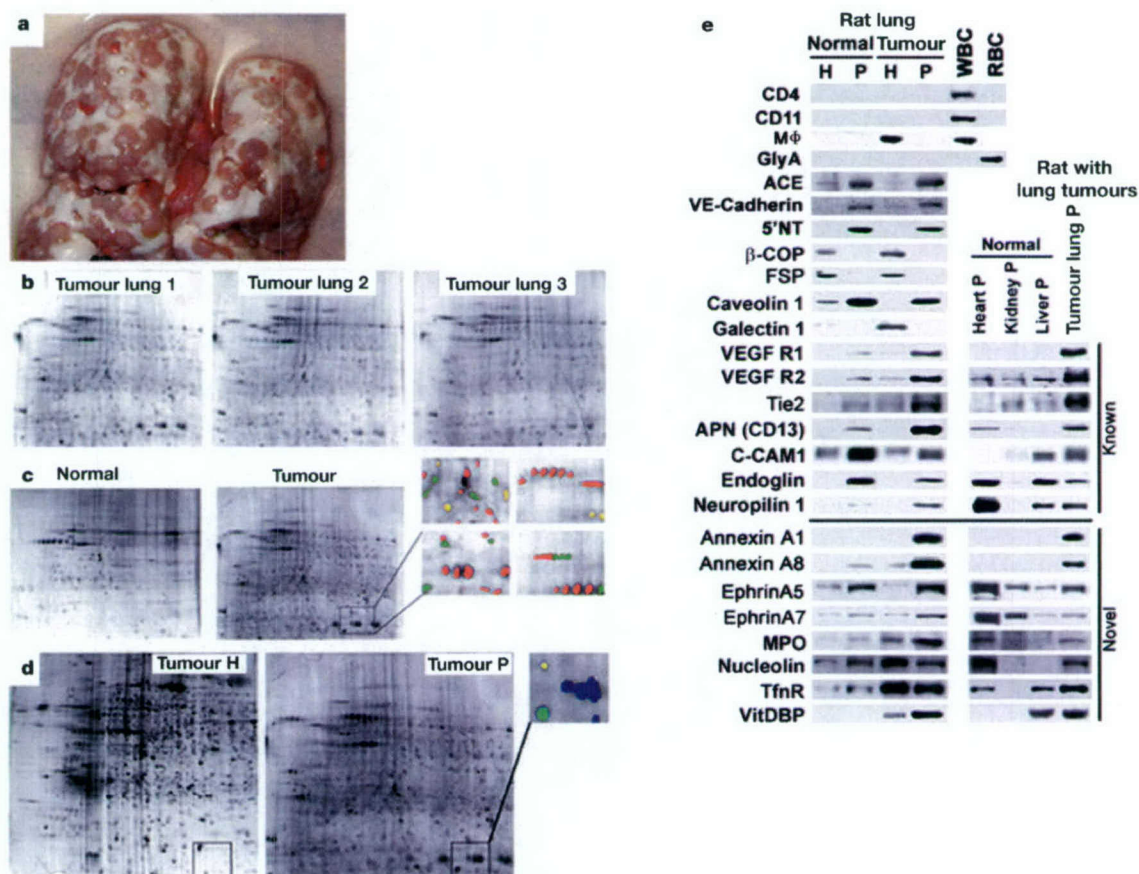


**Figure 3** Mapping rat lung tumours and organs for differential endothelial cell surface protein expression *in vivo*. **a**, Image of representative lungs with multiple solid tumours. **b**, 2D gel analysis of silica-coated luminal endothelial plasma membranes isolated from breast adenocarcinoma tumour-bearing lungs of three different animals. **c**, 2D gel analysis of endothelial plasma membranes from normal rat lungs (left) and lungs bearing breast adenocarcinoma tumours (right). A colour difference map of four small gel regions between normal and tumour endothelial plasma membrane proteins shows relative abundance of protein spots. Green, tumour endothelial plasma membranes > normal endothelial plasma membranes. Yellow, tumour endothelial plasma membranes < normal endothelial plasma membranes. Red, only in the tumour endothelial plasma membranes. Red-edged, tumour endothelial plasma

membranes = normal endothelial plasma membranes. **d**, 2D gel analysis of tumour homogenate (H) (left) and endothelial plasma membranes (P) (right). Yellow, protein spots enriched in the homogenate over plasma membranes. Green, protein spots enriched in plasma membrane over homogenate. Blue, detected only in tumour endothelial plasma membranes and not homogenate. **e**, Western blot analysis of proteins (10 µg) from rat lung homogenate (H) and endothelial plasma membranes (P) from normal organs or tumour-bearing rat lungs using antibodies to the indicated proteins. RBC, red blood cell; WBC, white blood cell; MΦ, macrophage; 5' NT, 5' nucleotidase; GlyA, glycophorin A; FSP, fibroblast surface protein; VEGF R, vascular endothelial growth factor receptor; APN, aminopeptidase N; MPO, myeloperoxidase; TfnR, transferrin receptor; VitDBP, vitamin D binding protein.



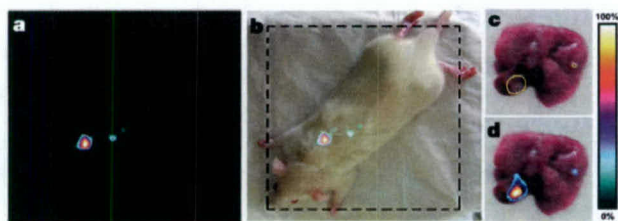


**Figure 4** Tumour-specific targeting of  $^{125}\text{I}$ -AnnA1 antibodies after intravenous injection into tumour-bearing rats. **a**, Whole-body planar  $\gamma$ -scintigraphic imaging 4 h after tail vein injection of  $^{125}\text{I}$ -AnnA1 antibodies ( $50\ \mu\text{Ci}$  of IgG at  $10\ \text{Ci g}^{-1}$ ) into lung-tumour-bearing female rats. **b**,  $^{125}\text{I}$ -AnnA1 antibody signal superimposed onto photo of experimental animal lying on the detector plate. **c, d**, Tumour-bearing lungs were excised for imaging *ex vivo*. Digital image of excised lungs showing location of tumours, circled in yellow (**c**). Overlay of planar images of tumour hot spots with excised tumour-bearing lungs (**d**).

shown), showing the specific ability of our antibodies to bind APP exposed on the endothelial cell surface of the lung but not other organs.

Consistent with OX-45 expression in various leukocytes<sup>38</sup>, we detected OX-45 (but not APP) in blood. Thus, imaging with the OX-45 antibody showed little targeting to the lung (data not shown). Biodistribution analysis confirmed only 2% of the injected dose per gram of tissue accumulating in the lung and greater than 70% of the injected dose per gram of tissue remaining in the blood, primarily bound to the buffy coat subfraction of the blood.

APP was reported to be expressed on mouse blood vessels of normal breast and mammary adenocarcinomas as a target for a homing peptide<sup>39</sup>. High resolution single photon emission computed tomography (SPECT) imaging of  $^{125}\text{I}$ -APP antibodies injected intravenously into female rats detected no accumulation in normal breast tissue (Fig. 2a) or in primary or metastatic breast tumour lesions (Fig. 2b; and multiple images taken over 36 hours (data not shown)). SPECT imaging provided a clear three-dimensional view of normal lungs (Fig. 2c) which was in striking contrast to the irregular images, with multiple nodular regions lacking signal, in rats with mammary adenocarcinomas in the lung (Fig. 2d). Thus, based on the immuno-targeting imaged *in vivo*, endothelial APP expression in the rat appeared quite specific for normal lung tissue, apparently induced by conditions present in the normal lung tissue microenvironment, but absent in the tumour

milieu *in vivo*, even when the tumour blood vessels are derived from the normal lung vasculature.

### Tumour-induced endothelial cell proteins

To determine whether the tumour microenvironment in the lung is sufficiently different to induce new endothelial protein expression, we isolated silica-coated luminal endothelial cell plasma membranes and their caveolae from normal rat lungs and lungs bearing breast adenocarcinomas<sup>35,36</sup> (Fig. 3a). As above, these isolates were significantly enriched relative to the tissue homogenates in endothelial cell surface markers (caveolin, 5' nucleotidase, ACE and VE-cadherin) and markedly depleted in markers of possible contaminants (including  $\beta$ -COP, CD4, CD11, glycophorin A, fibroblast surface protein and galectin-1, that is expressed by the tumour cells<sup>40</sup>) (Fig. 3e and data not shown). The endothelial plasma membranes isolated from tumours expressed multiple angiogenesis markers (enriched relative to both tumour homogenates and normal lung endothelial cell plasma membranes). Lastly, markers of immune cells known to infiltrate solid tumours were detected in tumour homogenates but not its endothelial cell plasma membranes.

We used 2D gels to visualize several hundred protein spots in endothelial cell plasma membranes from normal lungs versus tumours in lungs. These maps were reproducible (Fig. 3b). Multiple protein spots were detected in these tumour but not normal endothelial plasma membranes (Fig. 3c). Prominent 2D spots easily detected in tumour plasma membranes were not detected in the homogenates (Fig. 3d), consistent with the small percentage of endothelial cell plasma membranes in the tumours. Tissue subfractionation appeared necessary to unmask differentially expressed tumour vascular proteins obscured by the molecular complexity of the total tumour.

Again, we applied a subtractive proteomic approach using antibody and mass spectrometric analysis of these plasma membranes and caveolae isolated from them to identify 15 differentially expressed proteins (Fig. 3e), including proteins already implicated in tumour angiogenesis: vascular endothelial growth factor (VEGF) receptors-1 and -2; Tie2; aminopeptidase-N; endoglin; carcino-embryonic antigen-related cell adhesion molecule 1 (CD66)<sup>1</sup> (C-CAM-1) and neuropilin-1<sup>27,28</sup>. These proteins were enriched in the tumour endothelial plasma membranes relative to tumour homogenates, consistent with proper subfractionation. Eight new tumour-induced vascular proteins were also identified: annexin A1; annexin A8; ephrin A5; ephrin A7; myeloperoxidase; nucleolin; transferrin receptor and vitamin D-binding protein. Consistent with the subtractive screen hypothesis, 12 out of 15 proteins were

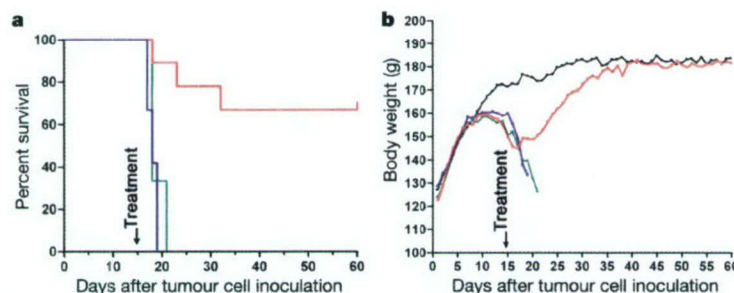


**Figure 5** AnnA1 targeted radio-immunotherapy increases survival in rats. Female Fisher rats were injected intravenously with 13762 cells to induce lung tumours (Day 0). **a**, Kaplan-Meier survival curve comparing the survival of tumour-bearing rats injected 15 days after tumour cell inoculation with  $^{125}\text{I}$ -AnnA1 antibodies ( $50\ \mu\text{g}$  of IgG at  $10\ \mu\text{Ci g}^{-1}$ , red line;  $n = 10$ ) versus control non-targeting  $^{125}\text{I}$ -IgG (blue line;  $n = 10$ )

versus untreated animals (green line;  $n = 3$ ). **b**, Body weights of rats were measured daily and plotted. Red, tumour-bearing rats treated with  $^{125}\text{I}$ -AnnA1 antibodies; blue, tumour-bearing rats treated with control  $^{125}\text{I}$ -IgG; green, untreated tumour-bearing animals; black, untreated normal rats.  $n = 3$ . Maximum standard deviation  $<10\ \text{g}$  for each weight plotted.



much more evident in tumour endothelial plasma membranes than in normal plasma membranes.

Expression profiling using endothelial plasma membranes isolated from major organs demonstrated that almost all of these proteins exist at the endothelial cell surface of at least one major organ, albeit mostly at levels much less than tumours (Fig. 3e). One promising tumour candidate target was the 34 KDa protein recognized by annexin A1 (AnnA1) antibodies only in tumour endothelial plasma membrane. Tissue immuno-histochemistry confirmed tumour blood vessel reactivity (data not shown). Thus, the tumour microenvironment appeared to induce distinct protein expression on the endothelial cell surface.

### Targeting and imaging of solid tumours

Annexins are cytosolic proteins that can associate with cell membranes in a calcium-dependent manner<sup>41</sup>. Some annexins may translocate the lipid bilayer to the external cell surface<sup>41</sup>. To test whether AnnA1 is sufficiently exposed and tumour vessel specific to permit immuno-targeting *in vivo*, we performed whole-body imaging using <sup>125</sup>I-labelled AnnA1 monoclonal antibodies.  $\gamma$ -scintigraphic planar images captured four hours postinjection showed a distinct focus of radioactivity in the lung and little signal elsewhere, in the bodies of rats with tumours (Fig. 4a, b). Non-targeting <sup>125</sup>I-labelled IgG did not show detectable selective tumour uptake (data not shown). When the lungs were imaged *ex vivo*, we observed <sup>125</sup>I-AnnA1 antibody accumulation in the tumour as hot spots corresponding to visible tumours (Fig. 4c, d). Furthermore, targeting was prevented by a 30-fold excess of unlabelled AnnA1 IgG but not by control IgG (data not shown). Region-of-interest and biodistribution analysis confirmed targeting *in vivo* with an average tumour accumulation at two hours of 34% injected dose per gram

of tissue. This compared favourably to VEGF receptor antibodies which accumulated at 6.4% injected dose per gram of tumour. When injected into rats without tumours, <sup>125</sup>I-AnnA1 antibodies showed no targeting of normal organs, including lung at levels less than 1% injected dose per gram of tissue, whereas VEGF receptor antibody accumulation was greater in multiple organs (data not shown). The uptake ratio in rat tumour-bearing lungs versus normal lungs was up to 2.0 and 70 for antibodies to VEGF receptor and AnnA1, respectively. Thus,  $\gamma$ -scintigraphic imaging rapidly validated AnnA1 as a tumour target that is readily accessible to antibody injected intravenously for tumour targeting and imaging *in vivo*. AnnA1 appeared to be selectively externalized on the endothelial cell surface in the solid tumours.

### Radio-immunotherapy of solid tumours

Many tumour-bearing rats imaged with the <sup>125</sup>I-AnnA1 antibody survived, so we performed a survival study and recorded animal body weights; 80% of the animals treated with the <sup>125</sup>I-AnnA1 antibody survived 8 days or longer compared with the <sup>125</sup>I-IgG-treated and untreated rats, which died within 7 days (Fig. 5a). The body weights of all tumour-bearing rats began to drop 7–10 days after tumour cell inoculation (Fig. 5b). The control rats continued to decrease in body weight to 23–30% less than normal at their death. In contrast, rats treated with <sup>125</sup>I-AnnA1 IgG began to gain weight within 3–4 days and reached a normal body weight after 25 days. This increased survival was striking because in this model many animals die within 2–4 days of treatment and thus may lack sufficient time to benefit from treatment. The survival rate of rats surviving the first week approached 90%. The one rat that died after 2 weeks required euthanasia because of a leg tumour and large tail tumour that were not apparent when treated. Thus, a single

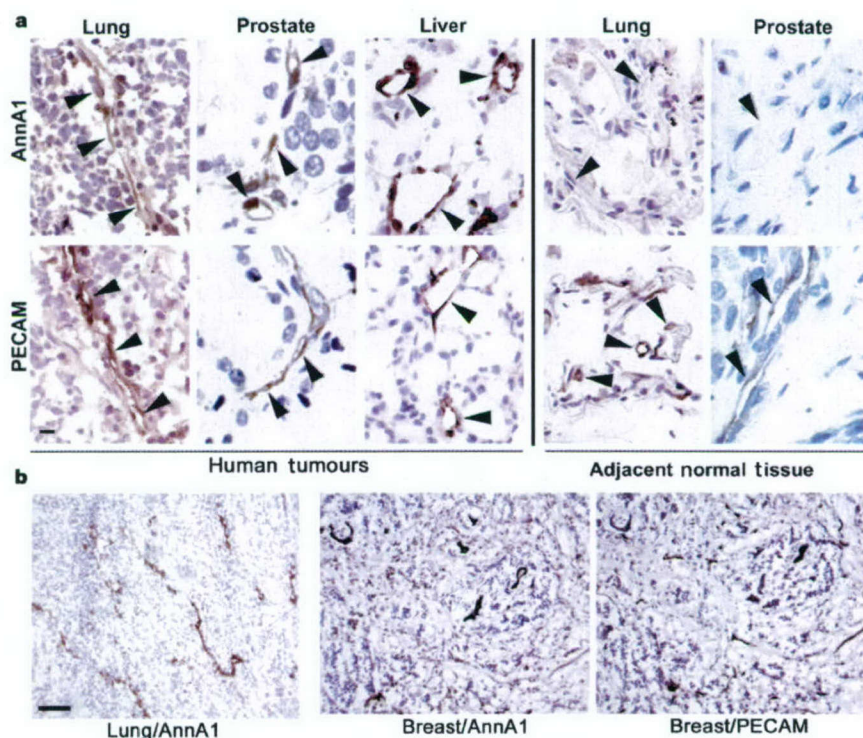


**Figure 6** Expression of AnnA1 on vascular endothelium of multiple primary human solid tumours. **a**, Immuno-staining of paraffin-embedded (prostate) or frozen (lung, liver) sections from human tumour specimens and normal tissues, as indicated, with antibodies to AnnA1 (top panels) and PECAM (bottom panels). Arrowheads indicate blood vessels.

Scale bar represents 10  $\mu$ m. **b**, Low magnification images of human lung and breast tumour specimens stained with antibodies to AnnA1 or PECAM, as indicated. Scale bar represents 100  $\mu$ m.



injection of  $^{125}\text{I}$ -AnnA1 antibody caused significant remission even in advanced disease.

## AnnA1 in human tumour neovasculature

We immuno-stained tissue sections of human solid tumours. AnnA1 antibody labelled blood vessels of human prostate, liver, breast and lung tumours but not matched normal tissues (Fig. 6). Antibodies to platelet endothelial cell adhesion molecule-1 (PECAM) stained both normal and tumour blood vessels. The lack of AnnA1 expression in vascular endothelium of multiple normal organs has been reported previously<sup>42–45</sup>. Thus, AnnA1 was selectively detected on the neovascular endothelium of multiple human solid tumours.

## Discussion

We describe a new logic-based discovery and validation approach that integrates newly developed, global analytical techniques to map the proteins expressed *in vivo* at the luminal endothelial cell surface. This approach has demonstrated distinct molecular signatures in normal and neoplastic tissues. We applied this strategy to rat lungs and solid tumours to uncover, from the vast number of proteins expressed in tissue, approximately 50 differentially expressed proteins, including two promising tissue-selective endothelial cell surface proteins that permitted rapid and specific immuno-targeting and imaging *in vivo*. Profiling the endothelial cell surface that is accessible *in vivo* is an important logical step for validating the hypothesis of tissue-modulated endothelial cell diversity *in vivo* and for discovering potential targets. This is important not only to direct pharmacodelivery and molecular imaging but also—by means of caveolae—to overcome the restrictive endothelial cell barrier to transport drugs or genes to the underlying tissue cells<sup>16,17</sup>.

Key features of our analysis included tissue subfractionation with subtractive proteomic and bioinformatic filters that together reduced tissue complexity by greater than five orders of magnitude, and unmasked a manageable subset of proteins at the inherently accessible blood–tissue interface. This has led to the creation of a database of vascular endothelial cell surface proteins containing accessible proteins apparently modulated by the tissue. After bioinformatic filtering, western blot analysis and/or tissue immuno-staining provided sensitive expression profiling to yield only a few candidate proteins exhibiting organ- or tumour-specificity. Planar and SPECT imaging, using intravenously injected antibodies specific to each protein, visualized targeting and tissue accumulation with high sensitivity and resolution. Imaging thus provided a rigorous and objective validation of accessibility and tissue-specificity of the few remaining candidate targets and ultimately demonstrated potential utility such as, how rapidly and to what extent the antibody targets single organs or solid tumours *in vivo*.

So far, *in vivo* imaging correlates well with the expression profiling using isolated endothelial plasma membranes. It showed lung-specific immuno-targeting for APP (Fig. 2), tumour-specificity for AnnA1 (Fig. 4) and targeting of multiple tissues for less specific target proteins (that is, PV-1, VEGF-R and podocalyxin) (our unpublished observations). Because of poor access inside many tissues, antibodies injected intravenously usually require significantly higher doses ( $\geq 250 \mu\text{g kg}^{-1}$  (ref. 46) compared with  $20 \mu\text{g kg}^{-1}$  used here) to get a small percentage into the tissue that binds and can then be visualized clearly a day or so later, after the background signal has been cleared from the blood. Here, the binding was direct and unhindered by barriers so that both tissue accumulation and blood clearance were rapid, thereby providing striking images within minutes to hours. The rapidity and high levels of specific targeting observed here meet the theoretical expectation of the vascular targeting strategy<sup>17</sup>. Although fast emerging as a standard for assessing targeting and specificity<sup>1–4</sup>, whole-body imaging may be underutilized in target validation despite being non-invasive and highly sensitive.

Using a new, integrated analytical approach we have found new tissue-specific endothelial cell surface proteins that can act as vascular targets to bring us one step closer to achieving the century-old elusive goal of targeting single organs or solid tumours *in vivo*<sup>1,2,4,6,10</sup>. The development and optimization of several key technologies has provided the sensitivity and throughput required for this new target discovery and validation process. We expect that site-directed vascular and caveolar targeting will benefit both drug and gene delivery in the treatment of many diseases<sup>16</sup>. We have demonstrated here, using a rat tumour model that monoclonal antibodies to AnnA1 can effectively direct low levels of radio-nuclides ( $100 \mu\text{Ci}$ ) to concentrate in, and thus destroy solid tumours, which ultimately increases animal survival. Because AnnA1 is also selectively detected in multiple human solid tumours, this target may similarly help to image and treat human disease. □

## Methods

A detailed description of the materials, 2D gel analysis, expression profiling *in vivo* of candidate proteins, rat tumour models,  $\gamma$ -scintigraphic imaging and biodistribution analysis is available in Supplementary Methods.

## Proteomic analysis

We used a three-pronged approach to resolve proteins/peptides for mass spectrometric analysis: (1) The proteins of silica-coated luminal endothelial cell plasma membranes and caveolae isolated from various normal organs or tumours were resolved by high resolution 2D gel analysis before excising potential organ- or tumour-specific protein spots for mass spectrometric analysis; (2) Proteins in the isolated endothelial plasma membranes and caveolae were separated using one-dimensional (1D) SDS–polyacrylamide gel electrophoresis (SDS–PAGE) and specific bands of interest were cut out or the whole gel lane was cut into 50 slices, and the proteins in each of the gel slices were analysed by mass spectrometry; and (3) Multi-dimensional Protein Identification Technology (MudPIT) was used to analyse tryptic peptides from a complex mixture of proteins extracted directly from the whole isolated endothelial plasma membrane fraction and caveolae isolates. Each gel spot/slice was de-stained and digested overnight with trypsin before extracting the cleaved peptides from the gel and then loading them onto a reverse phase micro-column for gradient acetonitrile elution directly into the mass spectrometer (LCQ Deca XP ion trap mass spectrometer (ThermoFinnigan) equipped with a modified micro-electrospray ionization source from Mass Evolution). For MudPIT, 150  $\mu\text{g}$  of complex peptide mixture was separated by 2D liquid chromatography, comprising a micro-column packed with three phases of chromatographic material as follows: 8.5 cm of 5  $\mu\text{m}$  reversed phase material (Polaris C18-A, Metachem); 4 cm of 5  $\mu\text{m}$  300 Å strong cation exchanger (PolyLC); and lastly 3.5 cm of  $\text{C}_{18}$  material, using a helium pressure cell operated at 600–900 psi (Mass Evolution). Peptides were directly eluted into the mass spectrometer using 2D chromatography with 18 step-elutions from the strong cation exchanger, followed by a gradient elution of the reversed phase material. Operation of the quaternary Agilent 1100 HPLC pump and the mass spectrometer was fully automated during the entire procedure using the Excalibur 1.2 data system (ThermoFinnigan). Continuous cycles of one full scan ( $m/z$  400 to 1,400) followed by three data-dependent MS/MS measurements at 35% normalized collision energy were performed. MS/MS measurements were allowed for the three most intense precursor ions with an enabled exclusion list of 25  $m/z$  values ( $\pm 1.5$  Da) or a maximum time limit of 5 min. The zoom scan function to determine the charge state was disabled in order to increase the duty cycle of the instrument.

## Database search and *in silico* analysis of tandem mass spectra

MS/MS spectra were extracted from raw files requiring a minimum of 21 signals with an intensity of at least  $4.75 \times 10^4$  arbitrary units (AU). Extracted MS/MS spectra were automatically assigned to the best matching peptide sequence using the SEQUEST algorithm and the Sequest Browser software package (ThermoFinnigan). SEQUEST searches were performed using a rat protein database containing 40,800 protein sequences that were downloaded as FASTA formatted sequences from ENTREZ (National Center for Biotechnology Information (NCBI); <http://www.ncbi.nlm.nih.gov/Entrez>). Sequence redundancies were removed using Perl script. The peptide mass search tolerance was set to 3 Da. Spectral matches were retained with a minimal cross-correlation score (XCorr) of 1.5, 2.2 and 3.3 for charge states +1, +2 and +3, respectively. DeltaCN (top match's XCorr minus the second-best match's XCorr, divided by top match's XCorr) had to be equal or less than 0.07. Retained spectral matches were filtered and re-assigned to proteins using DTASelect. DTASelect outputs of independent measurements were entered into the AVATAR database. AVATAR was designed to store a large amount of mass spectrometric data and to provide tools to analyse the data to extract valuable information. We used relational models for database design based on entity relationship and implemented the database in the MySQL relational database management system (MySQL) to support database query and management. This relational database plus the Perl-based interface greatly improved data organization, data consistency and integrity, and facilitated data comparison and information retrieval. In the case of the 1D gel and MudPIT approaches, AVATAR was used to subtract the data to find proteins detected only at the lung endothelial cell surface *in vivo* versus *in vitro* or on the tumour but not normal endothelium.



# In silico bioinformatic interrogation

To identify possible candidates for intravenously accessible targets from the subset of proteins identified as lung or tumour induced, we determined their currently known membrane-associated structure (bilayer spanning versus lipid anchor (intra- or extracellular) versus peripheral interaction) from scientific reports and/or protein databases, such as SwissProt (<http://us.expasy.org/sprot/sprot-top.html>) and the NCBI ENTREZ protein database (<http://www.ncbi.nlm.nih.gov/entrez/query.fcgi>). We also used web-based prediction programs to identify candidates that may harbour transmembrane spanning alpha helices (Prediction of Transmembrane Regions and Orientation (TMPred), [http://www.ch.embnet.org/software/TMPRED\\_form.html](http://www.ch.embnet.org/software/TMPRED_form.html)) or glycosylation sites to indicate a possible ectodomain exposed to the circulating blood (Prosit Scan, [http://npsa-pbil.ibcp.fr/cgi-bin/npsa\\_automat.pl?page=npsa\\_prosite.html](http://npsa-pbil.ibcp.fr/cgi-bin/npsa_automat.pl?page=npsa_prosite.html)). Only 100% probabilities were taken into consideration.

Received 28 January; accepted 19 April 2004; doi:10.1038/nature02580.

1. Massoud, T. F. & Gambhir, S. S. Molecular imaging in living subjects: seeing fundamental biological processes in a new light. *Genes Dev.* **17**, 545–580 (2003).
2. Herschman, H. R. Molecular imaging: looking at problems, seeing solutions. *Science* **302**, 605–608 (2003).
3. Rudin, M. & Weissleder, R. Molecular imaging in drug discovery and development. *Nature Rev. Drug Discov.* **2**, 123–131 (2003).
4. Weissleder, R. Scaling down imaging: molecular mapping of cancer in mice. *Nature Rev. Cancer* **2**, 11–18 (2002).
5. Drews, J. Drug discovery: a historical perspective. *Science* **287**, 1960–1964 (2000).
6. Lindsay, M. A. Target discovery. *Nature Rev. Drug Discov.* **2**, 831–838 (2003).
7. Workman, P. New drug targets for genomic cancer therapy: successes, limitations, opportunities and future challenges. *Curr. Cancer Drug Targets* **1**, 33–47 (2001).
8. Anzick, S. L. & Trent, J. M. Role of genomics in identifying new targets for cancer therapy. *Oncology (Huntingt.)* **16**, 7–13 (2002).
9. Cavenee, W. K. Genetics and new approaches to cancer therapy. *Carcinogenesis* **23**, 683–686 (2002).
10. Huber, L. A. Is proteomics heading in the wrong direction? *Nature Rev. Mol. Cell Biol.* **4**, 74–80 (2003).
11. Perou, C. M. *et al.* Molecular portraits of human breast tumours. *Nature* **406**, 747–752 (2000).
12. Jain, R. K. The next frontier of molecular medicine: delivery of therapeutics. *Nature Med.* **4**, 655–657 (1998).
13. Dvorak, H. F., Nagy, J. A. & Dvorak, A. M. Structure of solid tumors and their vasculature: implications for therapy with monoclonal antibodies. *Cancer Cells* **3**, 77–85 (1991).
14. von Mehren, M., Adams, G. P. & Weiner, L. M. Monoclonal antibody therapy for cancer. *Annu. Rev. Med.* **54**, 343–369 (2003).
15. Farah, R. A., Clinchy, B., Herrera, L. & Vitetta, E. S. The development of monoclonal antibodies for the therapy of cancer. *Crit. Rev. Eukaryot. Gene Expr.* **8**, 321–356 (1998).
16. Carver, L. A. & Schnitzer, J. E. Caveolae: mining little caves for new cancer targets. *Nature Rev. Cancer* **3**, 571–581 (2003).
17. Schnitzer, J. E. Vascular targeting as a strategy for cancer therapy. *N. Engl. J. Med.* **339**, 472–474 (1998).
18. Madri, J. A. & Williams, S. K. Capillary endothelial cell culture: Phenotype modulation by matrix components. *J. Cell Biol.* **97**, 153–165 (1983).
19. Schnitzer, J. E. in *Vascular Endothelium: Physiology, Pathology and Therapeutic Opportunities* (eds Born, G. V. R. & Schwartz, C. J.) 77–95 (Schattauer, Stuttgart, 1997).
20. Aird, W. C. *et al.* Vascular bed-specific expression of an endothelial cell gene is programmed by the tissue microenvironment. *J. Cell Biol.* **138**, 1117–1124 (1997).
21. Janzer, R. C. & Raff, M. C. Astrocytes induce blood–brain barrier properties in endothelial cells. *Nature* **325**, 253–257 (1987).
22. Stewart, P. A. & Wiley, M. J. Developing nervous tissue induces formation of blood–brain barrier characteristics in invading endothelial cells: a study using quail–chick transplantation chimeras. *Dev. Biol.* **84**, 183–192 (1981).
23. Auerbach, R. *et al.* Specificity of adhesion between murine tumor cells and capillary endothelium: an *in vitro* correlate of preferential metastasis *in vivo*. *Cancer Res.* **47**, 1492–1496 (1987).
24. Pasqualini, R. & Ruoslahti, E. Organ targeting *in vivo* using phage display peptide libraries. *Nature* **380**, 364–366 (1996).
25. Rajotte, D. *et al.* Molecular heterogeneity of the vascular endothelium revealed by *in vivo* phage

display. *J. Clin. Invest.* **102**, 430–437 (1998).

26. Papetti, M. & Herman, I. M. Mechanisms of normal and tumor-derived angiogenesis. *Am. J. Physiol. Cell Physiol.* **282**, C947–C970 (2002).
27. Ferrara, N. VEGF and the quest for tumour angiogenesis factors. *Nature Rev. Cancer* **2**, 795–803 (2002).
28. Kerbel, R. & Folkman, J. Clinical translation of angiogenesis inhibitors. *Nature Rev. Cancer* **2**, 727–739 (2002).
29. St Croix, B. *et al.* Genes expressed in human tumor endothelium. *Science* **289**, 1197–1202 (2000).
30. Huang, X. *et al.* Tumor infarction in mice by antibody-directed targeting of tissue factor to tumor vasculature. *Science* **275**, 547–550 (1997).
31. McIntosh, D. P., Tan, X.-Y., Oh, P. & Schnitzer, J. E. Targeting endothelium and its dynamic caveolae for tissue-specific transcytosis *in vivo*: A pathway to overcome cell barriers to drug and gene delivery. *Proc. Natl Acad. Sci. USA* **99**, 1996–2001 (2002).
32. Sipkins, D. A. *et al.* Detection of tumor angiogenesis *in vivo* by alphaVbeta3-targeted magnetic resonance imaging. *Nature Med.* **4**, 623–626 (1998).
33. Hu, Z. & Garen, A. Targeting tissue factor on tumor vascular endothelial cells and tumor cells for immunotherapy in mouse models of prostatic cancer. *Proc. Natl Acad. Sci. USA* **98**, 12180–12185 (2001).
34. Hood, J. D. *et al.* Tumor regression by targeted gene delivery to the neovasculature. *Science* **296**, 2404–2407 (2002).
35. Oh, P. & Schnitzer, J. E. in *Cell Biology: A Laboratory Handbook* (ed. Celis, J.) 34–36 (Academic Press, Orlando, 1998).
36. Schnitzer, J. E., McIntosh, D. P., Dvorak, A. M., Liu, J. & Oh, P. Separation of caveolae from associated microdomains of GPI-anchored proteins. *Science* **269**, 1435–1439 (1995).
37. Schnitzer, J. E. gp60 is an albumin-binding glycoprotein expressed by continuous endothelium involved in albumin transcytosis. *Am. J. Physiol.* **262**, H246–H254 (1992).
38. Henniker, A. J., Bradstock, K. F., Grimsley, P. & Atkinson, M. K. A novel non-lineage antigen on human leucocytes: characterization with two CD-48 monoclonal antibodies. *Dis. Markers* **8**, 179–190 (1990).
39. Essler, M. & Ruoslahti, E. Molecular specialization of breast vasculature: a breast-homing phage-displayed peptide binds to aminopeptidase P in breast vasculature. *Proc. Natl Acad. Sci. USA* **99**, 2252–2257 (2002).
40. Perillo, N. L., Marcus, M. E. & Baum, L. G. Galectins: versatile modulators of cell adhesion, cell proliferation, and cell death. *J. Mol. Med.* **76**, 402–412 (1998).
41. Gerke, V. & Moss, S. E. Annexins: from structure to function. *Physiol. Rev.* **82**, 331–371 (2002).
42. Dreier, R., Schmid, K. W., Gerke, V. & Riehemann, K. Differential expression of annexins I, II and IV in human tissues: an immunohistochemical study. *Histochem. Cell Biol.* **110**, 137–148 (1998).
43. Eberhard, D. A., Brown, M. D. & VandenBerg, S. R. Alterations of annexin expression in pathological neuronal and glial reactions. Immunohistochemical localization of annexins I, II (p36 and p11 subunits), IV, and VI in the human hippocampus. *Am. J. Pathol.* **145**, 640–649 (1994).
44. Ahn, S. H., Sawada, H., Ro, J. Y. & Nicolson, G. L. Differential expression of annexin I in human mammary ductal epithelial cells in normal and benign and malignant breast tissues. *Clin. Exp. Metastasis* **15**, 151–156 (1997).
45. McKanna, J. A. & Zhang, M. Z. Immunohistochemical localization of lipocortin 1 in rat brain is sensitive to pH, freezing, and dehydration. *J. Histochem. Cytochem.* **45**, 527–538 (1997).
46. Bredow, S., Lewin, M., Hofmann, B., Marecos, E. & Weissleder, R. Imaging of tumour neovasculature by targeting the TGF-beta binding receptor endoglin. *Eur. J. Cancer* **36**, 675–681 (2000).

Supplementary Information accompanies the paper on [www.nature.com/nature](http://www.nature.com/nature).

**Acknowledgements** We thank A. Wempen, K. Hearn, M. Bourne, L. Randall and T. Smith for technical assistance. This research was supported by the National Institute of Health (Heart, Lung and Blood), National Cancer Institute, Sidney Kimmel, Schutz Foundation, California Tobacco-related Disease Research Program and California Breast Cancer Research Program.

**Competing interests statement** The authors declare that they have no competing financial interests.

**Correspondence** and requests for materials should be addressed to J.E.S. ([jschnitzer@skcc.org](mailto:jschnitzer@skcc.org)).



## Subtractive proteomic mapping of the endothelial surface in lung and solid tumours for tissue-specific therapy

Phil Oh, Yan Li, Jingyi Yu, Eberhard Durr, Karolina M. Krasinska, Lucy A. Carver, Jacqueline E. Testa, and Jan E. Schnitzer

*Sidney Kimmel Cancer Center; 10835 Altman Row; San Diego, CA 92121*

### Supplementary methods.

**Materials.** Antibodies were obtained: AnnA1 (C19, polyclonal), AnnA8, EphA5, Eph A7, ACE, APN, caveolin-1, E-cadherin, Tie 2, and VE-Cadherin from Santa Cruz Biotechnology (Santa Cruz, CA); human AnnA1 (II-29, polyclonal) from ICN Biomedicals (Irvine, CA); aquaporin-1, was obtained from BD Biosciences/Pharmingen (San Diego, CA);  $\beta$ -COP,  $\beta$ -actin, M $\Phi$ , and fibroblast surface protein from Sigma (Saint Louis, MO); RAGE from Affinity Bioreagents (Golden, CO); TfnR, VEGF R2, and ECE were from Zymed Lab, Inc. (San Francisco, CA); nucleolin from Leinco Technologies (St. Louis, MO); CD4 from Serotech (Raleigh, NC); DPPIV from BD Biosciences (San Diego, CA); TM from Covance (Princeton, NJ); MPO from Accurate Chemicals (Westbury, NY), and Vitamin D binding protein from DAKO (Carpinteria, CA). Antibodies against carbonic anhydrase IV were a kind gift of W.S. Sly, St. Louis University (St. Louis, MO); APP, PV-1, and podocalyxin were produced in house; seven transmembrane receptor was a kind gift of Dr. Shigehisa Hirose, Tokyo Institute of Technology (Yokohama, Japan); OX-45 was a kind gift of Dr. Neil Barclay, University of Oxford (Oxford, UK); galectin 1 was a kind gift of Dr. M. Huflejt, Sidney Kimmel Cancer Center (San Diego, CA); VEGF receptor 1 was a kind gift of Dr. D. Sanger, Beth Israel Deaconess Medical Center (Boston MA); endoglin



was a kind gift of Dr. Yamashita, Ludwig Institute for Cancer Research; neurophilin 1 was a kind gift of Dr. Ginty, Johns Hopkins School of Medicine (Baltimore, MD); C-CAM1 was a kind gift of Sue-Hwa Lin, The University of Texas M.D. Anderson Cancer Center (Houston, TX). After testing commercially available AnnA1 monoclonal antibodies, we found it necessary to generate our own panel of monoclonal antibodies using recombinant AnnA1.

**Expression profiling in vivo of candidate proteins.** To assess expression of candidate endothelial cell proteins in different tissues, proteins from the tissue homogenate and P isolated from normal rat lung, heart, kidney, liver, and/or tumour-bearing lungs were solubilized with CLB buffer (6M urea, 0.5M Tris pH 6.8, 9mM EDTA, 9% sodium dodecyl sulfate), separated by SDS-PAGE, and electrotransferred to nitrocellulose filters for immunoblotting with the appropriate antibodies as described<sup>1</sup>.

**Immunohistochemical staining of tissues.** Tissue samples were provided by the Cooperative Human Tissue Network which is funded by the National Cancer Institute. Frozen tissues were cut (5  $\mu$ m) on a Microm HM505E cryomicrotome. Sections were fixed with neutral buffered formalin for 5 min at room temperature then incubated for one hour at room temperature in blocking solution (5% FBS, 0.1% Tween 20 in PBS). After a 2-hour incubation at room temperature in primary antibodies (diluted in blocking solution) the sections were washed then treated with the appropriate biotin-conjugated secondary antibody (KPL Laboratories, Gaithersburg, MD) for 1 hour at room temperature, washed again then treated with a streptavidin-conjugated horseradish peroxidase (KPL Laboratories) for 1 hour at room temperature. Immune complexes were detected using a Liquid DAB staining kit from BioGenex (San Ramon, CA). Formalin-fixed, paraffin-embedded sections (5  $\mu$ m) were cut on a Microm HM340E microtome. Antigen retrieval



was performed using acid citrate buffer following standard procedures. After the sections were washed in water to remove the citrate buffer, they were blocked and immunostained as above.

**Rat tumor models.** Female Fisher rats (100-150 gms) were injected via the tail vein with a cell suspension of 13762 breast adenocarcinoma cells to give ample, well circumscribed, and highly vascularized tumours in the lung. To create a maximum density of tumour lesions of 3-8 mm in diameter that are clearly visible in the lungs (as shown in Fig. 3A), we injected  $5 \times 10^5$  13762 cells 14-15 days prior to perfusion and isolation of tumour-bearing lung P. To obtain a few well-circumscribed tumours of 3-6 mm in diameter, we injected  $1 \times 10^5$  cells 21 days prior to performing the imaging experiments.

**Gamma scintigraphic imaging and biodistribution analysis.** Monoclonal antibodies were isolated using GammaBind Plus Sepharose (Amersham, Piscataway, NJ) and conjugated to  $^{125}\text{I}$  using Iodogen as described<sup>2</sup>. Biodistribution analysis was performed as described<sup>2</sup>. Imaging was performed using an A-SPECT imaging system, a dedicated small animal radiotracer imaging system (Gamma Medica, Inc., Northridge, CA)<sup>3</sup>, fitted with a parallel-hole collimator. Normal and tumour-bearing female Fisher rats were anaesthetized and injected via the tail vein with  $^{125}\text{I}$ -labeled monoclonal antibody (5  $\mu\text{g}$  IgG; 10  $\mu\text{Ci}/\mu\text{g}$ ) before being subjected to planar gamma scintigraphic imaging captured over 10 min. For tomographic studies, the images were captured in  $6^\circ$  increments for 64 frames (30 sec/frame). After whole body imaging, in some cases, the lungs were excised for planar imaging captured over 10 min ex vivo.



1. Schnitzer, J. E., McIntosh, D. P., Dvorak, A. M., Liu, J. & Oh, P. Separation of caveolae from associated microdomains of GPI-anchored proteins. *Science* **269**, 1435-9 (1995).
2. McIntosh, D. P., Tan, X.-Y., Oh, P. & Schnitzer, J. E. Targeting endothelium and its dynamic caveolae for tissue-specific transcytosis in vivo: A pathway to overcome cell barriers to drug and gene delivery. *Proc. Natl. Acad. Sci. USA* **99**, 1996-2001 (2002).
3. McElroy, D. et al. Performance evaluation of A-SPECT: A high resolution desktop pinhole SPECT system for imaging small animals. *IEEE Trans Nucl Sci NS* **49**, 2139-2147 (2002).